Graduate School Form 30
Updated 1/15/2015

PURDUE UNIVERSITY
GRADUATE SCHOOL
Thesis/Dissertation Acceptance

This is to certify that the thesis/dissertation prepared

By Steven Hunt

Entitled

Thermoacoustic Oscillations in Supercritical Fluid Flows

For the degree of Doctor of Philosophy

Is approved by the final examining committee:

Stephen Heister
Chair

Carlo Scalo

J Stuart Bolton

Stephen Heister for L. Qiao

To the best of my knowledge and as understood by the student in the Thesis/Dissertation Agreement, Publication Delay, and Certification Disclaimer (Graduate School Form 32), this thesis/dissertation adheres to the provisions of Purdue University's "Policy of Integrity in Research" and the use of copyright material.

Approved by Major Professor(s): Stephen Heister

Approved by: W. Chen 3/2/2016

Head of the Departmental Graduate Program Date

THERMOACOUSTIC OSCILLATIONS IN SUPERCRITICAL FLUID FLOWS

A Dissertation

Submitted to the Faculty

of

Purdue University

by

Steven A. Hunt

In Partial Fulfillment of the

Requirements for the Degree

of

Doctor of Philosophy

May 2016

Purdue University

West Lafayette, Indiana

It's what you learn after you know it all that counts.

-John Wooden

ACKNOWLEDGMENTS

I am deeply appreciative of my colleagues at Zucrow Labs, with whom I have made what will certainly be lasting friendships. My gratitude goes to my labmates who have afforded me an abundance of support and time; special thanks are due to Jesse Adams and Heather Wiest for helping me design, build, and operate my experiment. I also thank the support staff at Zucrow Labs and Purdue University for their assistance and expertise.

It has been a pleasure working with Prof. Carlo Scalo, who has provided instrumental insight toward my data analysis. I have also been fortunate to receive helpful feedback from Professors Li Qiao and J. Stuart Bolton.

My project funding has been provided by Rolls-Royce, under the auspices of the Rolls-Royce University Technology Center in Advanced Thermal Management Systems at Purdue University with Pat Sweeney as technical monitor; I am grateful for the input and guidance provided by Pat and the many Rolls-Royce personnel with whom I have worked.

Many thanks go to my advisor, Prof. Stephen Heister. I am grateful for the wonderful opportunity he has given me to work at Zucrow Labs, for his deep wisdom and guidance, and for his relentless positivity and patience.

TABLE OF CONTENTS

Page

LIST OF TABLES

LIST OF FIGURES

SYMBOLS

a	speed of sound
D	tube internal diameter
f	frequency
P	pressure
P_c	critical pressure
P_r	reduced pressure (P/P_c)
Re_D	Reynolds number based on tube inner diameter
St	Strouhal number based on tube length
St_D	Strouhal number based on tube inner diameter
T	temperature
T_c	critical temperature
T_r	reduced temperature
V	flow velocity
μ	fluid dynamic viscosity
ρ	fluid density

ABSTRACT

Hunt, Steven A. PhD, Purdue University, May 2016. Thermoacoustic Oscillations in Supercritical Fluid Flows. Major Professor: Stephen Heister.

Pressure oscillations in supercritical Jet-A fuel flowing through four parallel, heated tubes connected to common manifolds have been observed in this study. Tests were performed with fuel inlet temperatures ranging from 70°F to 700°F, and fuel pressures ranging from 360-700 psi. Total fuel flow rate ranged from 5-55 lb/hr. Tubes were heated by blowing 800-950°F nitrogen over them. Acoustic-mode oscillations, typically ranging from 100-500 Hz, occurred only when a large temperature gradient was created inside the heated fuel tubes. Pressure oscillation amplitudes ranged from 0.1-1.0 psi. Oscillations at the inlet and outlet manifolds that were caused by a mode with the characteristic length of a single fuel tube were separated by a phase lag that was a function of the manifold cross-passage diameter. A lower-frequency mode was also observed, which had a characteristic length based of the summed lengths of a single fuel tube and a single manifold passage. An acoustic simulation using the COMSOL Acoustics Module was performed to predict frequencies based on geometry and flow conditions of the experiment.

1. INTRODUCTION

The field of thermoacoustics pertains to coupled oscillations of pressure, motion, and heat transfer in a fluid. These oscillations occur under many conditions, and are applicable to many fields. Researchers have performed physical experiments under a wide range of conditions, and analytical research on the subject has progressed from purely qualitative, to simplified mathematical models, to numerical analysis using computational fluid dynamics (CFD).

Some of the earliest documented oscillations were encountered by glassblowers from the 19th century [1]. Loud noises emanated from glass tubes as they were heated at a single end [2]. This prompted early study of thermoacoustics. More mathematically-rigorous studies were performed by cryogenics researchers [3] who encountered spontaneous vibrations in tubes of helium, particularly when one end of the tube was much colder than the other. More recently, nuclear power engineers [4] have experienced oscillations of moderating fluid as it is heated, and aerospace engineers have encountered oscillations of combusting gas inside turbine engine combustion chambers [5], as well as supercritically-heated fuels flowing through fuel-air heat exchangers. The latter scenario motivates this study, as pressure spikes associated with thermoacoustic oscillations can damage tubes and other hardware.

1.1 Previous Works

Griffith [5] took Schlieren photos and measured the heat transfer coefficient of Freon 114A near its critical point. The fluid flowed through a 2-inch ID tube, and was heated with nichrome wire inside the test section. Griffith observed bubble-like activity in the fluid, which is likely what others have described as pseudoboiling. Bubble-like activity occurred in fluids near the critical point, both above and below.

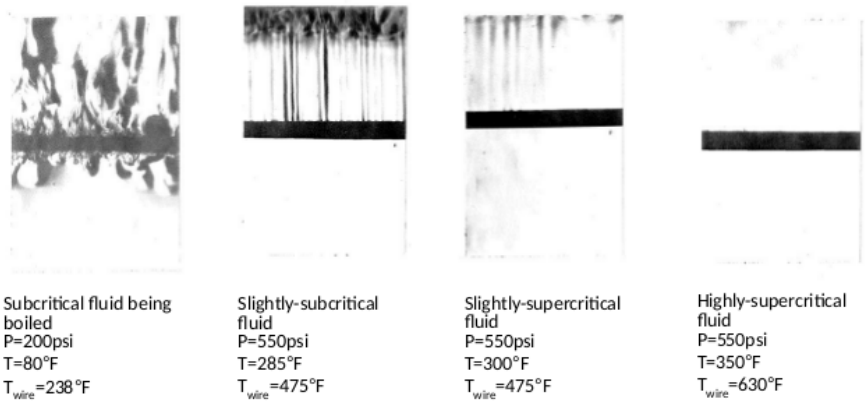

Figure 1.1. Schlieren photos of pseudoboiling, courtesy of Griffith [5]

However, it never occurred in highly-supercritical fluids. This activity did not affect the heat transfer rates Griffith measured.

Hines and Wolf [6] performed early experiments to show thermoacoustic oscillations in supercritical fuels. They tested turbulent flows of supercritical RP-1 and diethylcyclohexane (DECH) through thin-walled tubes designed to replicate flowpaths found in rocket cooling jackets. They found the slope of heat transfer coefficient vs. the difference between bulk and wall temperature increased substantially just above Tcr. At this temperature the heat transfer coefficient rose by up to 40 percent. A similar increase is experienced with subcritical fluids when nucleate boiling begins, although often larger in magnitude. Tests performed by Griffith [5], however, did not show a significant change in heat transfer. Oscillations were often audible in their tests; oscillations of well-defined frequency with uniform amplitude caused a sound described as a clear and steady scream, whereas oscillations of varying amplitude caused chugging or pulsing noises. Dominant frequencies encountered ranged from 1000-7500 Hz, and pressure amplitudes ranged from 50-380psi. Hines and Wolf unsuccessfully attempted to eliminate these oscillations by placing the tube in cement to damp the vibrations during a run.

Several tubes failed during testing. In three experiments at 2000psi, tubes ruptured without any evidence of oscillations. In experiments at 700psi, thin-walled test sections developed hairline longitudinal cracks after a few minutes of oscillations.

Linne et al. [7] performed a design of experiments to generate a statistical model predicting the stability of a flow. Their tests involved supercritical JP-7 fuel flowing through a vertical, resistively-heated tube. An upstream preheater helped heat the fuel to the necessary temperatures. Five independent variables were selected for this study: test section length, test section inside diameter, mass flow rate, inlet fluid temperature, and heat flux. Buoyancy was originally proposed as a driver of oscillations, but based on the Reynolds and Grashof numbers calculated, buoyancy was deemed negligible for all tests.

$$
\begin{aligned}
RMS(P_{out})_{1.0} = {} & 44.82 + 31.98\left(\frac{L-17.0}{3.0}\right) + 37.50\left(\frac{D_i-0.14875}{0.03125}\right) + 17.30\left(\frac{\dot{m}-0.1118}{0.0401}\right) - 31.22\left(\frac{T_i-121.6}{78.9}\right) \\
& + 27.15\left(\frac{L-17.0}{3.0}\right)\left(\frac{D_i-0.14875}{0.03125}\right) - 29.65\left(\frac{L-17.0}{3.0}\right)\left(\frac{T_i-121.6}{78.9}\right) + 18.20\left(\frac{D_i-0.14875}{0.03125}\right)\left(\frac{\dot{m}-0.1118}{0.0401}\right) \\
& - 24.00\left(\frac{D_i-0.14875}{0.03125}\right)\left(\frac{T_i-121.6}{78.9}\right) + 24.80\left(\frac{\dot{m}-0.1118}{0.0401}\right)\left(\frac{Q-3.005}{1.016}\right) - 21.11\left(\frac{T_i-121.6}{78.9}\right)\left(\frac{Q-3.005}{1.016}\right)
\end{aligned}
$$

Figure 1.2. Statistical model courtesy of Linne et al.

The stability analysis was based on the magnitude of RMS pressure. RMS waveforms led to probability distributions of fluid pressure occurring in each test case. The authors arbitrarily selected an RMS pressure of 10 psi as the threshold between a stable and an unstable condition.

To determine the reproducibility of the experiments, Linne et al. repeated several test cases and compared the repeat results with the original results. The authors claimed overall reproducibility to be less than optimal. The percent difference in RMS pressure between repeat tests led them to generate three categories of reproducibility: good, fair, and poor. Out of nine repeat experiments: three had good reproducibility, three had fair, and three had poor. The cause of the irreproducibility could not be determined.

The statistical model estimating RMS pressure is provided in 1.2, in terms of test section length (L), inside diameter (D_i), mass flow rate ($\dot{m}$), inlet temperature (T_i), and heat flux ($\dot{Q}$).

Certain terms describe the effects of a single variable, while others describe coupled effects of two variables.

The model correctly predicted most, but not all, test points as being stable or unstable. Figure 1.3 shows all the test points; incorrectly predicted points are circled.

Several trends can be inferred from this statistical model:

- All inlet temperature coefficients, direct and indirect, are negative.
  - Instabilities should weaken with increasing inlet temperature.

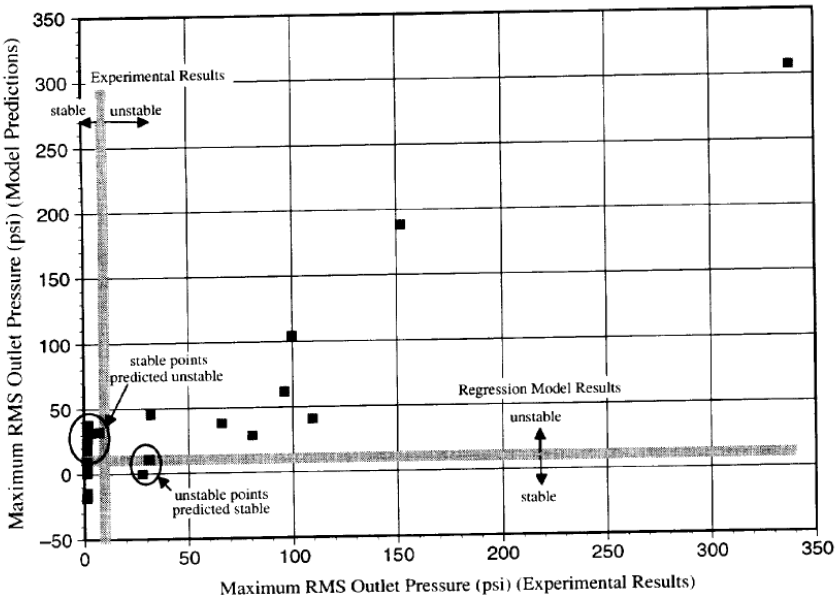

Figure 1.3. Statistical stability analysis courtesy of Linne et al.

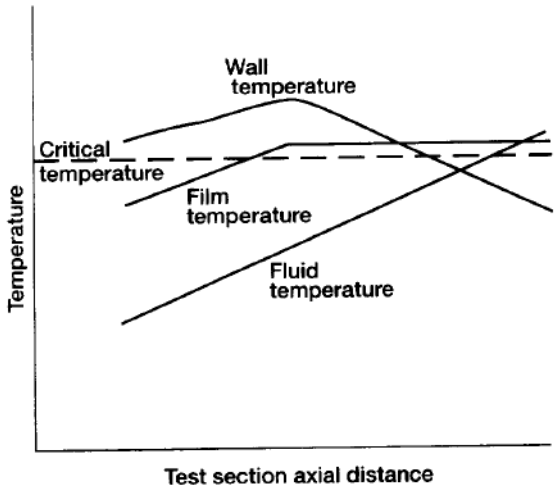

Figure 1.4. Temperature profile conducive to thermoacoustic oscillations - courtesy of Linne et al.

- All mass flow rate coefficients, direct and indirect, are positive.
  - Instabilities should strengthen with increasing mass flow rate.
- Coefficients of tube length diameter vary in sign, and are strongly coupled with other variables. Overall, though, positive terms tend to cancel out negative terms.
  - Instabilities should strengthen (to varying degrees) with increasing tube diameter and length.

Linne et al. hypothesized the temperature distribution shown in Figure 1.4 is conducive to thermoacoustic oscillations.

This temperature distribution has the inlet fluid temperature below the critical temperature, most of the wall above the critical temperature, and the fluid reaching the critical temperature midway through the test section. Many other studies,

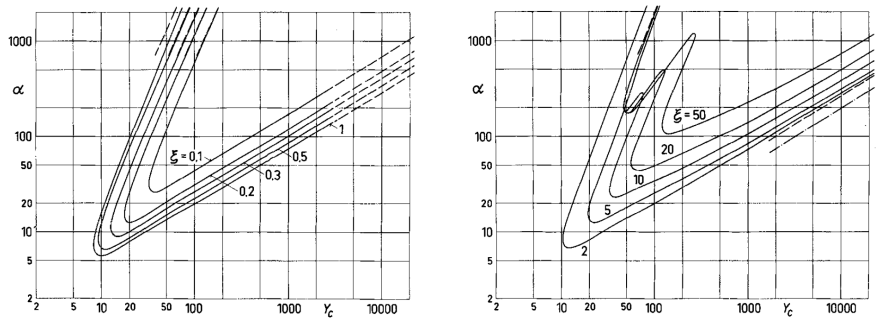

Figure 1.5. Stability limit curves for helium courtesy of Rott

discussed below, also noted that oscillations would not occur if the fluid inlet temperature were above the critical temperature.

This point in the tube where the critical temperature is reached may hold importance to oscillations, as fluid properties such as specific heat vary the greatest in this section. These rapid changes in fluid properties may lead to high derivatives of temperature with respect to axial tube position ($\frac{dT}{dx}$). In a cryogenic fluids study, Rott treated this large temperature gradient as a step discontinuity in his analytical studies [8] and [9]. He investigated acoustic resonance in tubes that are closed at one end and contain a temperature discontinuity.

Rott formulated and solved two-dimensional, time-varying equations of continuity, axial momentum, and energy. A stability limit for helium, which bounds the maximum magnitude of temperature discontinuity (α), was generated in terms of the location of temperature discontinuity in the tube (ξ), and the ratio of boundary layer thickness to tube radius (Y_c).

Temperature ratios below the curves cause stable flow, and temperature ratios above the curves cause instabilities.

Faith et al. [10] experimented with supercritical Jet-A fuel, flowing it through first a preheater, and then one of several types of resistively-heated tubes. They installed 21 equally-spaced tube wall thermocouples: some atop, and some underneath the

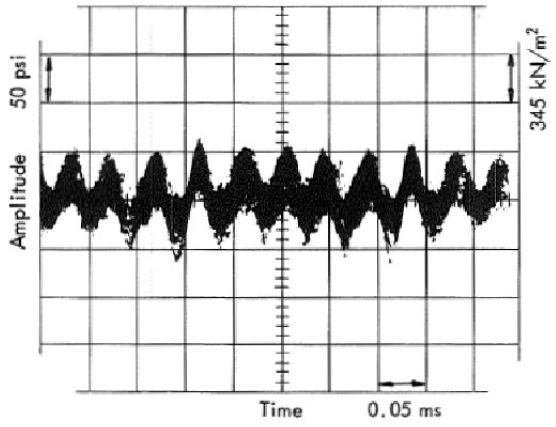

Figure 1.6. Sample waveform courtesy of Faith et al.

tube. Mean pressure was varied between tests. Heat transfer power was increased over a 5-10 minute period until oscillations began.

Heat transfer coefficient correlations were developed for laminar and turbulent flows. Low heat transfer coefficients were often observed when the fuel was near its pseudocritical temperature. Under low heat-flux conditions, the temperature varied substantially from tube bottom to top.

Oscillations manifested in the form of whistling noises. Pressure fluctuations for 0.32-cm ID tubes ranged up to 350 psi. 150-psi amplitudes were seen in 0.16-cm ID tubes. Primary frequencies varied between 1000 and 5000 Hz. A sample waveform is shown in Figure 1.6.

Test runs at a lower mean pressure (500 psi) more frequently produced noises than those at a higher mean pressure (1000 psi). Moreover, noises tended to be louder in the lower pressure cases than the high pressure cases. This trend was explained by the fact that larger viscosity and density gradients exist at lower pressures.

During certain tests lasting 20 hours, whistling only began after several hours. Coking may have caused this in part, as it was reported to increase turbulence, increase the heat transfer coefficient, and decrease the tube temperature.

Hitch and Karpuk [11] studied vertical flow of MCH and JP-7 through a tube heated by band heaters. Flow was driven by a positive-displacement pump. Their test section consisted of eleven solid nickel cylinders. The length of each section was 2.5 in, making for a 26-in total length. The tube outer diameter was fixed at 2.25 in and the ID varied between 0.13 in and 0.065 in.

They observed two distinct types of oscillations near the critical point: Helmholtz oscillations (also known as bulk-mode oscillations) and acoustic-scale oscillations. Helmholtz oscillations occurred with high amplitude and low frequency (1-2 Hz), whereas acoustic oscillations occurred with low amplitude and high frequency (75-450 Hz). Flows were always stable when the fluid pressure was much higher than the critical pressure.

Aiming to eliminate oscillations and increase heat transfer, Hitch and Karpuk tested several turbulating inserts: a twisted-tape insert, a louvered-tape insert, and a static mixer. All three inserts were found to increase the heat transfer coefficient over that of a basic tube. The static mixer caused the largest heat transfer improvement, and reduced Helmholtz oscillations substantially. Flow stability could be maintained with a static mixer until pressure was reduced to less than 1.1 times the critical pressure. Hitch and Karpuk successfully eliminated oscillations even below the critical pressure by using a damping valve to cause a flow restriction before the test section.

Herring's [12] research was aimed at developing a robust and high-performance fuel-air heat exchanger able to accept fuels near or above the supercritical point. Supercritical JP-10 flowed through a single resistively-heated tube in his experimental tests. Flows remained in the laminar regime. Independent variables included inlet temperature, mass flow rate, input power, heated length, and total pipe length. He also tested vertical and horizontal flows to determine the effect of buoyancy, and

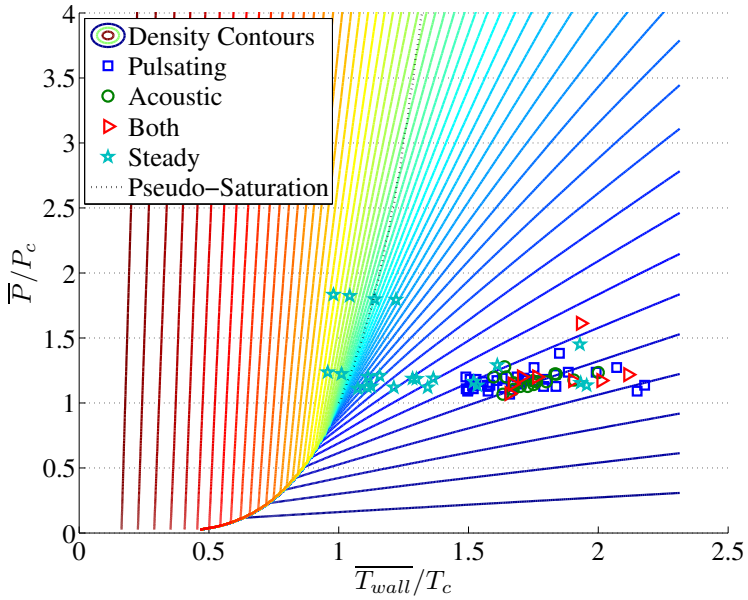

Figure 1.7. Oscillations encountered as function of reduced temperature and pressure, courtesy of Herring

several types of wire coil inserts in an attempt to improve heat transfer and suppress oscillations.

Similar to the results of Hitch and Karpuk, Herring observed bulk-mode oscillations for reduced pressures up to 1.5. He attributed the inability to produce oscillations above this pressure to the insufficient wall temperatures his apparatus was capable of. Linne et al. and Hines & Wolf reported oscillations at reduced pressures over 2.

Figure 1.7 shows all Herring's test points in terms of their dimensionless pressures and temperatures. Different markers for test points are used to depict what type(s) of oscillation, if any, were detected. In Herring's nomenclature, pulsating oscillations are equivalent to bulk-mode or Helmholtz oscillations.

Like many other experimenters, Herring only experienced oscillations when the wall temperature was above the pseudocritical temperature and the fuel inlet temperature was below. Unlike the results of Hitch and Karpuk, however, the use of an upstream damping valve did not prevent bulk-mode oscillations. Herring postulated the dissimilarity was due to the different flow systems used: Hitch and Karpuk used a pump-fed system, so the upstream section could be considered incompressible; Herring (and Linne et al.) drove flows with high-pressure gaseous nitrogen, which could apply a restoring force causing Helmholtz oscillations.

In an attempt to numerically predict oscillations, Herring developed a 1-D CFD code based on inviscid, compressible Euler equations. Heat diffusion in the fluid was ignored. For the test-section exit boundary condition, he originally intended to choke the flow with an area change and set the outlet to atmospheric pressure. This caused the code to become unstable, though, so he changed the pressure at the outlet boundary to be closer to the test section pressure.

The output of his code did not match pressure fluctuations seen in experimental tests. The code predicted pressure fluctuations of about 10 Hz, which was on a different order than that of bulk-mode and acoustic oscillations. One particular assumption in Herring's code has fallen into question: wall temperature was assumed to be steady with time. However, his proposed driving mechanism involves wall temperatures changing with time. It is plausible, although unproven, that considering varying wall temperature would lead to the correct prediction of oscillations. Other authors have postulated the boundary layer mechanics and radial temperature distributions play an important role in oscillations; if this is true, then the improved 1-D model suggested by Herring might not capture all the relevant mechanics.

Palumbo [13] expanded upon Herring's thermoacoustic research by further investigating and attempting to predict oscillations in a supercritically-heated fuel. He flowed supercritical methanol, a simulant to JP-10, through a resistively-heated apparatus similar to Herring's. The independent variables considered were: tube inner

diameter, reduced pressure, mass flow rate, input power, and heated length. The baseline quantities were as follows:

- Tube inner diameter: 0.069 in
- Tube length: 6 in
- Reduced pressure: 1.2
- Flow rate; 6 lb/hr
- Heat input: 600W

The baseline tests produced stable-looking acoustic vibrations at the onset of bulk-mode oscillations. Bulk-mode oscillations occurred at 1.77 Hz and acoustic oscillations occurred at 425 Hz.

Increasing the diameter to 0.093 in caused the bulk-mode frequency to decrease and the acoustic mode to increase. Decreasing the diameter to 0.027 in caused the bulk-mode frequency to drastically decrease to 0.07 Hz, and completely eliminated acoustic oscillations.

Increasing the reduced pressure to 1.4 decreased the strength of both types of oscillations. By decreasing the reduced pressure to 1.0, bulk-mode oscillations decreased in strength, while acoustic oscillations remained strong.

The lowest flow rate (4 lb/hr) tests produced stable-looking acoustic vibrations at the onset of bulk-mode oscillations. An audible pinging noise, described as a hammer on metal, emanated during this run. The highest flow rate (7 lb/hr) produced a sloppy bulk-mode oscillations signal, and a smaller and less-uniform acoustical signature.

The baseline (and highest) heat input was 600W. Decreasing the heat input to 300W caused the frequency of bulk-mode oscillations to decrease to 0.35 Hz, drastically lower than the 1.77 Hz oscillations from the baseline case. The lower heat input setting had a small effect on acoustic frequency, decreasing it to 400 Hz. A higher heat input setting was not tested because of hardware limitations.

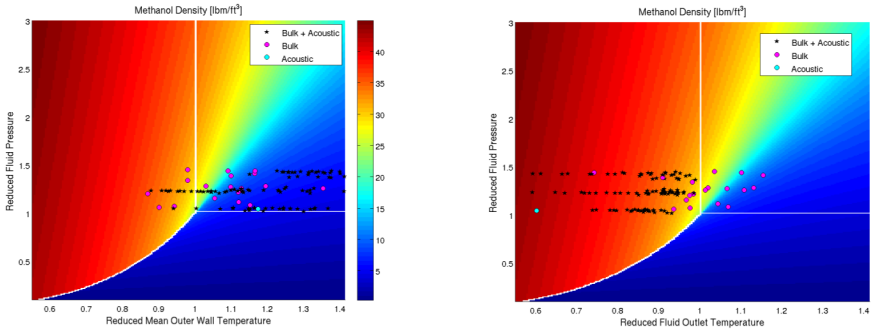

Figure 1.8. Oscillations encountered as a function of reduced temperature and pressure, courtesy of Palumbo

Figure 1.8 shows all test points in terms of their dimensionless pressures and temperatures. The left graph considers the wall temperature at outlet, and the right graph considers fluid temperature at outlet. Different markers for test points are used to depict what type(s) of oscillation, if any, were detected.

These graphs imply that acoustic oscillations occur when the wall temperature is above the pseudocritical temperature, and the fluid is below.

Palumbo highlighted the following as causes of bulk-mode oscillations:

- Oscillations occur because tube wall's thermophysical properties, viz, resistivity, change due to temperature variation.
- Resistivity changes cause wall's periodic heating and cooling.

Fluid properties have large variability near critical point, as depicted by the graph of the gradient of density vs. temperature and pressure:

A critical gradient of density for the onset of oscillation may exist for a given combination of physical parameters.

In addition to physical tests, Palumbo wrote a lumped parameter model to predict the outlet fluid temperature of the test rig. Stagnation pressure and atmospheric pressure were assumed to be constant, as was the density outside the test section.

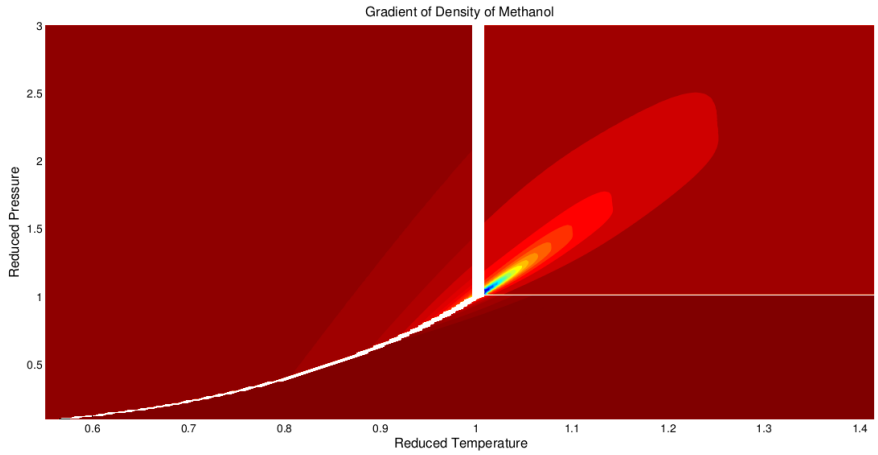

Figure 1.9. Gradient of Density of Methanol, courtesy of Palumbo

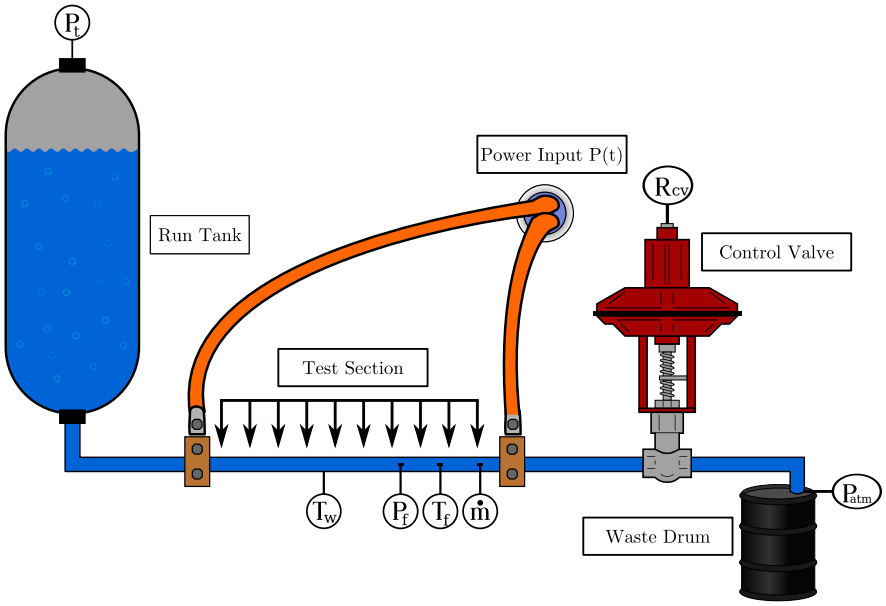

Figure 1.10. Illustration of Palumbo's testing apparatus, courtesy of Palumbo

Initial pressure, temperature, and mass flow rate could be specified in the code. Other properties were evaluated via the NIST database.

The initial pressure in the tube was calculated with the Bernoulli equation with respect to stagnation properties in the tank. Power input into the tube was calculated using Ohm's law. A first law energy balance was performed between the tube and the fluid, considering heat loss through outside insulation. From the energy balance, the change in wall temperature with respect to time was solved for. The Dittus-Boelter equation was used to calculate the heat transfer coefficient. MATLAB's ode45 solver solved for the temperature for all time steps. Given the temperature, the fluid pressure, density, and mass flow rate at the next time step were then calculated.

The model matched experimental results under subcritical conditions, but severely over-predicts the outlet temperature after the fluid reaches the critical temperature. Palumbo believed that major heat loss was likely to occur over a two-inch non-insulated section of the tube between the test section outlet and the thermocouple, so the actual outlet temperatures from the test section were much higher than measured. Also, the analysis assumed a constant tube thermal resistivity, when it actually could vary substantially with temperature.

1.1.1 Selected test results from other experiments

The following table provides a sample of results from some of the cited publications. Several quantities in this table were not reported by the original authors, but were calculated based on their reported data. These quantities include Reynolds and Strouhal numbers, as well as T/Tr, which describes the heat input to the system. Most tests were performed at pressures and temperatures near the critical point of the associated fluid; Linne and Meyers tests broke this trend, with extremely high reduced pressures and low reduced temperatures. Correlations between flow conditions and pulsation characteristics are weak. Tests under high reduced pressure tended to produce high acoustic-mode frequencies. Herrings results deviated from

the norm; Herrings experiments often ran at above-average reduced pressures, and below-average acoustic-mode frequencies. Little correlation can be made across studies regarding the individual effect of reduced temperature, tube diameter, heat input, or the type of fuel used. It follows that oscillatory effects of flow conditions are strongly coupled.

1.2 Hypotheses Describing Thermoacoustic Oscillations

Several authors hypothesized driving mechanisms for thermoacoustic oscillations. This section paraphrases, illustrates, and compares these hypotheses.

1.2.1 Hines and Wolf Hypothesis

Hines and Wolf [6] proposed a mechanism for the oscillations they encountered.

1. For reduced pressure less than 2.5, a small temperature increase near the critical point appreciably thins the laminar boundary layer due to a reduction in viscosity.

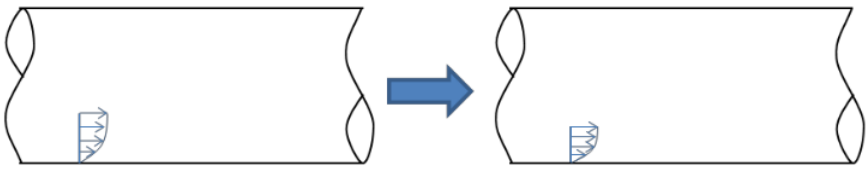

2. The thinner boundary layer leads to cooler wall temperatures.

3. A cooler wall decreases heating of incoming fluid, and the boundary layer thickens.

Table 1.1. Selected test cases for previous works

Researcher	Tube ID	Tube length	P_r	T_r	Re_D	Temperature rise	Fluid
Palumbo	0.027-0.093	11	1-1.4	0.6-1.2	5,000-8,000	40-500	Methanol
Herring	0.069	9-11	1.1-1.9	0.5-0.9	2,000-4,000	100-700	JP-10
Hitch & Karpuk	0.065-0.13	26	1.1-1.7	0.6-1.1	1,000-100,000	200-500	MCH and JP-7
Hines & Wolf	0.314-0.326	9-11	1.9-5.5	0.5-0.8	7,000-43,000	100-400	DECH and RP-1
Faith et al.	0.027-0.093	24	1.5-3	1.0-1.2	$\sim$12,000	700-900	Jet-A
Linne et al.	0.125	18	3.3	0.7-1.4	7,000-52,000	600	JP-7

Table 1.2. Results summary of selected test cases from previous works

	Bulk-mode			Acoustic			
Researcher/case	f(Hz)	St	$\Delta P/P$	f (Hz)	St_D	St	$\Delta P/P$
Palumbo (baseline)	1.77	0.49	0.028	425	0.731	117	0.0014
Palumbo (#154057)	2.22	0.61	0.038	425	0.725	116	0.0027
Herring (#131156)	1.97	0.34	0.017	150	0.195	26.8	0.0017
Hitch & Karpuk (MCH3 Point D)	0.625	0.1	0.018	N/A			
Hitch & Karpuk (JP7-2 Point C)		N/A		325	1.28	256	0.032
Hines & Wolf (Case 3)		N/A		3,600	2.51	154	0.27
Faith et al. (Run 42)		N/A		1,500	0.309	117	0.08
Linne et al. (Test Matrix 22)		N/A		1,900	1.43	158	0.4

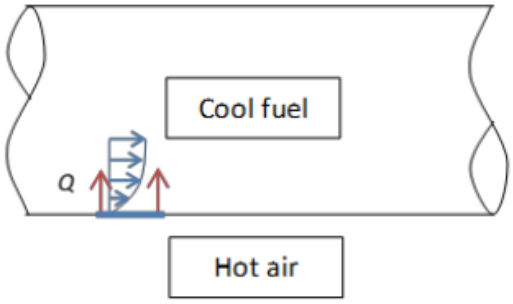

4. The thicker boundary layer causes hotter wall temperature, and cycle repeats.

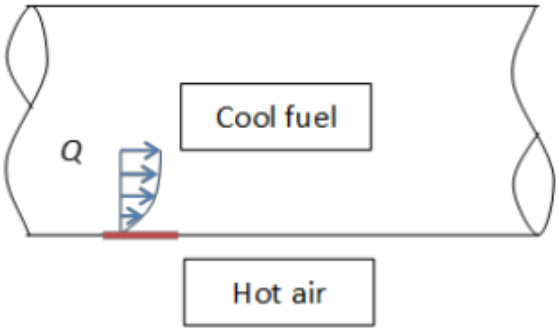

No measurements of such wall temperature oscillations could be made with the recording equipment Hines and Wolf employed.

1.2.2 Faith et al. Hypothesis

Faith et al. [10] proposed a mechanism that is effectively the same as Hines and Wolfs:

1. Fuel heats up, causing viscosity to drop. The viscosity gradient is especially high near critical point.

2. Viscosity drops, causing boundary layer to thin.

3. Thinner boundary layer causes heat transfer coefficient to rise.
4. Higher heat transfer coefficient causes lower film temperature.
5. Lower film temperature causes viscosity to increase, and cycle repeats.

1.2.3 Herring Hypothesis

Herring proposed the following driving mechanism for bulk-mode oscillations:

1. Wall temp reaches threshold causing a sudden increase in heat flux.

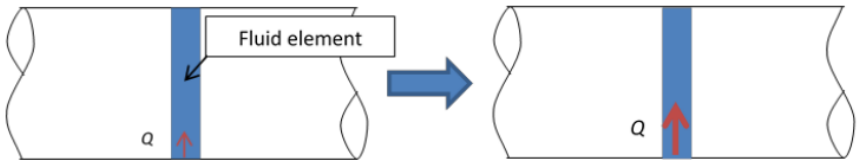

2. Increased heat flux results in large fuel temperature change, and fuel expands.

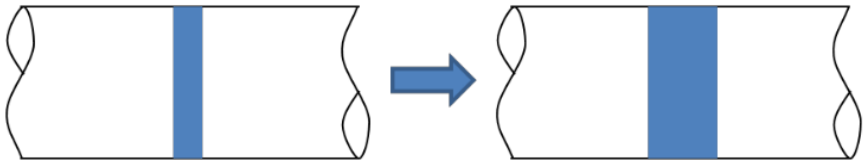

3. Rapidly-expanding fuel is ejected from tube and creates pressure wave that transmits the increased pressure throughout the system.

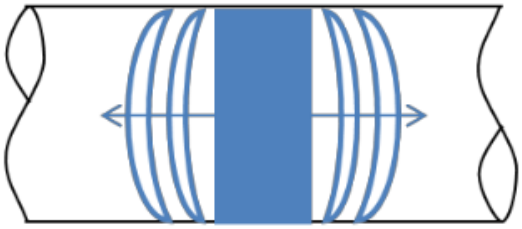

4. Increased heat flux rapidly cools the tube.

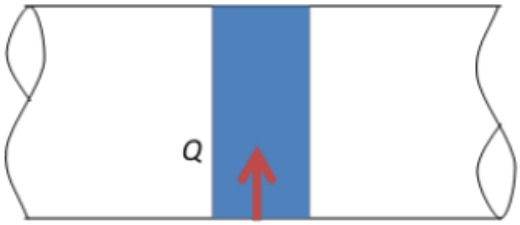

5. Hot, low-density fuel is ejected into plenums, and is cooled by surrounding fuel.

6. This cooling causes fuel to compress and create more pressure fluctuations.

7. Cool fuel from the inlet re-enters tube as wall temperatures rise, and cycle repeats.

Herring remarked that the time between bulk-mode oscillations is related to the amount of time for fuel to completely fill the tube, and the time for the wall temperature to exceed the threshold value.

1.2.4 Summary of hypotheses

The three hypotheses discussed all attribute oscillations to periodic heating and cooling of the fluid and tube wall. The theories disagree about the manner in which oscillations manifest themselves. Hines & Wolf and Faith et al. described oscillations in the form of growing and shrinking boundary layers, a function of the fluids viscosity. Herrings description was more one-dimensional; periodic heating and cooling of the fuel was said to cause changes in its density, thereby forcing the fluid in and out of the heated tube with longitudinal waves. While these theories seem to differ in their description of thermoacoustic waves, it is plausible they are both correct. Thurston [14] characterized five distinct categories of oscillations, including acoustic-scale and bulk-mode oscillations discussed in this report. The above hypotheses may describe different categories of oscillation. However, no physical experiment or numerical simulation has yet corroborated any of these proposed mechanisms.

1.2.5 Other causes of oscillations

Drivers besides thermoacoustic effects can cause oscillations in heat exchangers. Although outside the scope of the present study, oscillations may be generated inside a tube from turbulence or vortex shedding in crossflow. Blevins and Bressler [15], [16] flowed air through a duct over an array of tubes instrumented with microphones to measure acoustic oscillations and pressure transducers to measure oscillations caused by turbulence. For low freestream air speeds, oscillations were detected due to vortex shedding. The frequency of these oscillations could be predicted with the Strouhal relationship; a Strouhal number of 0.22 was typical. Eisinger and Sullivan [17] studied various tube bundle geometries and flow conditions, and encountered several oscilla-

tion modes. These oscillations did not perfectly match those expected from vortex shedding or turbulence, but it was suggested that oscillations from each of these sources would interact, creating what was termed fluid-acoustic instabilities. Eisinger and Sullivan attempted to use several preexisting criteria to predict oscillations, but none of these criteria could predict oscillations with certainty. They were able to suppress oscillations by several means: adding baffles and turning vanes inside the ducting, and installing barriers inside the duct to increase acoustic damping.

2. FACILITY DESCRIPTION

2.1 Design objectives and options

The present study requires a test article capable of generating conditions conducive to supercritical fuel oscillations. Previous works have considered oscillations in a single tube. This experiment considers four parallel tubes connected to common inlet and outlet manifolds to more accurately simulate the flow paths of a fuel-air heat exchanger. Non-uniform heating has been hypothesized to create oscillations as flow is diverted from tubes with higher heating toward tubes with lower heating.

The test apparatus must provide a means for controlling and measuring the following independent variables: fuel pressure, fuel mass flow rate, fuel inlet temperature, and fuel temperature at the outlet of each of the four tubes. The manifold cross passage diameter has also been chosen as an independent variable, so manifolds are required to be interchangeable. The ability to use an infrared camera to measure the wall temperature of each tube is also desired. With these requirements under consideration, four design options were proposed for heating fuel to its critical temperature:

- Option 1: Cartridge heating of tubes placed in copper block
- Option 2: Inductive heating of tubes
- Option 3: Resistive heating of tubes
- Option 4: Air-heated tubes

2.1.1 Design option 1: cartridge heating of tubes placed in copper block

One proposed design would use nine 800W cartridge heaters installed inside a copper block with four fuel flow paths drilled into it. Cartridge heaters could be

controlled individually to create differential heating between each flow path. This design is illustrated in Figure 2.1. The main advantage of this design was that it posed the fewest safety hazards of the four designs. However, a copper block of the required size would have a large thermal mass, making the changing of test conditions very slow. Flow paths would require large spacing because of the positioning of cartridge heaters. Such a large spacing does not accurately model the geometry of actual fuel-air heat exchangers. This design option would also preclude the use of an infrared camera to obtain a temperature distribution over the flow path.

2.1.2 Design option 2: inductive heating of tubes

Another proposed design involved inductive heating of tubes. To achieve this, an oval-shaped coil would be wrapped around four tubes. Mutual inductance between the coil and the tubes would cause the tubes to be heated if a current were placed through the coil. Heat input to individual tubes could be adjusted by moving the coil with respect to the tube bundle, or by applying flux intensifiers to individual tubes. This option allowed for the use of an infrared camera to measure tube wall temperatures, and great flexibility for tube spacing. Responsiveness for inductive heating was expected to be better than that for cartridge heating because the thermal mass is much smaller for the inductive heating option. However, the feasibility of this option was unknown, as few experiments have been performed with such a device. Instrumentation noise due to electromagnetic fields was deemed worrisome.

2.1.3 Design option 3: resistive heating

The third option considered uses a voltage source to generate a current across fuel tubes, causing Joule heating. Such a design is extremely controllable; a rheostat for each tube could be used to directly control heat input. Tube spacing is also flexible in this design. Moreover, most previous supercritical fuel experiments heated fuel via resistive tube heating, so the design is known to be capable of heating fuel to the

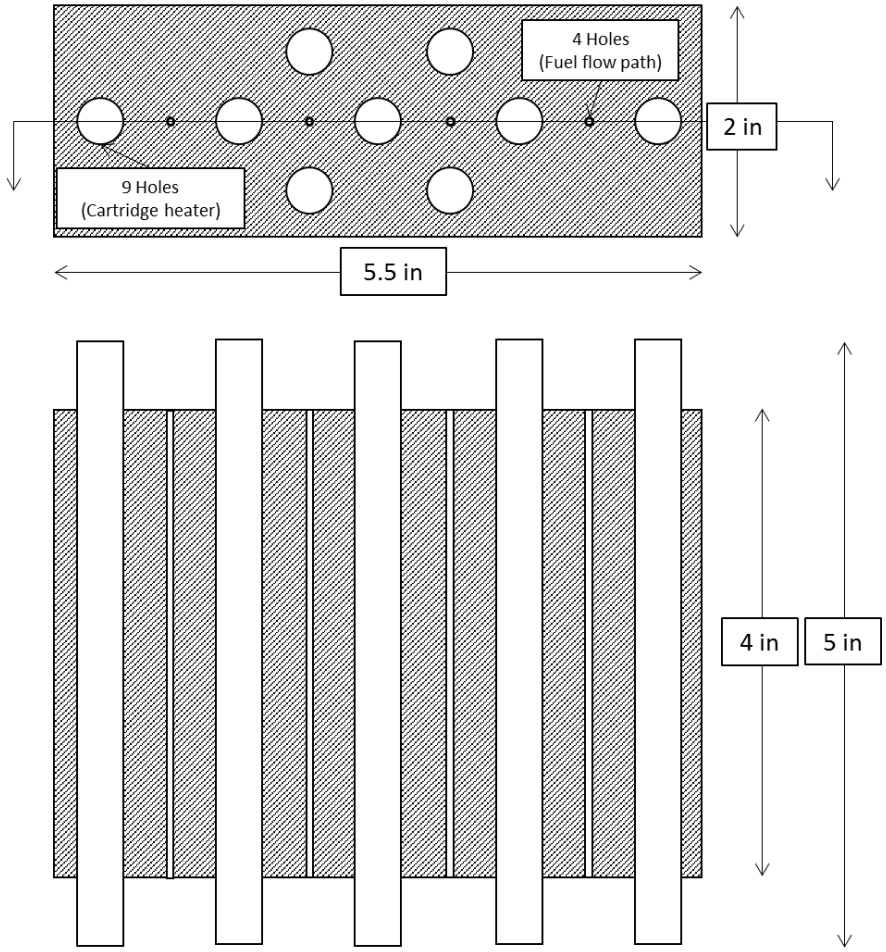

Figure 2.1. Drawing of design option 1 - cartridge heating

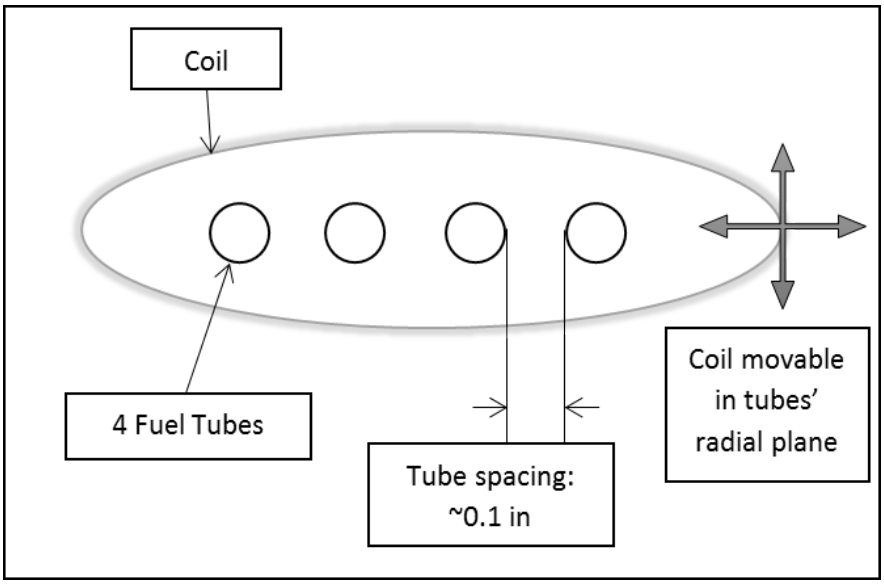

Figure 2.2. Drawing of design option 2 - inductive heating

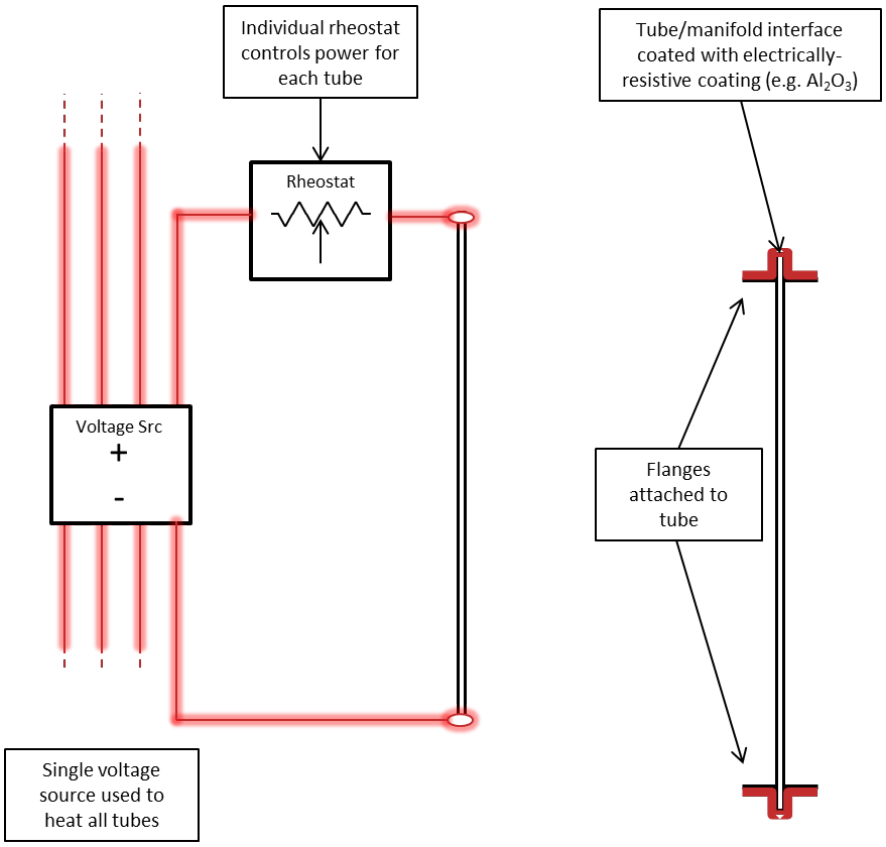

Figure 2.3. Drawing of design option 3 - resistive heating

desired conditions. However, for individual tubes to be given differential heating, all four tubes must be electrically insulated from one another. Sealing an electrically-insulated interface between tubes and manifolds requires relatively complicated manufacturing processes. The large potential for hot leaks at the tube ends make this the most hazardous design option considered. This design option is illustrated in Figure 2.3.

2.1.4 Design option 4: air heating

The fourth design option involved flowing heated air across the fuel tubes. Hot air used to heat each fuel tube would flow through separate channels with adjustable louvers that would control how much air would flow through each channel. This design option is illustrated in Figure 2.4. The air heating option offered many advantages over the other options. The lack of current through the tubes and electric fields around the tubes minimizes the risk of instrumentation interference. Metal-to-metal contact between tubes and manifolds is permissible with air heating. Such a design could be made optically accessible, so an infrared camera could be used to measure tube wall temperatures. Air heating also heats tubes in a manner most-similar to actual fuel-air heat exchangers, as the windward side of the tube will be receive more heat flux than the leeward side. Unfortunately, the amount of heat transfer to each tube is difficult to quantify with air heating. The extra working fluid also adds complexity to the design and operation of the test article.

For the reasons noted above, Design option 4 was selected as the best option. Nitrogen was selected as the working fluid rather than air because it could help suppress a fire in the event of a fuel tube leak. The following sections provide a detailed description of the resulting facility and instrumentation suite.

2.2 Facility overview

2.2.1 Flow paths

Experiments in the initial test campaign were performed in the High Pressure Laboratory Gas Turbine Cell at Purdue University's Zucrow Laboratories. A schematic of the fuel flow path is shown in Figure 2.5.

Jet-A fuel was stored in a tank and delivered to the test article using an electric fuel pump. The pump and tank are shown in Figure 2.6. The fuel's dissolved oxygen content was measured with a Mettler-Toledo Inpro 6850 oxygen sensor. The dissolved

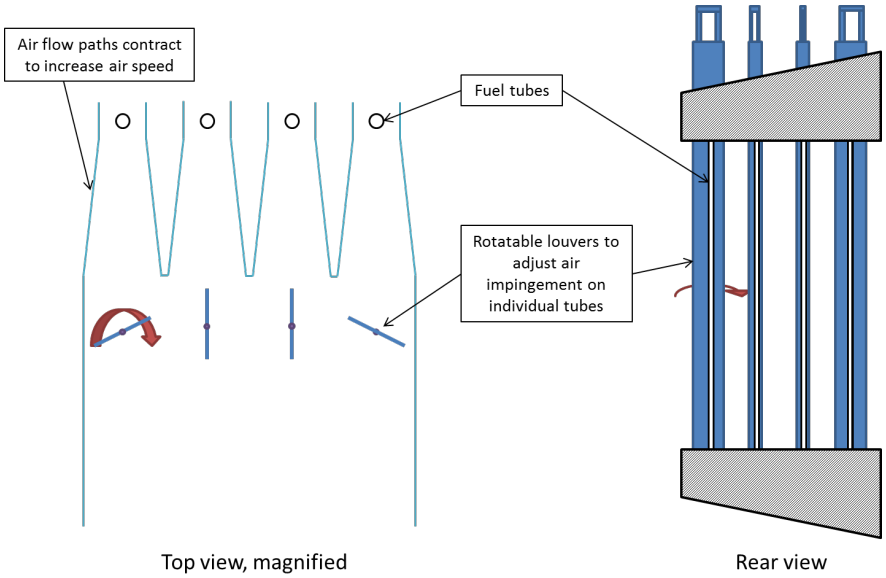

Figure 2.4. Drawing of design option 4 - air heating

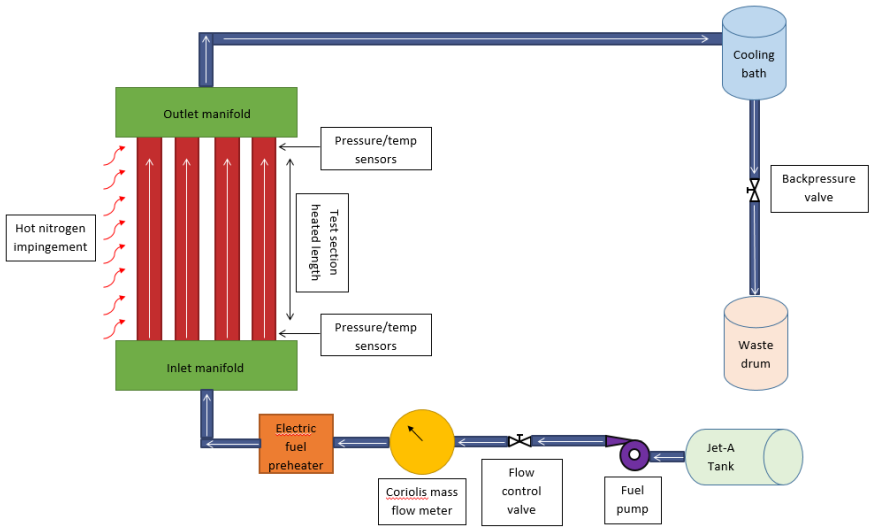

Figure 2.5. Fuel flow path schematic

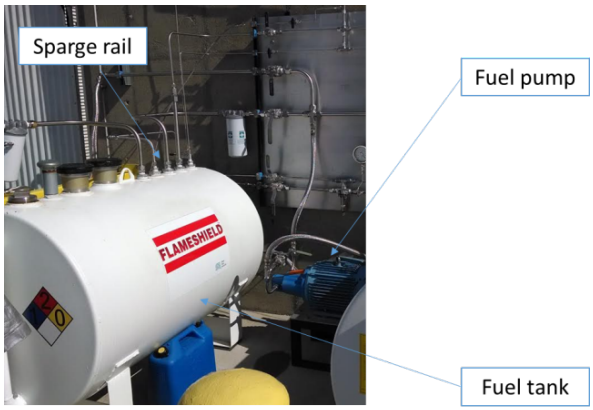

Figure 2.6. Fuel tank and pump

oxygen content was reduced to below one percent of saturation by sparging it in its tank with nitrogen before all tests. A nitrogen blanket purge prevented oxygen buildup in the tank during testing.

Fuel flow rate was measured with a Coriolis flow meter (MicroMotion CMFS015M232N2BAEC downstream of the oxygen sensor and upstream of the fuel preheater. A computer-actuated control valve upstream of the preheater controlled the fuel flow rate. The fuel flow path upstream of the preheater, including an isolation valve, mass flow meter and control valve, is shown in Figure 2.7.

The fuel preheater consists of 30 Watlow FIREROD cartridge heaters and eight 1/8-in diameter fuel tubes sandwiched between copper blocks. Figure 2.8 is a model of a copper block used in the preheater. Figure 2.9 is a photo of the preheater as installed in the laboratory. Two Omega CN616 controllers controlled the cartridge heaters to maintain a desired preheater block temperature. Fuel enters and exits the preheater through two inlet and outlet manifolds. This preheater has been described further by Wiest.

The test section fuel tubes had an outer diameter of 1/8 in, inner diameter of 0.069 in, and length of 7.5 in. They were brazed to the manifolds in a parallel and

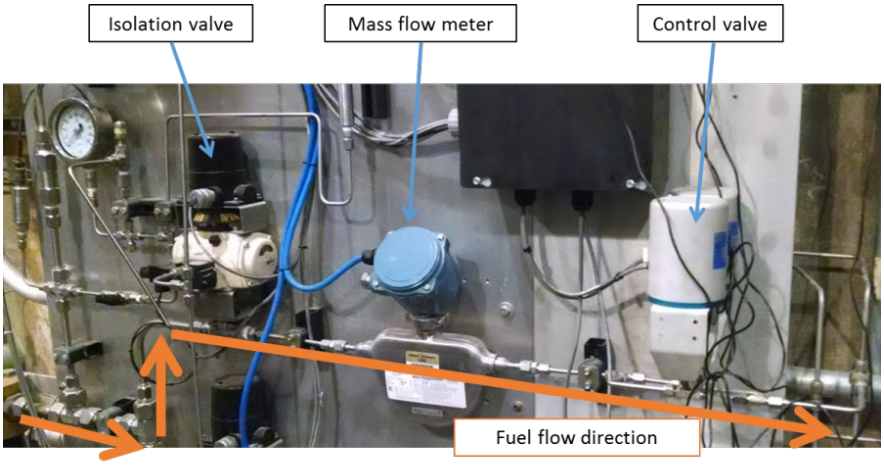

Figure 2.7. Fuel flow path upstream of preheater

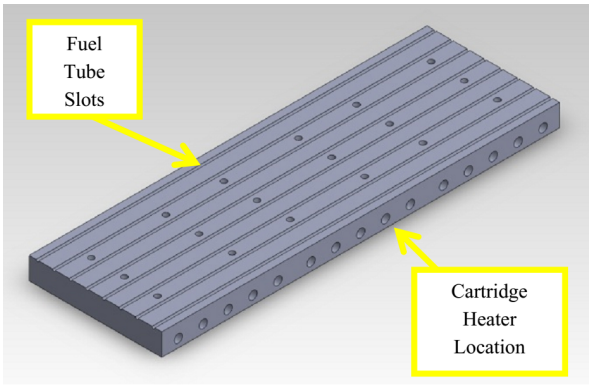

Figure 2.8. Drawing of copper block used in fuel preheater, courtesy of Wiest

Figure 2.9. Fuel preheater photo

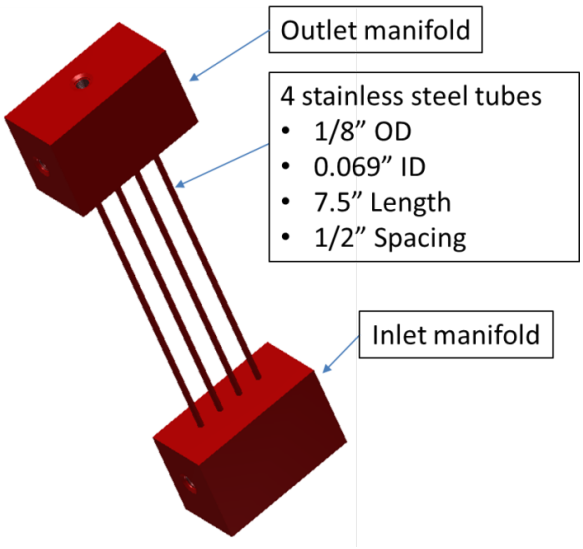

Figure 2.10. Manifold and tube assembly

coplanar orientation, with center-to-center spacing of 1/2 in. Manifolds and fuel tubes were made of SS304 stainless steel. The manifolds used in the current study had cross-passage diameters of 1/8 in and 1/4 in. Manifolds were also fabricated with cross-passage diameters of 3/16 in, and may be used in future experiments. The tube-manifold assembly is shown in Figure 2.10 and a cut-away view of a fuel manifold is shown in Figure 2.11.

Fuel exiting the outlet manifold was cooled in a cooling bath, which consisted of a coiled fuel tube submerged in a drum of water. The cooled fuel flowed through a Swagelok SS-SS4 metering valve, which controlled the backpressure for the test article. The flow coefficient of this valve is adjustable between 10-4 and 410-3. The valve was controlled with a Hanbay MCL-050AF-1-SS4MG actuator. Fuel exited this valve into a waste drum.

Fuel was heated in the test article by flowing hot nitrogen over the fuel tubes. A schematic of the hot nitrogen flow path is provided in Figure 2.12. Nitrogen was heated with an electrical heater, capable of heating 0.1 lb/hour of nitrogen to 1200F.

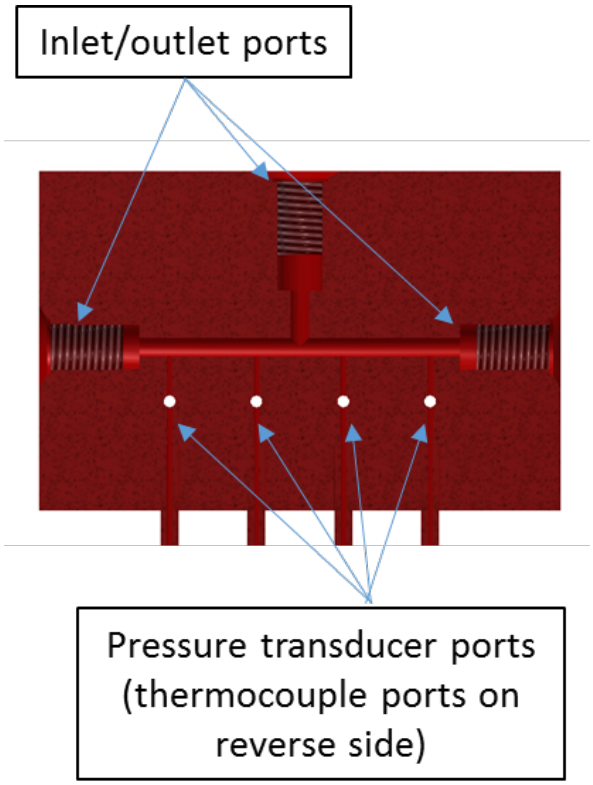

Figure 2.11. Cut-away view of fuel manifold

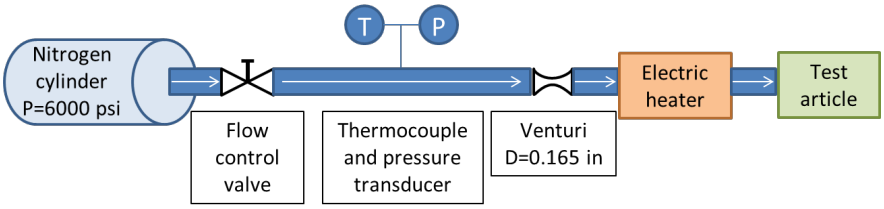

Figure 2.12. Nitrogen flow path schematic

The nitrogen flow rate was calculated using pressure and temperature measurements upstream of a choked venturi. Each tube received heated nitrogen from a separate channel of rectangular cross-section; nitrogen flow through individual channels was adjusted with servo-actuated louvers upstream of the fuel tubes.

Upstream of the flow control louvers, a perforated plate equalized flow through the four channels. Five layers of mesh with 1/16 inch diameter openings were placed immediately downstream to break up jets created by the perforated plate. These layers of mesh were held into place by the perforated plate and a reinforcement plate, both of which were welded into the nitrogen flow path. The flow conditioning layers are illustrated in Figure 2.13.

Nitrogen channels were cut into a SS304 block using wire EDM (electrical discharge machining). The nitrogen channel width contracted from 7/8 in to 3/8 in to increase the flow speed over the fuel tubes, thereby increasing heat transfer between nitrogen and fuel. The nitrogen and fuel flow paths are shown together in Figure 2.14. A flow control louver is shown in Figure 2.15. A cut-away view of the nitrogen flow path is shown in Figure 2.16.

Figure 2.17 and figure 2.18 are labeled photos of the test article as installed in the laboratory. Thermafiber FRF insulation was placed over the hot nitrogen flow path to minimize heat loss to the surroundings. This insulation was secured with aluminum tape. Hot nitrogen, after flowing across the fuel tubes, exhausted directly to the test cell.

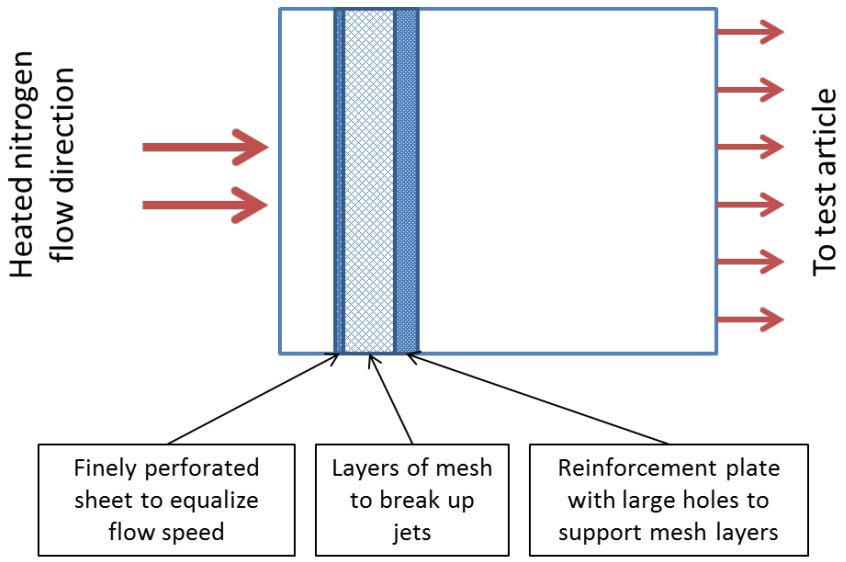

Figure 2.13. Nitrogen flow conditioning illustration

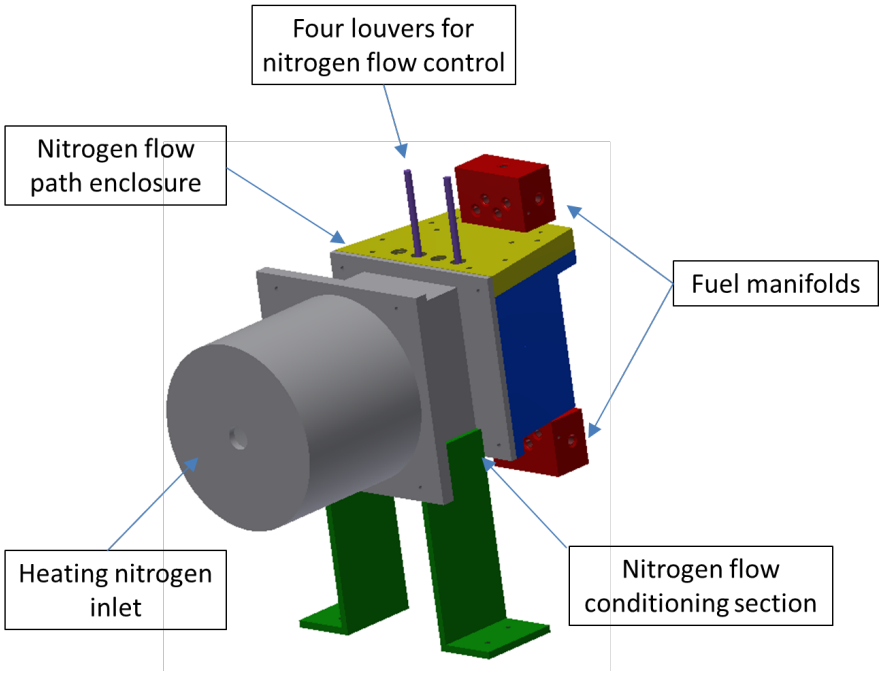

Figure 2.14. Test article overall view

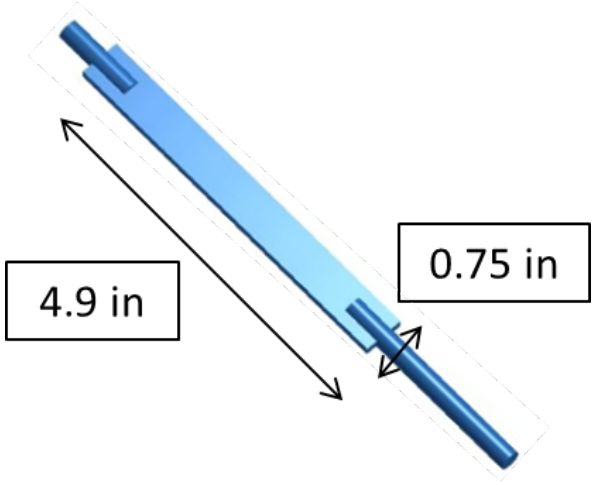

Figure 2.15. Flow control louver

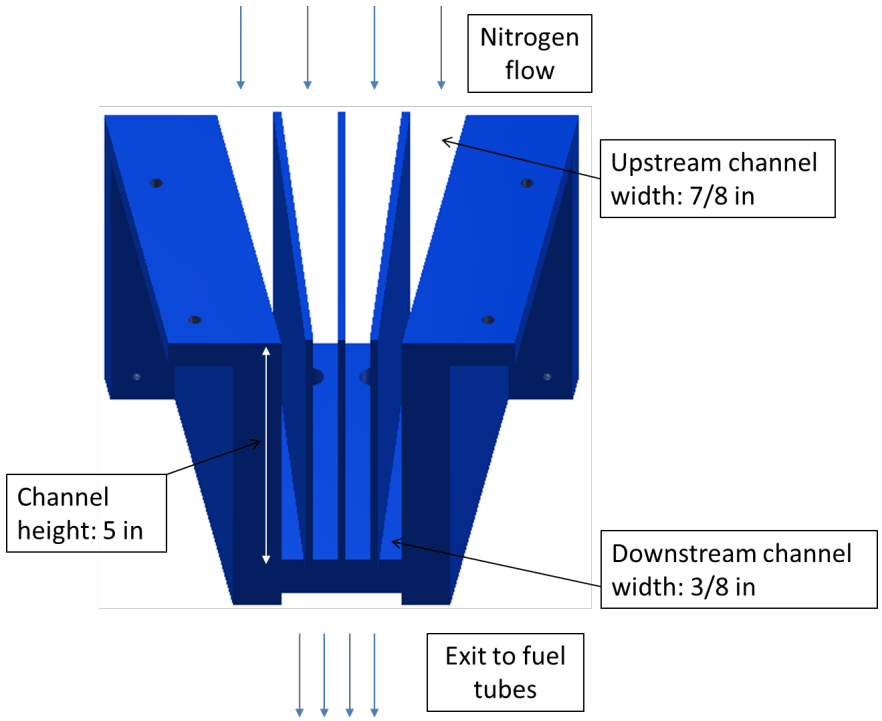

Figure 2.16. Nitrogen flow path cut-away view

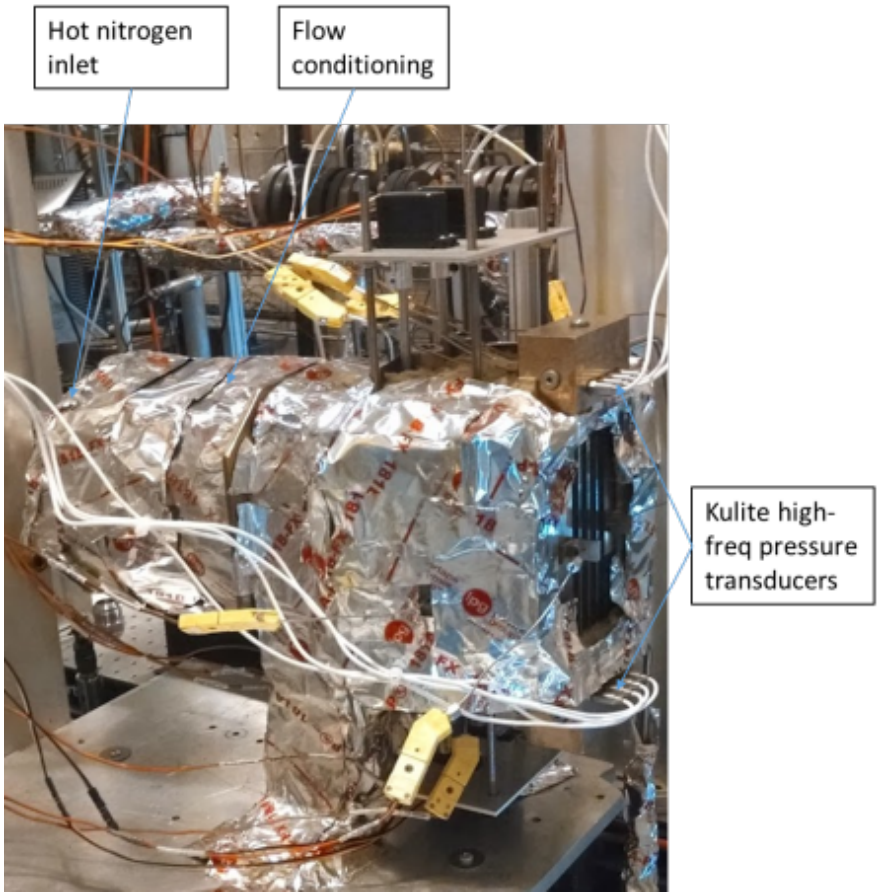

Figure 2.17. Test article - side view

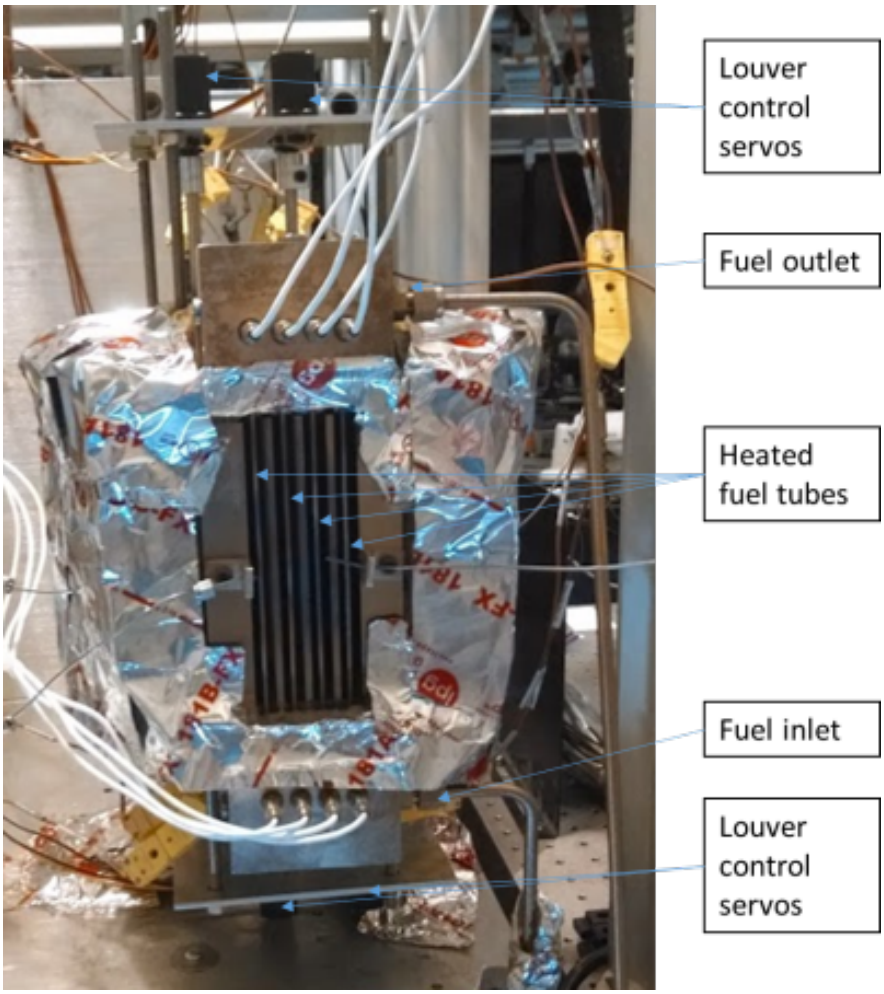

Figure 2.18. Test article - rear view

Figure 2.19. Micro Maestro 1350 USB servo controller, courtesy of Pololu

2.2.2 Instrumentation and uncertainty analysis

Oscillations were measured with fuel pressure transducers (Kulite ETL-GTS-190) and type-K thermocouples (Omega GKMQSS-062U-6) installed inside inlet and outlet manifolds one upstream and downstream of each fuel tube. Fuel mass flow rate was measured with a Coriolis flow meter (MicroMotion CMFS015M232N2BAECZZ), located upstream of the fuel preheater.

Each nitrogen flow control louver was actuated with its own Hitec HS-485HB servo motor. All four servos were controlled by a computer via a Pololu Micro Maestro 1350 USB servo controller, shown in Figure 2.19. All valves were controlled with an interface developed in LabVIEW 2007, shown in Figure 2.20. This software also recorded pressures, temperatures and flow rates obtained from nearly all of the sensors used in the experiment. Fuel manifold pressures were recorded through a separate acquisition system (DSPCon DataFlex-1000A).

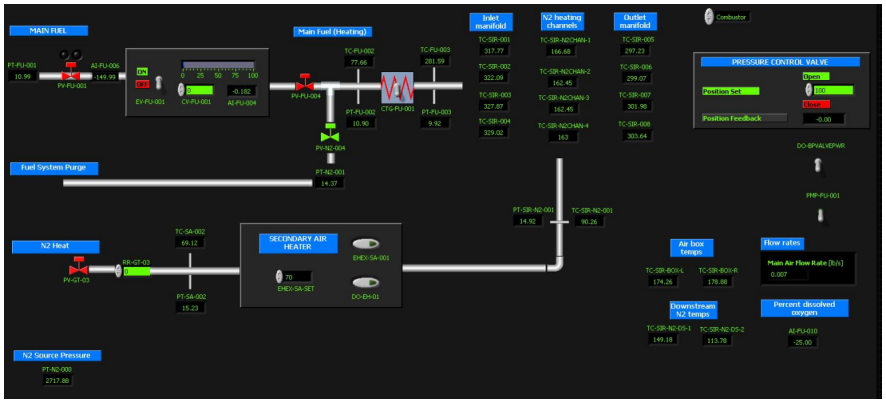

Figure 2.20. Screenshot of LabVIEW data acquisition and control program

Table 2.1. Bias errors for sensing equipment

Device	Bias error
Fuel manifold pressure transducers	+/- 60 psi
Nitrogen-side pressure transducer	+/- 30 psi
All thermocouples	+/- 8.7F
Fuel flow meter	+/- 0.04 lb/hr
Tube diameter	0.006 in
Fuel properties	+/- 15%

2.2.3 Uncertainty analysis

The uncertainty for several outputs was calculated with consideration to bias errors present in the hardware used. Because outputs were sampled many times for each recording, precision error was assumed negligible, and was ignored for the uncertainty analysis. The bias errors for relevant dimensions and sensors used in the experiments were calculated and are presented in Table 2.1.

The uncertainty of a calculated value Y, which is calculated using independent measurements Xi containing uncertainties Pi, is calculated by the following equation provided by Mills [18].

$$P_Y = \sqrt{\sum_{i=1}^{n} (\frac{\partial Y}{\partial X_i} P_i)^2} \tag{2.1}$$

The uncertainty of heat transfer was calculated with the following formula:

$$P_{\dot{Q}} = \sqrt{(\frac{\partial \dot{Q}}{\partial \dot{m}} P_{\dot{m}})^2 + (\frac{\partial \dot{Q}}{\partial c_p} P_{c_p})^2 + (\frac{\partial \dot{Q}}{\partial T_1} P_{T_1})^2 + (\frac{\partial \dot{Q}}{\partial T_2} P_{T_2})^2} \tag{2.2}$$

Substituting for heat transfer partial derivatives:

$$P_{\dot{Q}} = \sqrt{[c_p(T_2 - T_1)P_{\dot{m}}]^2 + (\dot{m}(T_2 - T_1)P_{c_p})^2 + (-\dot{m}c_p P_{T_1})^2 + (\dot{m}c_p P_{T_2})^2} \tag{2.3}$$

For the worst-case scenario, the heat transfer uncertainty was calculated to be 33.2W (113.2 BTU/hr), which was 15.8% the total heat transfer. This case (ID 20140524_0359509) was determined the worst-case scenario because of its relatively large temperature gradient (244F) which dominated over other terms in the calculation.

3. RESULTS OF FIRST TEST CAMPAIGN

Tests were performed under nominal conditions of 360-700 psi fuel inlet pressure and mass flow rate of 1.75-9.25 lb/hr per tube. Fuel manifold assemblies having cross-passage diameters of 1/8 in and 1/4 in were used. Fuel preheating and nitrogen flow control louver settings were varied between test cases. Hot nitrogen was either blown on all tubes (when all channels were wide-open), or a single tube (when only one channel was wide-open). Individual tube heating was investigated to determine whether an oscillation beginning in one heated tube could cause oscillations to occur in neighboring unheated tubes. Table 3.1 outlines variables that were varied for each test case. A detailed test matrix is provided in the appendix. A total of 108 cases were run, excluding cold-flow tests.

Table 3.1. Outline of test parameters

Manifold cross-passage diameter	1/8, 1/4 in
Inlet temperature	200, 300, 400, 500, 600, 700F
Fuel pressure	360, 400, 500, 600, 700 psi
Fuel mass flow rate (4 tubes combined)	7 - 37 lb/hr
Tube heating condition	All tubes heated, one tube heated

Nitrogen was typically heated to the maximum temperature the heater was capable of, flowing at around 0.3 lb/s. The nitrogen temperature inside the test article varied from case to case because of heat loss inside tubing, and was recorded for every test condition. The fuel flow configuration is described in Figure 3.1. Only inlet and outlet ports adjacent to Tube 4 were used. Pressure measurements were taken at the

Table 3.2. Ranges of flow properties

Nitrogen speed	200 - 800 ft/s
Fuel flow speed	0.45 - 3.12 ft/s
Fuel Reynolds number (Re_D)	900 - 8700
Fuel reduced temperature (outlet)	0.27 - 0.94
Fuel reduced pressure	1.05 - 2.06
Fuel temperature change along tube length	0 - 180F
Fuel density change along tube length	0 - 4.4 lb/ft^3

inlets and outlets of tubes 1-3. Pressure measurements for Tube 4 were unavailable due to malfunctioning transducers in both manifolds.

A preliminary acoustic analysis was performed to predict frequencies for three oscillatory modes: the fundamental acoustic resonant frequency for the tube, the frequency for bulk-mode oscillations, and the frequency related to nitrogen vortex shedding off fuel tubes. The fundamental acoustic frequency for a tube is given by the equation:

$$f_{acoustic} = \frac{a}{2L} \tag{3.1}$$

Here, a is the speed of sound of the fluid in the tube, and L is the length of the tube. The bulk-mode frequency was predicted based on the residence time of the fuel inside the tube.

$$f_{bulk} = \frac{1}{t_{residence}} \tag{3.2}$$

The frequency of oscillations caused by nitrogen vortex shedding off of fuel tubes is predicted based on the Strouhal number for the nitrogen flow. Typically, vortex shedding off of a cylinder corresponds to a Strouhal number of 0.2. The Strouhal number based on tube outer diameter is defined by the following equation:

$$St_D = \frac{f_{vs} D}{v_{gas}} \tag{3.3}$$

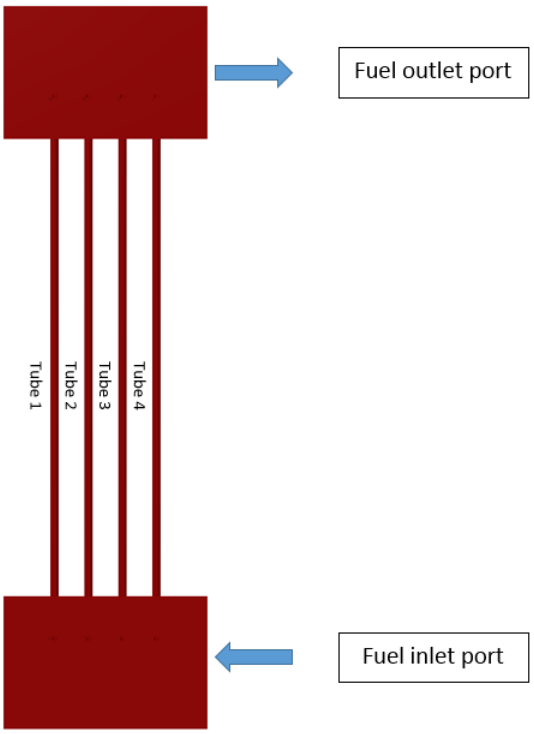

Figure 3.1. Fuel flow configuration used for all tests

Table 3.3. Preliminary acoustic analysis inputs and predicted frequencies

Fundamental Acoustic Frequency	
Speed of sound in fuel	1,437 ft/s
Tube length	7.5 in
Longitudinal acoustic mode	1,150 Hz
Bulk Mode Frequency	
Fuel flow speed	0.45 - 3.12 ft/s
Fuel residence time in tubes	0.20 - 1.39 s
Bulk mode frequency	1.08 - 7.44 Hz
Fuel residence time in manifolds	1.7 - 49.3 s
Vortex Shedding Frequency	
Assumed Strouhal number for vortex shedding	0.2
Fuel tube outer diameter	1/8 in
Nitrogen freestream speed over tube	200 - 800 ft/s
Vortex shedding frequency	3.8 - 15.4 kHz

where f_{vs} is the frequency of vortex shedding, D is the outer diameter of the cylinder in cross flow (or the fuel tube outer diameter), and v_{gas} is the freestream speed of nitrogen over the tube.

Table 3.3 outlines inputs and results for these preliminary analyses.

Two distinct modes of oscillations were encountered during testing. Bulk-mode oscillations are characterized by relatively high amplitudes (above 2 psi) and low frequencies (under 3 Hz). Acoustic-mode oscillations occurred with lower amplitudes (under 1 psi) and higher frequencies (300-350 Hz). Many test cases exhibited both oscillation modes superposed atop one another.

A low-pass filter with 1 kHz cutoff frequency was used to reduce instrumentation noise for manifold pressure traces intended to show bulk-mode oscillations. The transducers produced noise signals with amplitudes of 0.6 psi. A band-pass filter allowing frequency content from 100-500 Hz was applied to pressure traces intended to show acoustic-mode oscillations. A complete list of test cases performed is provided in the appendix. Trends proposed in this report reflect the results of every test case run; however, pressure traces are only provided for select test cases.

3.1 Bulk-mode oscillations

Table 3.4 describes conditions for cases examined in this document for bulk-mode oscillations.

Figure 3.2 shows measured manifold pressures for Case 1b (T_{inlet}=166.7degF, p=404.2 psi). The temperature remained far below the critical temperature in this case, and no significant oscillations occurred within the test section. Figure 3.3 shows fuel and nitrogen temperature traces for Case 1b.

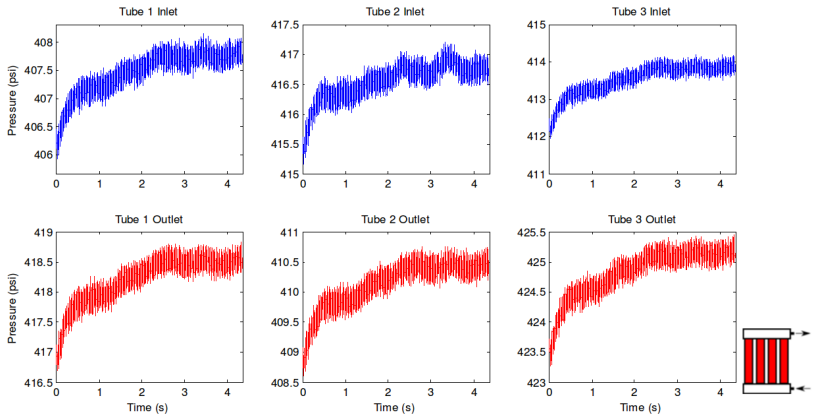

Figure 3.2. Case 1b manifold pressure traces (T_{inlet}=166.7degF, p=404.2 psi, all channels open)

Table 3.4. Conditions for select cases involving bulk-mode oscillations

Case num	Inlet fuel temp (F)	Fuel pressure (psi)	Fuel flow rate (lb/hr)	Re_D	Heating setting	File ID
1b	166.7	404.2	21.1	1,118	All open	20140524_0359509
2b	372.2	378.7	22.5	2,384	All open	20140524_0425131
3b	465.1	388.7	22.5	3,198	All open	20140524_0436466
4b	594.1	479.7	20.2	4,533	All open	20140531_0149370
5b	624.4	515.3	20.6	4,432	No N2 flow	20140716_2204064

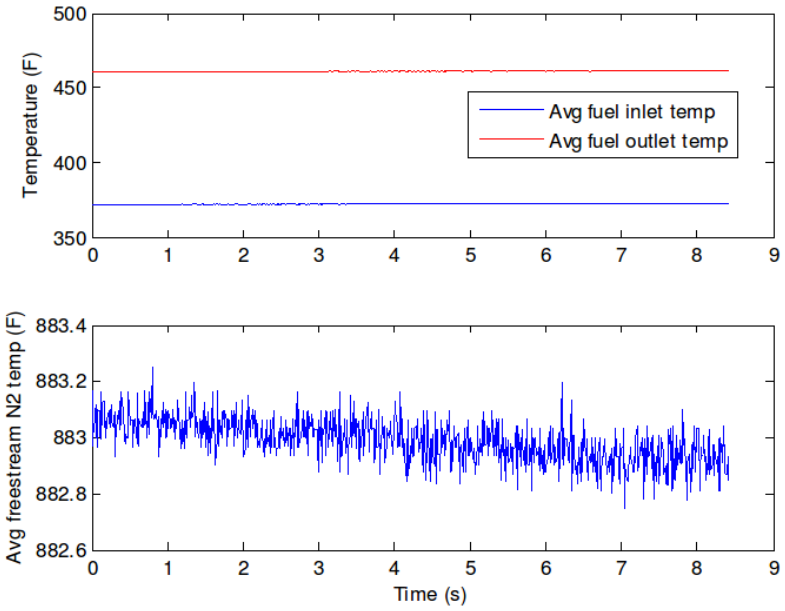

Figure 3.3. Case 1b temperature traces (T_{inlet}=166.7degF, p=404.2 psi, all channels open)

Figure 3.4 shows pressure oscillations for Case 2b (T_{inlet}=400°F, p=400 psi). Oscillations with amplitudes of 1-2 psi were measured in the center tubes (2 and 3). Lower-amplitude oscillations were encountered in the end tube (Tube 1), which carried the coldest fuel. Fuel in Tube 1 was coldest because of heat loss through the outside nitrogen channel wall and the longer residence time for fuel in the uninsulated inlet manifold.

Figure 3.5 shows pressure oscillations for Case 3b (T_{inlet}=500degF, p=400 psi). Oscillations of over 2 psi were encountered in this case. Smaller oscillations were once again observed in the coolest channel.

Figure 3.6 shows pressure oscillations for Case 4b (T_{inlet}=600degF, p=500 psi). The largest oscillations had amplitudes of 6 psi, and occurred in Tube 2.

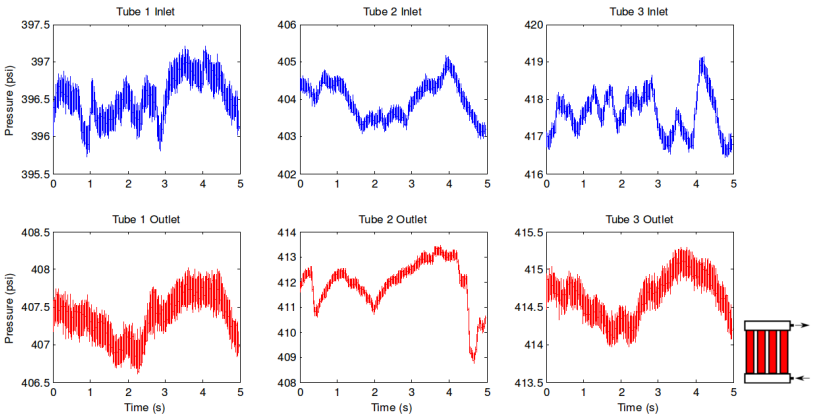

Figure 3.4. Case 2b manifold pressure traces (T_{inlet}=372.2degF, p=378.7 psi, all channels open)

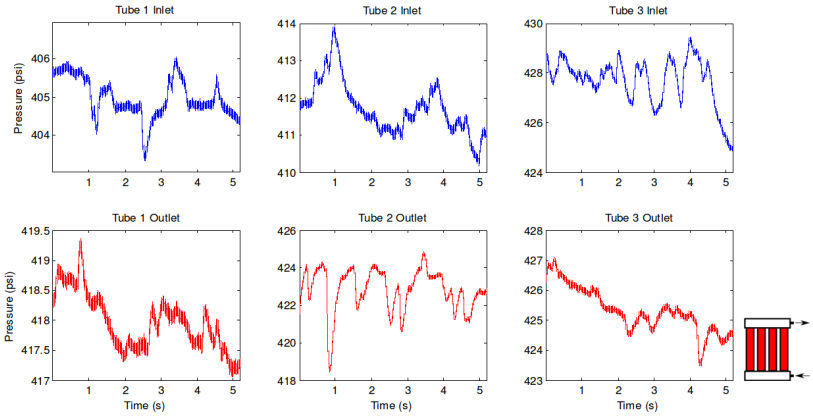

Figure 3.5. Case 3b manifold pressure traces (T_{inlet}=500degF, p=400 psi, all channels open)

Figure 3.7 is an autocorrelation plot for the six pressure signals in Case 4b, generated by the xcorr function in MATLAB [19]. The lack of any nonzero-lag peaks in all

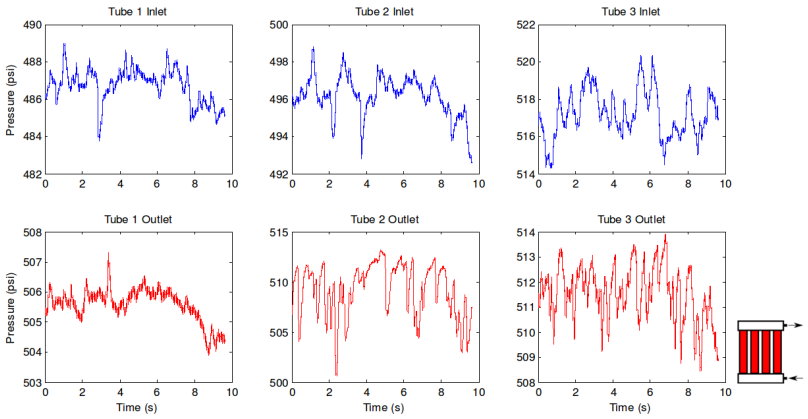

Figure 3.6. Case 4b pressure traces (T_{inlet}=600degF, p=500 psi, all channels open)

signals signifies that these bulk-mode oscillations are random, rather than periodic, in nature. No discrete frequencies were found for any cases.

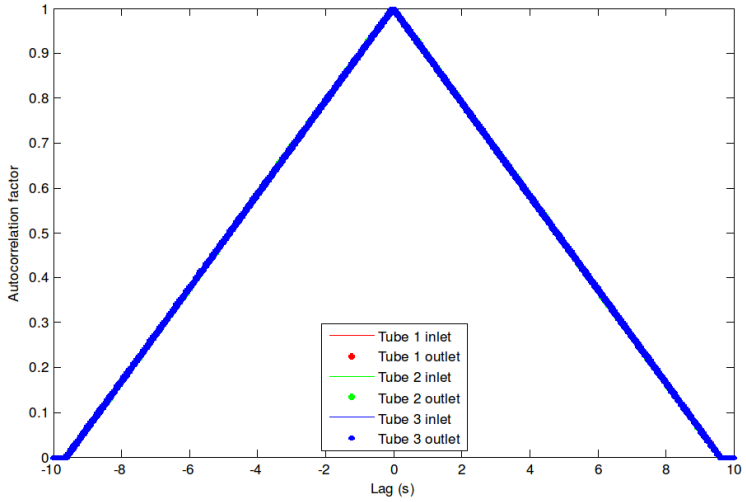

Figure 3.7. Case 4b pressure autocorrelation

Bulk-mode oscillation amplitude was directly correlated with fluid temperature over the range studied. Figure 3.8 compares the largest oscillation amplitudes observed for each inlet temperature.

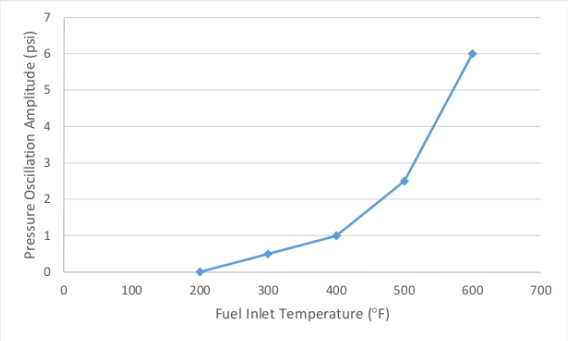

Figure 3.8. Comparison of pressure oscillation amplitude vs. fuel inlet temperature

All of the data reported for bulk-mode oscillations came from tests involving the manifold with a 1/8 in diameter cross passage. Test data with the 1/4 in manifold passage diameter were also examined, and indicate that the cross passage diameter does not significantly affect the character of bulk-mode oscillations. The parameters of fuel pressure, fuel mass flow rate, and differential heating were also found to have no clear or consistent effect on the character of bulk-mode oscillations. Two sets of cases are presented below where fuel mass flow rate is varied, and other parameters are intended to be held constant. Figure 3.9 compares oscillation amplitudes vs. fuel mass flow rate for several cases with the small manifold passage, inlet temperature of 500degF and fuel pressure of 500 psi. Figure 3.10 compares oscillation amplitudes vs. fuel mass flow rate for several cases with the large manifold passage, inlet temperature of 600degF and fuel pressure of 400 psi.

Although Figure 3.10 displays a linear correlation between flow rate and pressure amplitude, this correlation does not hold for the cases in Figure 3.9, or several other

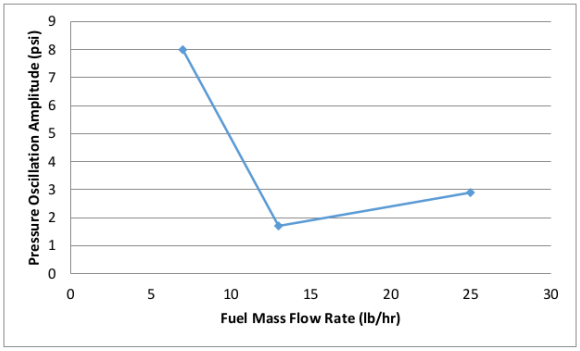

Figure 3.9. Bulk mode oscillation amplitude vs fuel mass flow rate for T=500degF, p=500 psi

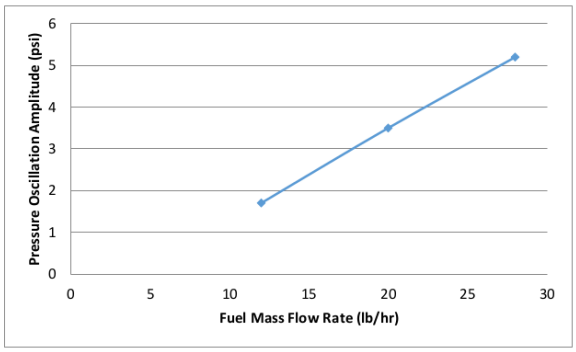

Figure 3.10. Bulk mode oscillation amplitude vs fuel mass flow rate for T=600degF, p=400 psi

cases in the test campaign where mass flow rate was investigated as a parameter. Bulk-mode oscillations may originate inside the test article, the preheater, or both. For some test cases with high inlet temperatures and low flow rates, the preheater flow path is the hottest surface the fuel contacts. Case 5b was run with fuel heated exclusively by the electric preheater; fuel flowed through the test section tubes in this case, but no heated nitrogen flowed over the tubes. Bulk-mode oscillations are

present for this case, and have amplitudes and frequencies close to those found with test-section heating.

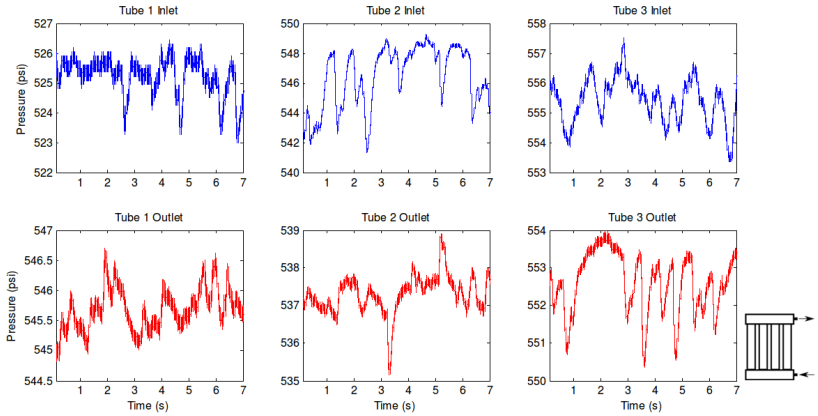

Figure 3.11. Case 5b pressure traces (T_{inlet}=500degF, p=500 psi, no nitrogen flow)

3.2 Acoustic-mode oscillations

Oscillations with frequencies between 300-350 Hz occurred in many test cases. The acoustic frequencies detected are far from those predicted for open tube resonance. Moreover, these frequencies cannot be predicted by scaling data from previous studies based on tube length. The 7.5-inch long tubes used in the present study were shorter than most of those used in previous studies, yet the frequencies were an order of magnitude lower than those found by Hines & Wolf [6], Faith et al. [10], and Linne et al. [7]. A basic tube resonance calculation would predict the opposite trend. The excited acoustic modes were therefore most likely characteristic of several tubes rather than a single tube. Table 3.5 describes conditions for cases examined in this document for acoustic-mode oscillations.

Table 3.5. Conditions for select cases involving acoustic-mode oscillations

1/4 in manifold cross passage cases					
Case num	Inlet Fuel Temp (F)	Fuel Pressure (psi)	Fuel flow rate (lb/hr)	Heating Setting	File ID
1a	592.2	551.4	38.6	Chan 1 open	20141028_1300083
2a	635.6	364.3	32.0	Chan 2 open	20141028_1340278
3a	614.3	600.4	36.5	Chan 1 open	20141028_1313025
4a	609.2	600.4	36.5	Chan 2 open	20141028_1314343
1/8 in manifold cross passage cases					
5a	598.4	605.5	20.4	Chan 1 open	20140621_0036317
6a	598.0	606.3	20.3	Chan 2 open	20140621_0038590
7a	305.8	484.5	19.9	Chan 2 open	20140531_0121427

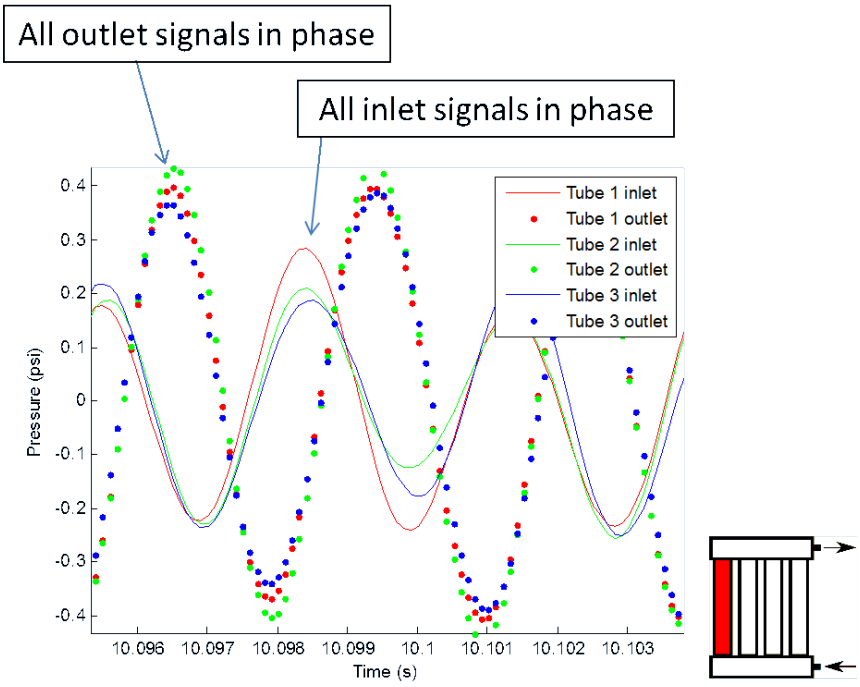

Figure 3.12. Case 1a pressure trace

Fuel manifold pressure traces and power spectral density plots for Case 1a are shown in Figures 3.12 and 3.13.

The spikes in the power spectral density (PSD) plot for Case 1a indicate frequency content between 338-342 Hz in all tubes. These oscillations showed coupling: all inlet pressure signals remained in phase with each other, and all outlet signals remained in phase with each other.

Figure 3.14 is an autocorrelation plot for the six pressure signals for Case 1a. The signals have autocorrelation factors ranging from 0.72 to 0.80, all peaking at 2.9ms intervals.

Figure 3.15 is a cross-correlation plot between each of the tubes inlet and outlet pressure signals, calculated with the xcorr [19] function in MATLAB. The x-position of each peak denotes the time lag between inlet and outlet signals. Average phase lag,

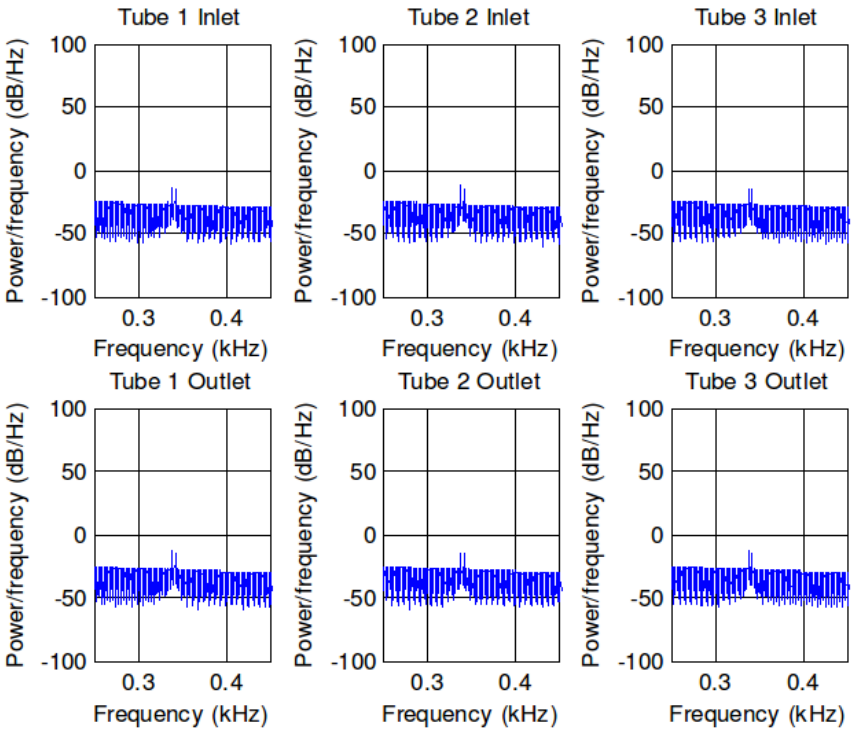

Figure 3.13. Case 1a power spectral density plot

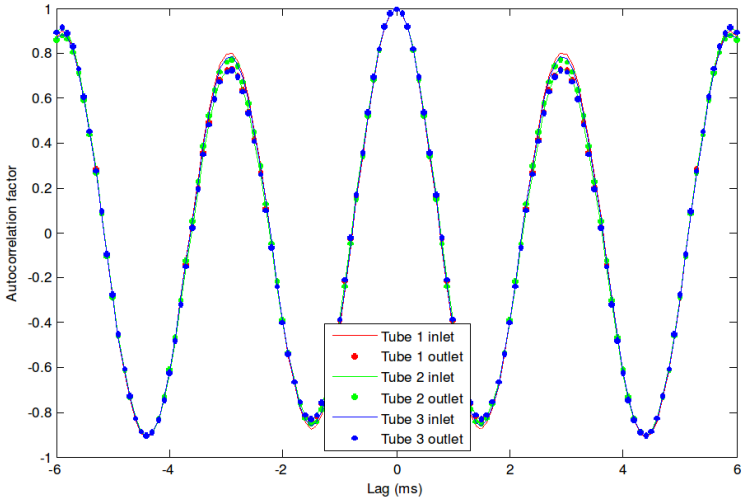

Figure 3.14. Case 1a pressure autocorrelation plot

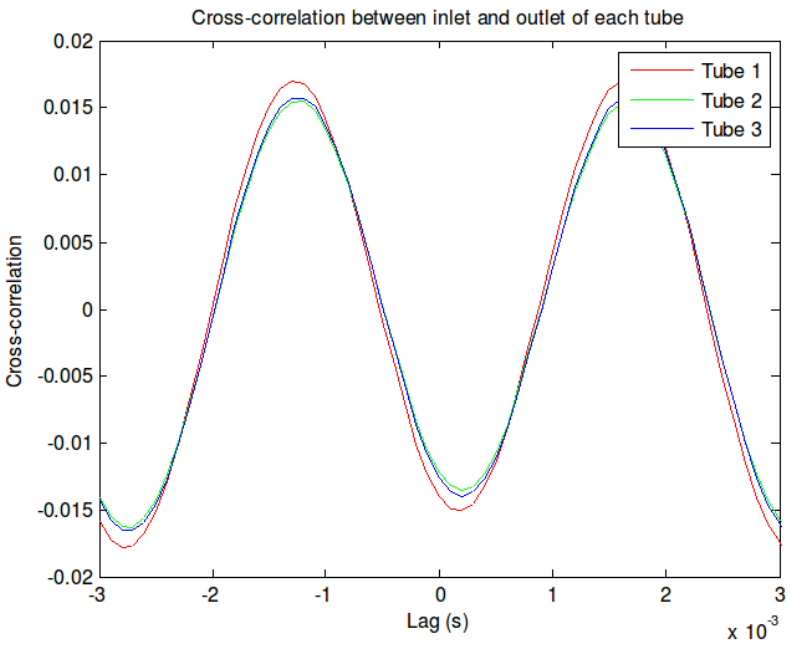

Figure 3.15. Case 1a pressure cross-correlation plot

defined as the average time lag divided by the average oscillation period, is tabulated for all acoustic cases in Table 3.7 near the end of the section.

Figure 3.16 plots the temperature rise across each tube as a function of time for Case 1a. Only Tube 1 received nitrogen heating, yet Tube 2 showed a larger temperature rise. This result was likely due to the location of the thermocouples inside the manifolds. Because of packaging constraints, thermocouples were installed in the manifolds in a staggered pattern. This pattern is can be seen in Figure 2.14. Half of the thermocouples in each transducer measured temperature inside a single tube, and the other half measured temperature inside the manifold cross-passage; the latter measured the temperature of a mixture of fuel from several tubes. Moreover, the long residence time for fuel inside the manifold cross passage allowed heat diffusion inside the manifold.

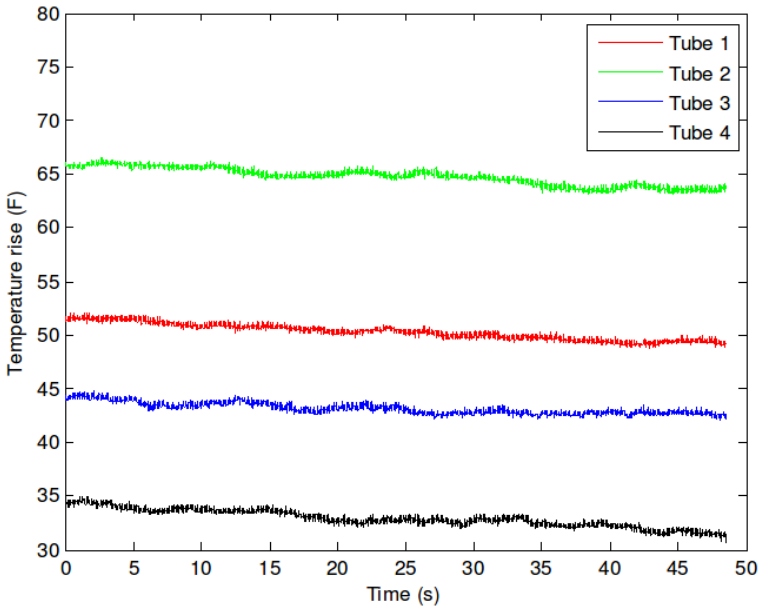

Figure 3.16. Case 1a tube temperature rise plots

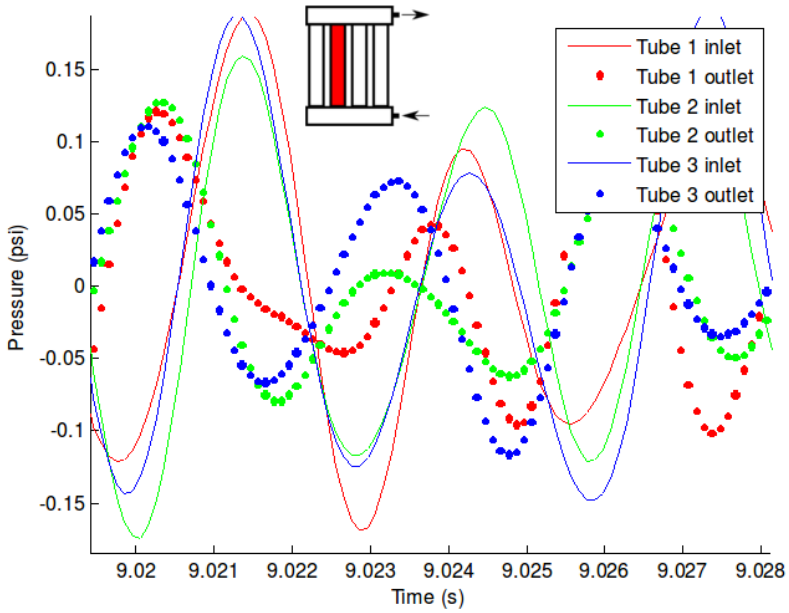

Figure 3.17. Case 2a pressure trace

Figures 3.17-3.18 provide a pressure trace and power spectral density plots for Case 2a. Figure 3.19 provides a cross-correlation for pressure signals.

These oscillations are less organized and weaker than those of case 1a. Coupled oscillations overtake one another more drastically in this case. Frequency content peaked between 337 and 338 Hz in all tubes. Oscillation amplitudes periodically decreased to those found in zero data (∼0.1 psi). Only Tube 1 was heated in Case 1a, and only Tube 2 was heated in Case 2a. For this pair of test runs, the case where Tube 1 was heated yielded stronger and more tightly-coupled oscillations than the case where Tube 2 was heated. However, this trend did not apply to all cases.

Case 3a showed little in the way of discrete frequency content. Slight peaks did appear on the PSD plot at 278 Hz and between 832 and 834 Hz. Oscillations show some coupling, but often overtake one another. Oscillation amplitudes periodically decreased to those found in zero data (0.1 psi).

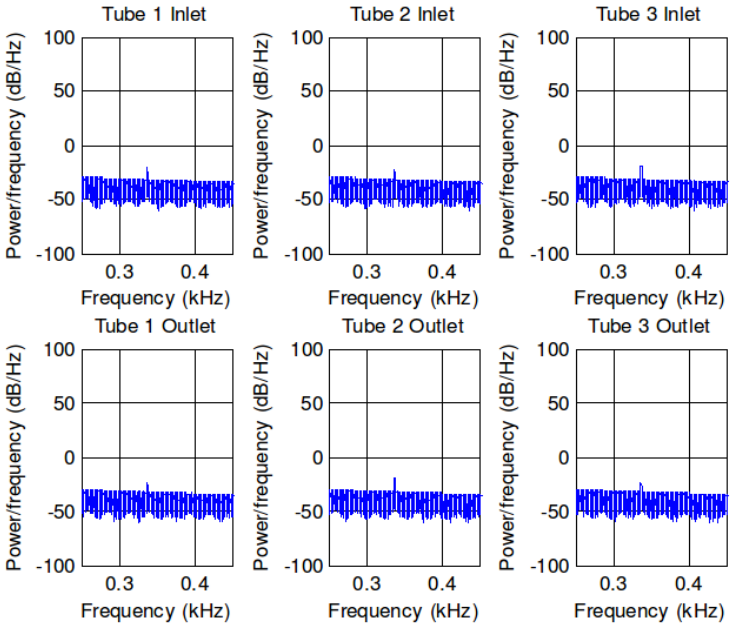

Figure 3.18. Case 2a power spectral density plot

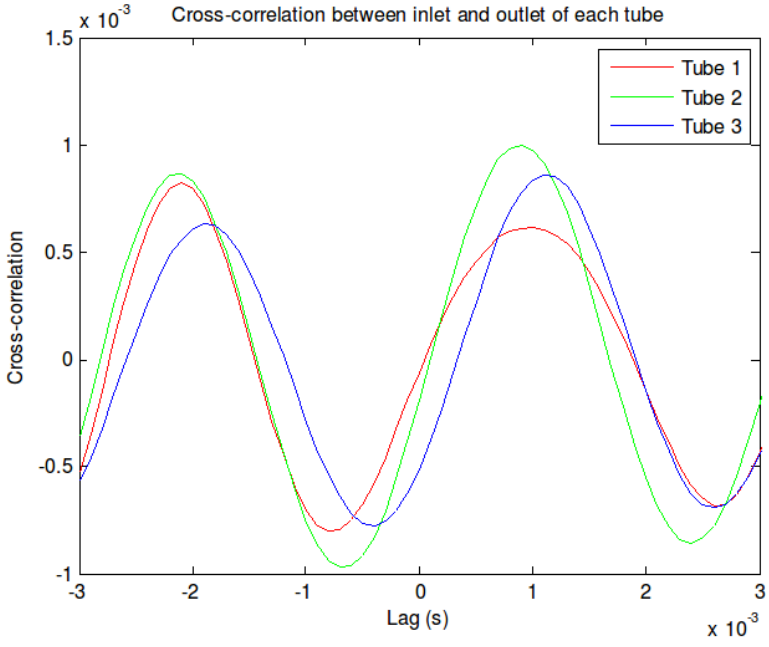

Figure 3.19. Case 2a pressure cross-correlation plot

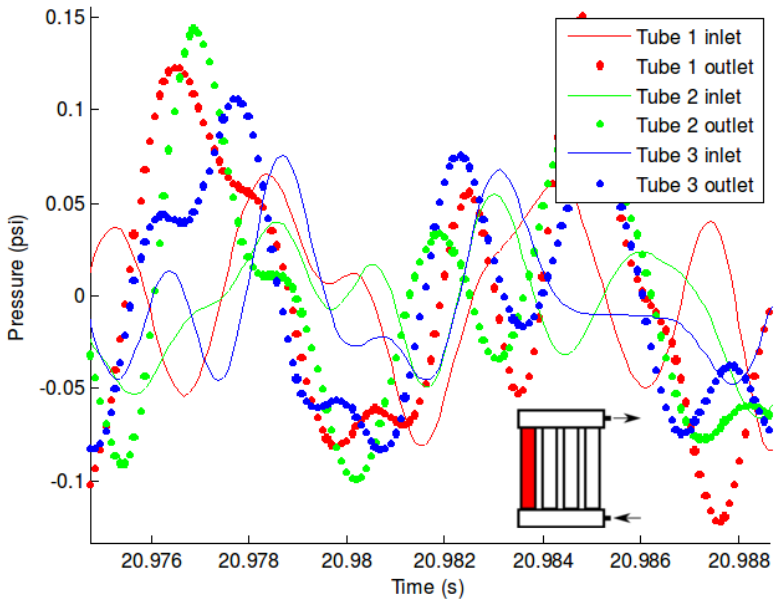

Figure 3.20. Case 3a pressure trace

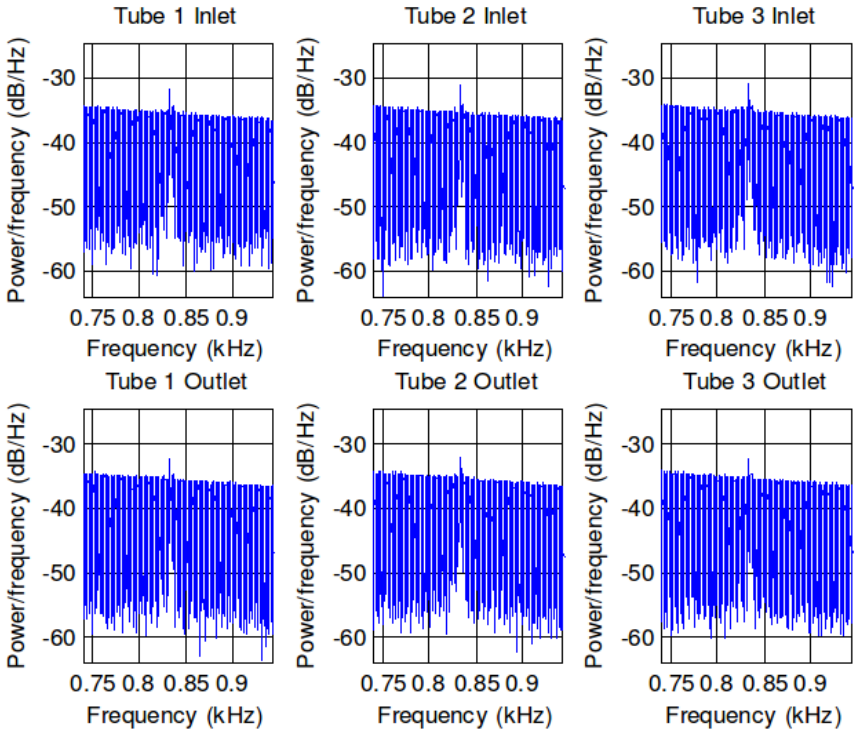

Figure 3.21. Case 3a power spectral density plot

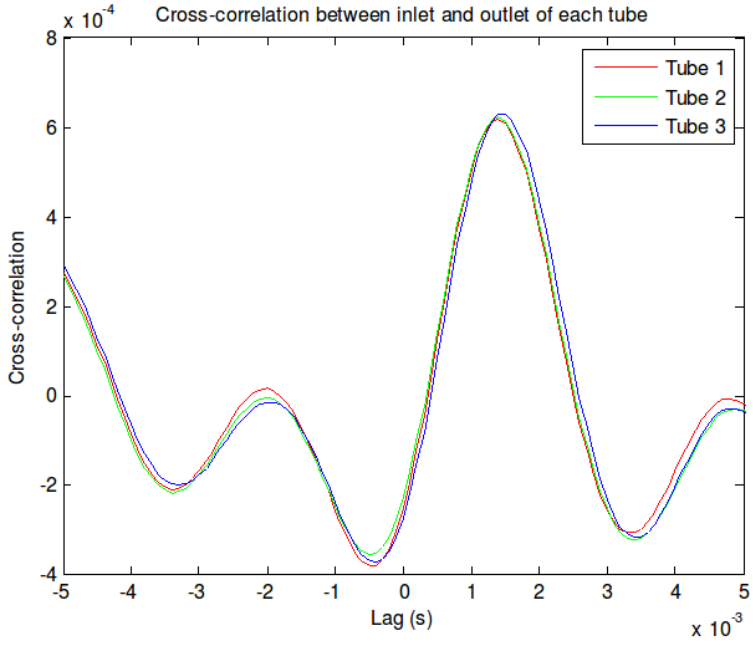

Figure 3.22. Case 3a pressure cross-correlation plot

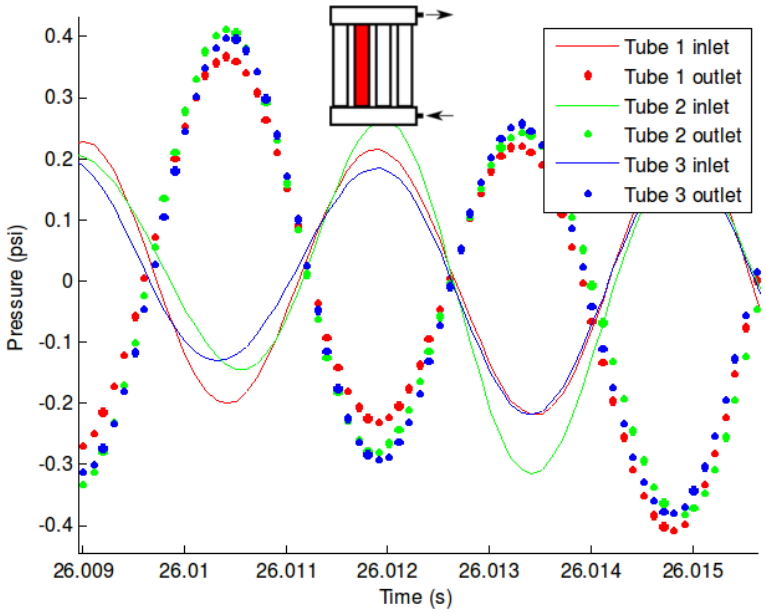

Figure 3.23. Case 4a pressure trace

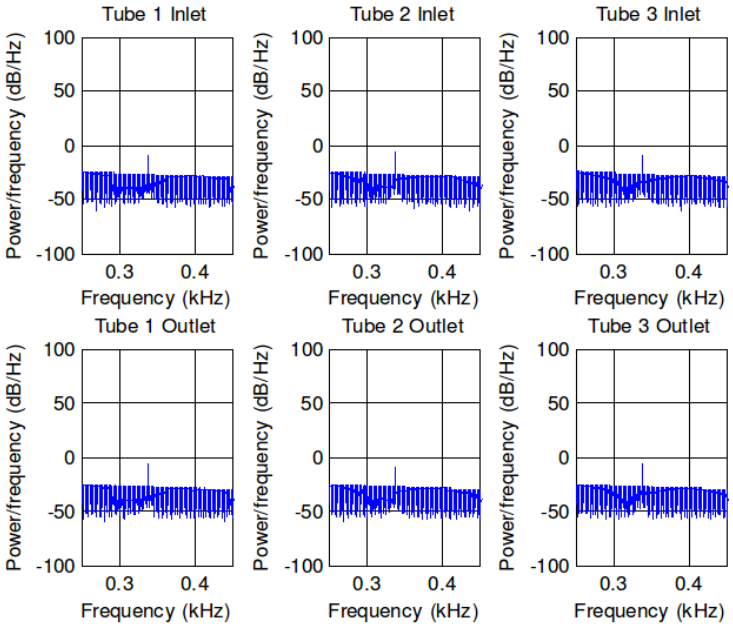

Figure 3.24. Case 4a power spectral density plot

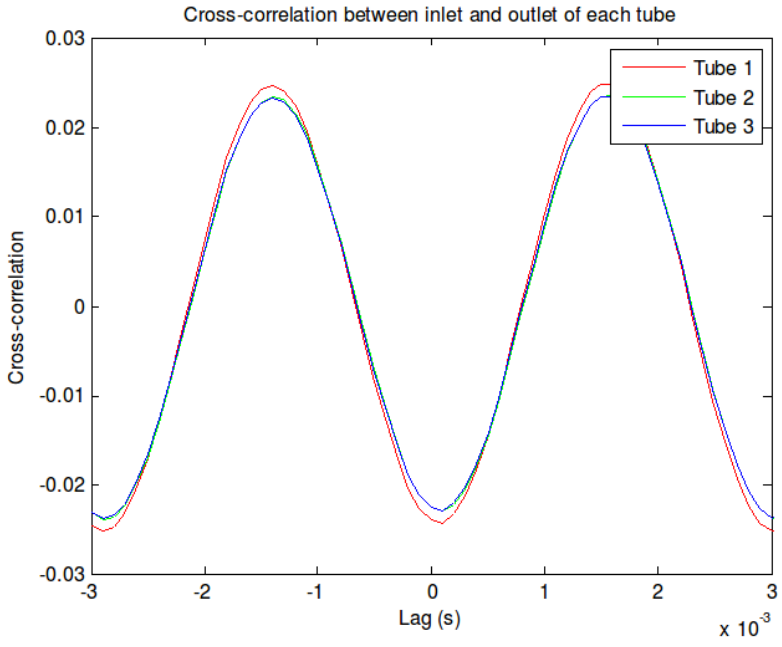

Figure 3.25. Case 4a pressure cross-correlation plot

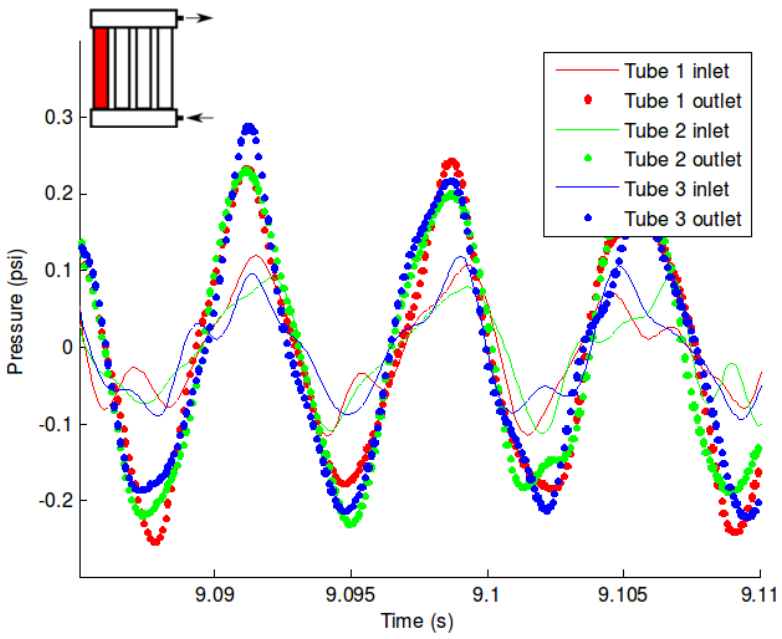

Figure 3.26. Case 5a pressure trace

Case 4a showed strong frequency content at 338 Hz for all tubes. The same two groups of oscillations described in Case 1a remained in phase for the entire data sample of Case 4a.

Cases 1a through 4a were run using manifolds with large cross passage diameters. Cases 5a through 7a used manifolds with small cross passage diameters.

Case 5a showed weak frequency content at 139 Hz. The two groups of oscillations have a smaller phase offset here than in the large-manifold cases.

Case 6a exhibited weak oscillations at 338 Hz. Coupling occurred between the inlet waveforms; however, the outlet waveforms followed each other less closely.

Case 7a exhibited the largest acoustic oscillation amplitudes seen (near 1 psi); it was also run with a particularly low inlet fuel temperature (300degF). Oscillations occurred at 337 Hz. The two groups of oscillations have a small phase offset, which is typical for cases with small manifold cross passages.

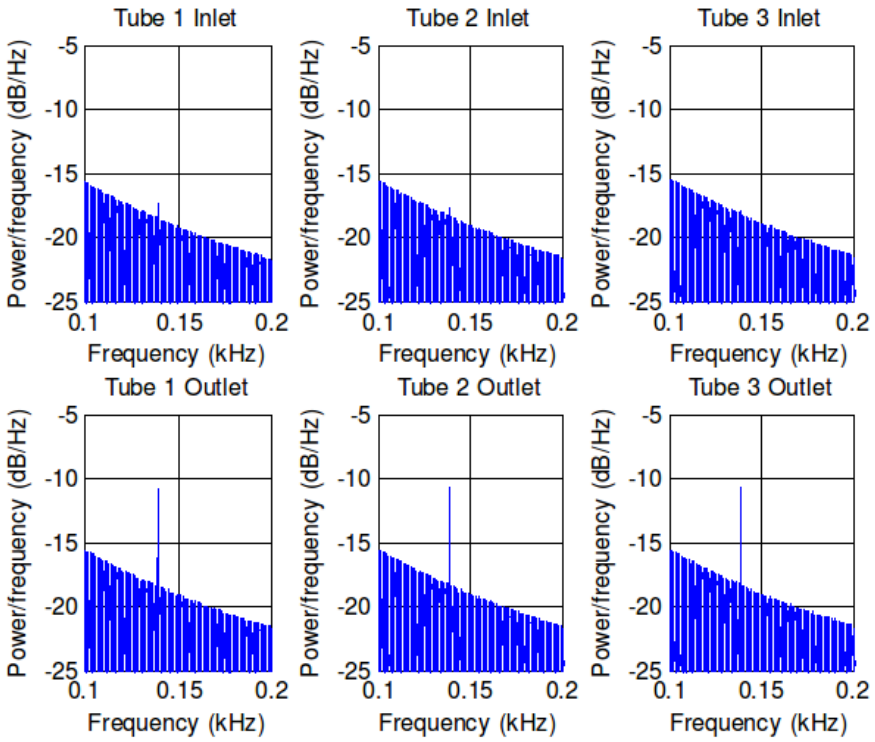

Figure 3.27. Case 5a power spectral density plot

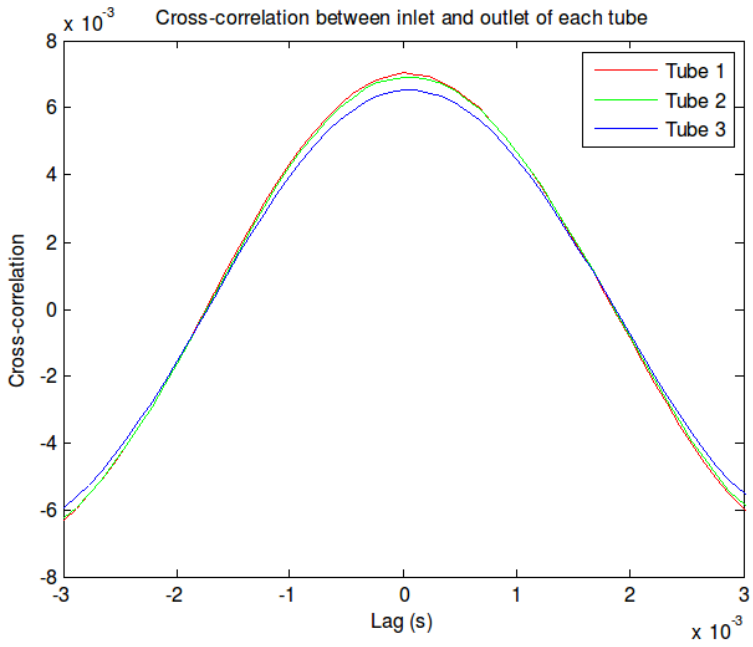

Figure 3.28. Case 5a pressure cross-correlation plot

Table 3.6. Summary of acoustic case results

Case num	Density drop	Acoustic-mode amplitude	Acoustic-mode frequency
(lb/ft^3)	(psi)	(Hz)	(Hz)
1a	2.08	0.35	338-342
2a	2.16	0.21	337-338
3a	1.88	0.20	832-834
4a	1.73	0.44	338
5a	1.62	0.29	139
6a	1.54	0.22	338
7a	3.65	1.05	337

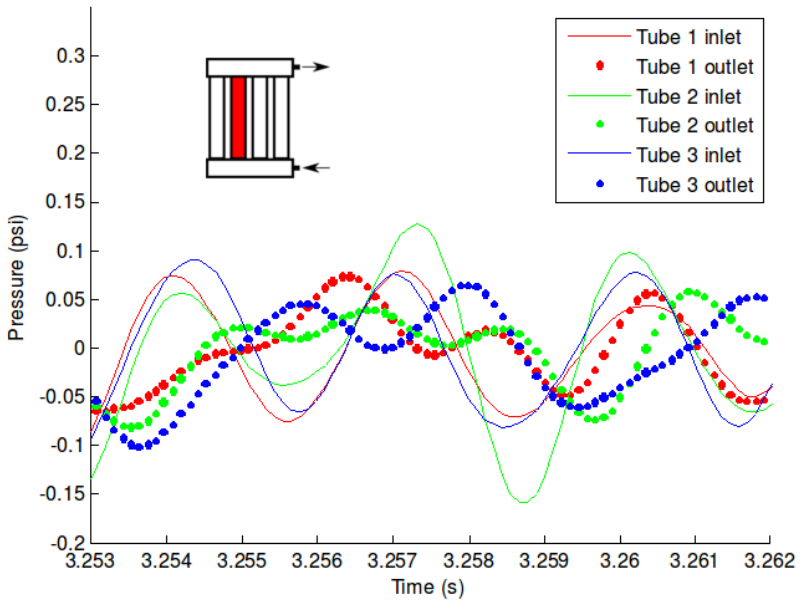

Figure 3.29. Case 6a pressure trace

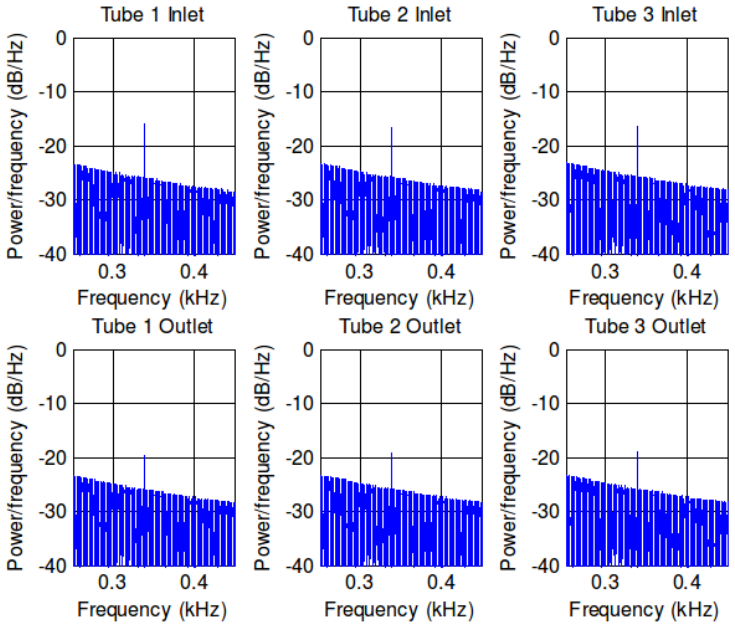

Figure 3.30. Case 6a power spectral density plot

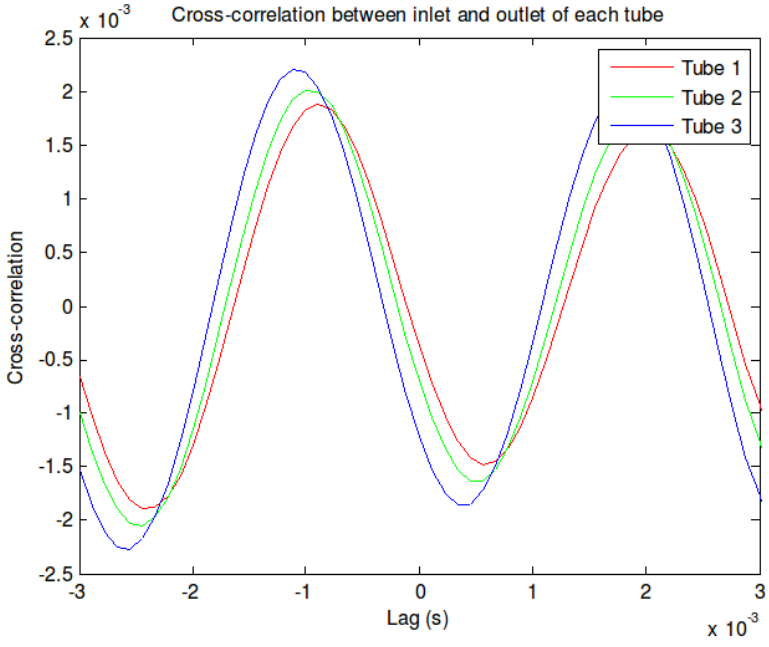

Figure 3.31. Case 6a pressure cross-correlation plot

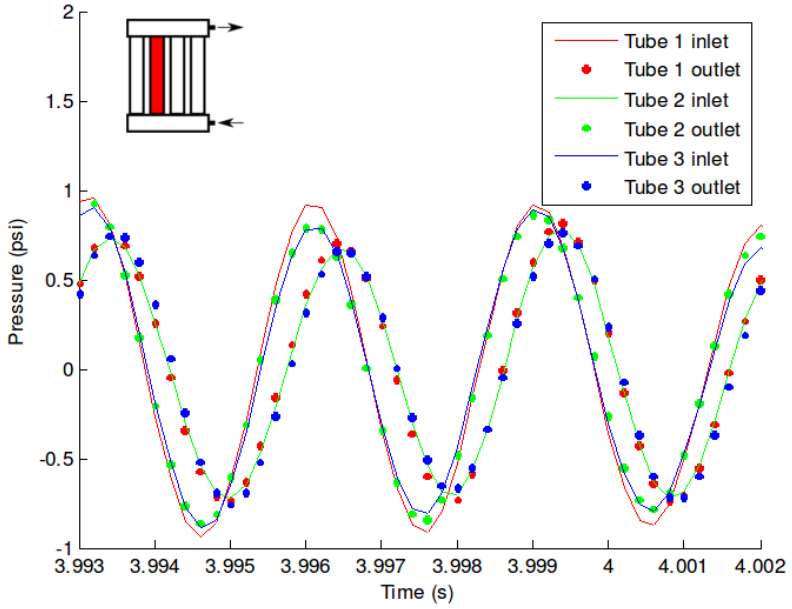

Figure 3.32. Case 7a pressure trace

Table 3.7 presents the average phase lag between the inlet and outlet of each tube in degrees. Because Cases 5a and 6a showed loose coupling, the phase lag was not calculated for these cases.

For all cases with substantial acoustic oscillations, large phase lags (greater than 90 degrees) were observed in cases run with the large manifold cross passage. Small phase lags (less than 60 degrees) were observed in cases run with the small manifold cross passage.

The following trends regarding acoustic oscillations are proposed:

- Acoustic oscillations occur when a single tube is heated, but never occur when all tubes are heated.
- No trends have yet been observed pertaining to which tube is heated.

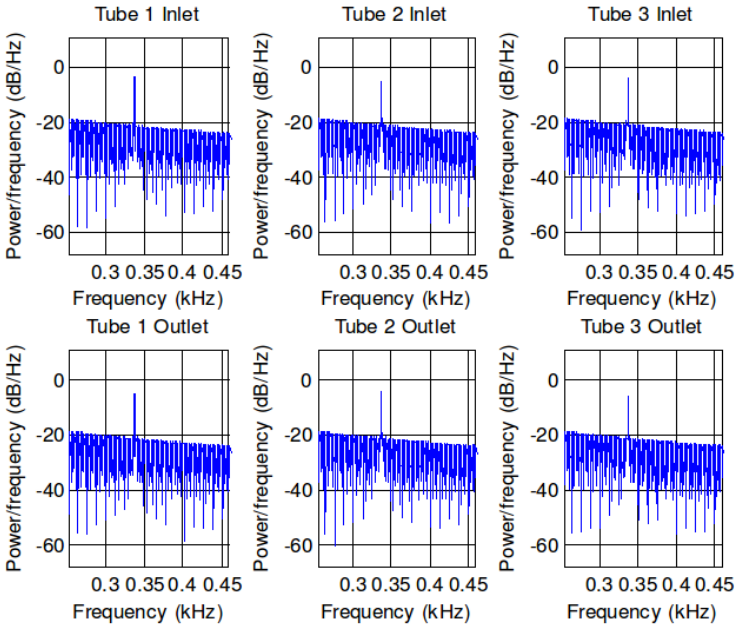

Figure 3.33. Case 7a power spectral density plot

Table 3.7. Inlet/outlet pressure oscillation phase lag for acoustic cases

Case num	Tube 1 inlet/outlet phase lag (degrees)	Tube 2 (degrees)	Tube 3 (degrees)
1a	157.8	146.6	146.6
2a	122.1	109.2	133.5
3a	110.9	112.6	115.0
4a	170.3	170.3	170.3
5a	N/A	N/A	N/A
6a	N/A	N/A	N/A
7a	38.8	38.8	41.3

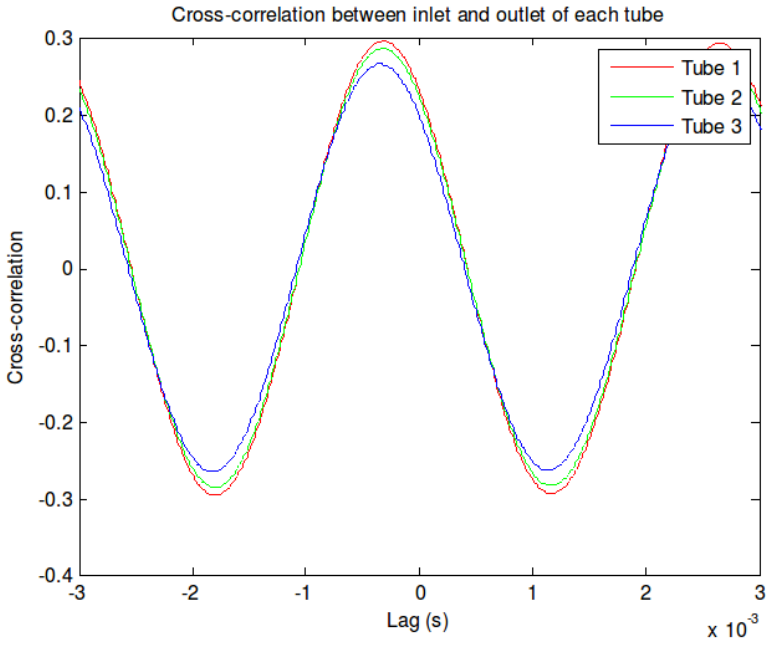

Figure 3.34. Case 7a pressure cross-correlation plot

- Cases with colder inlet temperatures tend to produce relatively large acoustic oscillations. This may due to the larger temperature rise across the test section in these cases.

- A large majority of oscillating cases had frequency content between 335 and 340 Hz, regardless of fuel temperature, pressure, mass flow rate, and manifold geometry. Weak oscillations were detected in other frequency ranges in select cases.

- The phase offset between the two groups of oscillations depends on cross passage diameter. A large cross passage diameter is conducive to larger offset. However, the passage diameter does not appear to affect the frequency or amplitude of acoustic oscillations.

4. RESULTS OF SECOND TEST CAMPAIGN

Tests were performed under nominal conditions of 400-700 psi fuel inlet pressure and mass flow rate of 0.25-13.75 lb/hr per tube. Only the fuel manifold assembly with 1/4 in cross passage diameter was used. Fuel preheating and nitrogen flow control louver settings were varied between test cases. Hot nitrogen was either blown on all tubes (when all channels were wide-open), a single tube (when only one channel was wide-open), or two tubes at a time. Table 4.1 outlines conditions for each test. A total of 77 cases were run. Trends proposed in this report reflect the results of every test case run; however, pressure traces are only provided for select test cases. A complete test matrix, detailing conditons for each case, is included in Appendix B.

Several modifications were made to the test article between the first and second test campaigns:

- The diameter of the fuel inlet tube, which connects to the inlet manifold shown in Figure 2.10, was reduced from 1/4 in to 1/8 in outer diameter. This smaller tube helps isolate acoustics inside the test section.
- The fuel inlet tube was heated with rope heaters to reduce the temperature drop between preheater and test section.
- Functioning pressure transducers were restored in all four tube inlets and outlets.

Nitrogen was heated to the maximum temperature the laboratory's electic air heater was capable of, yielding temperatures between 811 and 957F at the test article. The nitrogen flow rate for baseline cases was 0.3 lb/s. In select cases, the nitrogen flow rate was decreased to 0.08 lb/s. The second campaign focused on very high and very low fuel preheating condition, whereas the first campaign focused on

Table 4.1. Outline of test parameters

Manifold cross-passage diameter	1/4 in
Inlet temperature	70, 200, 300, 650, 675, 700F
Fuel pressure	400, 450, 500, 700 psi
Fuel mass flow rate (4 tubes combined)	1 - 55 lb/hr
Tube heating condition	One, two, or all tubes heated

moderate conditions. Results of the previous campaign indicated that high preheating is conducive to bulk-mode oscillations because associated temperatures more closely approach the critical temperature, whereas low preheating is conducive to acoustic-mode oscillations due to the larger temperature gradients and resulting density drops that occur under such conditions.

The same two distinct modes of oscillations were encountered during the second test campaign: bulk-mode oscillations occurred with relatively high amplitudes (above 2 psi) and low frequencies (under 3 Hz), while acoustic-mode oscillations occurred with lower amplitudes (under 1 psi) and higher frequencies (140-450 Hz). Many test cases exhibited both oscillation modes superposed atop one another. A band-pass filter allowing frequency content from 100-1000 Hz was applied to pressure traces intended to show acoustic-mode oscillations.

Bulk-mode behavior in the second test campaign was generally unchanged from the first. Cases with substantial preheating tended to experience these oscillations. However, it would appear that these oscillations originated from the fuel preheater; the heating in the test section was inadequate to induce bulk-mode oscillations, as bulk-mode oscillations were unchanged when fuel was heated exclusively in the preheater.

While it was once theorized that oscillations were caused by the preheater's individual elements cycling on and off to maintain a target temperature, oscillations of similar magnitude and character also occurred when heater elements maintained steady heat output. The analysis of the second test campaign shall be restricted to acoustic-mode oscillations, as the bulk-mode oscillations originating in preheater, have been discussed in the previous chapter.

Oscillations with frequencies between 140-450 Hz occurred in many test cases. The observed oscillation frequencies in the second campaign strongly depended on which tube was heated. As in the first test campaign, however, the 340 Hz oscillations frequently appeared in the second campaign. Table 4.2 describes conditions for cases examined in this document for acoustic-mode oscillations. Excited mod es from

Table 4.2. Conditions for select cases involving acoustic-mode oscillations

1/4 in manifold cross passage cases					
Case	T_{inlet} (F)	p_{fuel} (psi)	$\dot{m}$ (lb/hr)	Heating Setting	File ID
8a	340.9	400.7	25.7	Chan 1 open	20150624_1537483
9a	340.8	427.5	30.9	Chan 1 low-flow	20150624_1547385
10a	333.2	418.3	24.1	Chans 1 and 4 open	20150624_1536095
11a	268.1	398.1	30.1	Chan 2 open	20150625_0915291
12a	318.9	420.3	29.8	Chan 3 open	20150624_1643232
13a	317.2	407.9	26.5	Chan 4 open	20150624_1534134

these cases are representative of what modes are typically excited for a given heating condition.

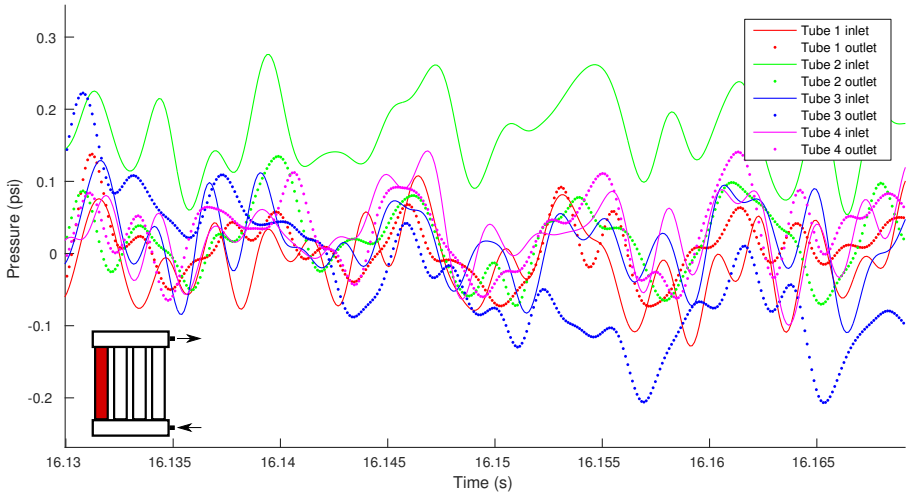

Figure 4.1. Case 8a pressure trace (T_{inlet}=340.9F, p=400.7 psi, Tube 1 heated)

Fuel manifold pressure traces and power spectral density plots for Case 8a are shown in Figures 4.1-4.2. The spikes in the power spectral density (PSD) plot for Case 8a indicate frequency content at 141, 282, 352, and 423 Hz in all tubes. These oscillations showed loose coupling between each tube's inlet and outlet signals, but the presence of many frequencies made the overall waveforms rather incoherent. The frequencies for this case were typical of cases in the second campaign in which Tube 1 was heated. Amplitudes for this particular case were of a similar order of magnitude as pressure transducer noise. However, the oscillations measured are likely acoustic in nature due to their discrete frequency content, in contrast to the broadband content typical of noise signals and hydrodynamic effects.

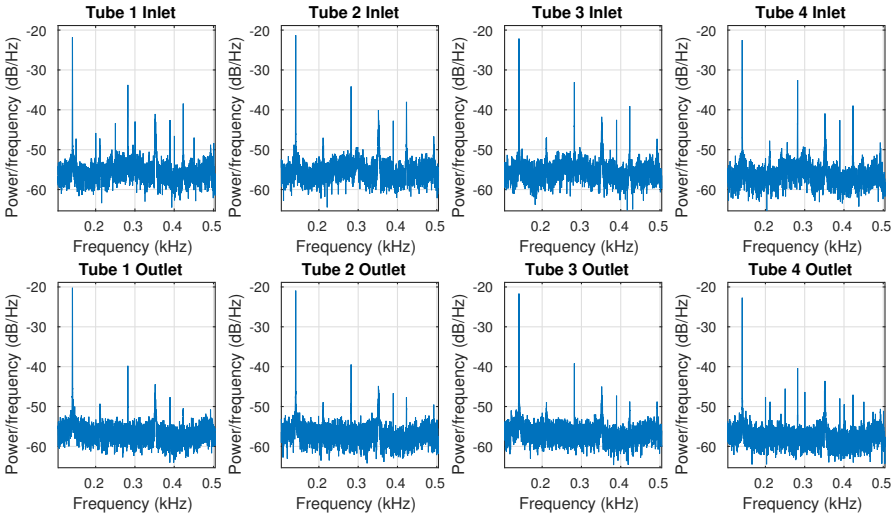

Figure 4.2. Case 8a power spectral density plot (T_{inlet}=340.9F, p=400.7 psi, Tube 1 heated)

Figure 4.3 and 4.4 provide a pressure trace and power spectral density plot for Case 9a. This case is similar to Case 8a, except that the nitrogen flow rate has been reduced by 75%. The rationale for this case was to test the theory from the first test campaign that uneven tube heating is required for oscillations to occur. Recall that cases in the first campaign often displayed oscillations when a single tube was heated, but never displayed oscillations when all tubes were heated. It was unknown whether the lack of oscillations during even tube heating was due to the fact that the tubes weren't heated unevenly, or that they each received only one fourth the flow rate of nitrogen used in single tube heating cases.

Oscillations in Case 9a are disorganized and weak, having amplitudes and characteristics similar to noise oscillations found in zero data ($\tilde{0}$.1 psi). Frequency content for the signal is broadband, which is not indicative of acoustic activity. All other cases with 1/4 the standard nitrogen mass flow rate yielded no oscillations as well. This would indicate that insufficient energy was input into the tube to drive measurable oscillations when all tubes were heated.

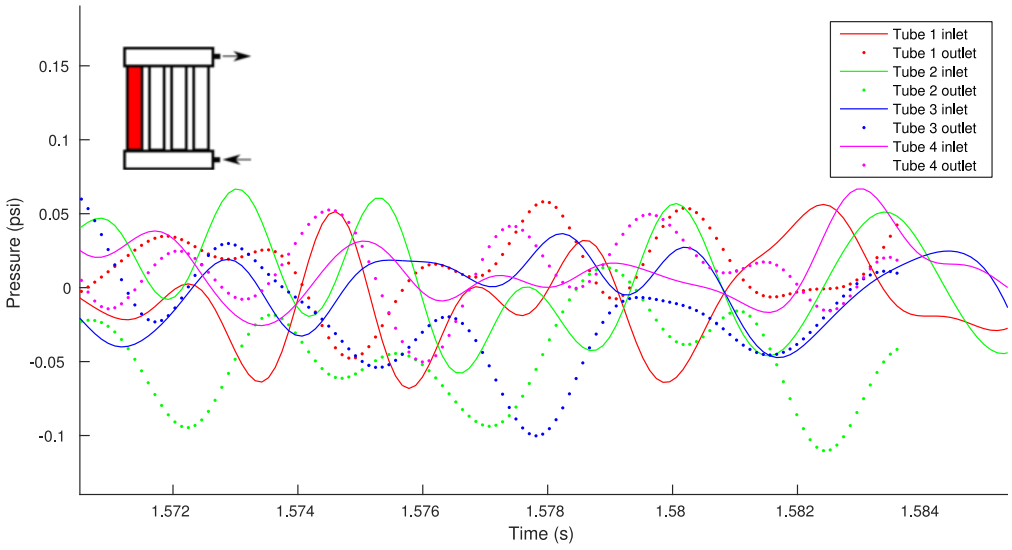

Figure 4.3. Case 9a pressure trace (T_{inlet}=340.8F, p=427.5 psi, Tube 1 heated, low nitrogen flow)

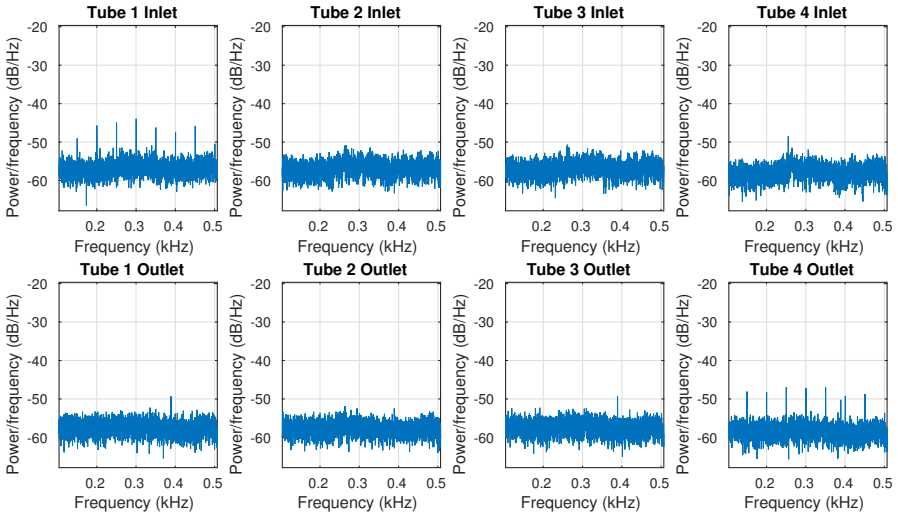

Figure 4.4. Case 9a power spectral density plot (T_{inlet}=340.8F, p=427.5 psi, Tube 1 heated, low nitrogen flow)

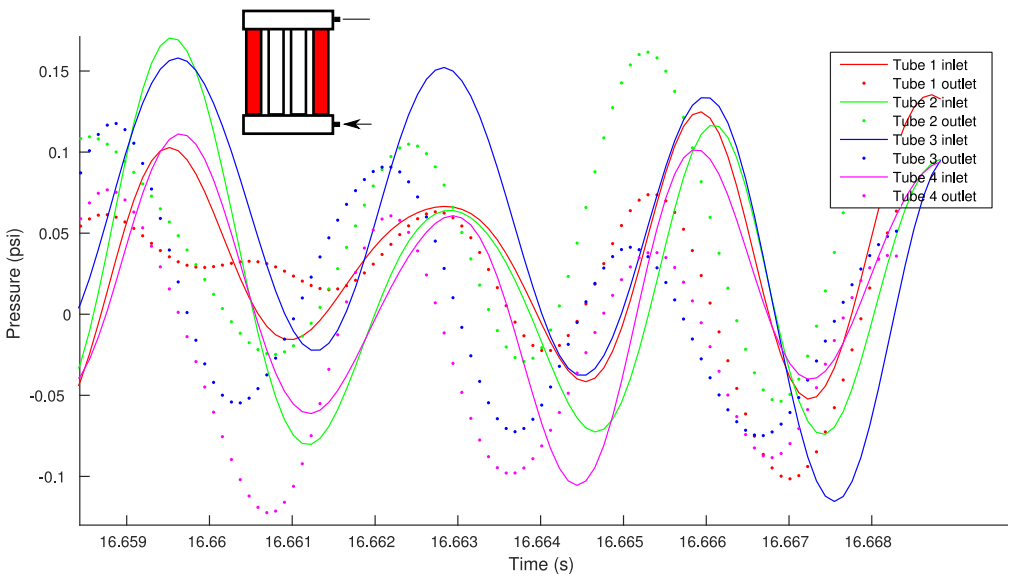

Figure 4.5. Case 10a pressure trace (T_{inlet}=333.2F, p=418.3 psi, Tubes 1 and 4 heated)

Case 10a was run with Tubes 1 and 4 heated. No cases in the first test campaign were performed with two tubes heated at a time. Figure 4.5 and 4.6 provide a pressure trace and power spectral density plot for Case 10a. Strong frequency content was detected at 341 Hz for Case 10a. Some frequency content was also detected at 389 and 482 Hz; however, these higher-frequency modes have amplitudes many orders of magnitude weaker than the 341 Hz mode. The presence of oscillations having large amplitude and discrete frequency content in the case in which several tubes were heated (Case 10a), and the lack thereof when tubes were heated with low power (Case 9a), indicates that differential tube heating is likely not required to produce acoustic oscillations.

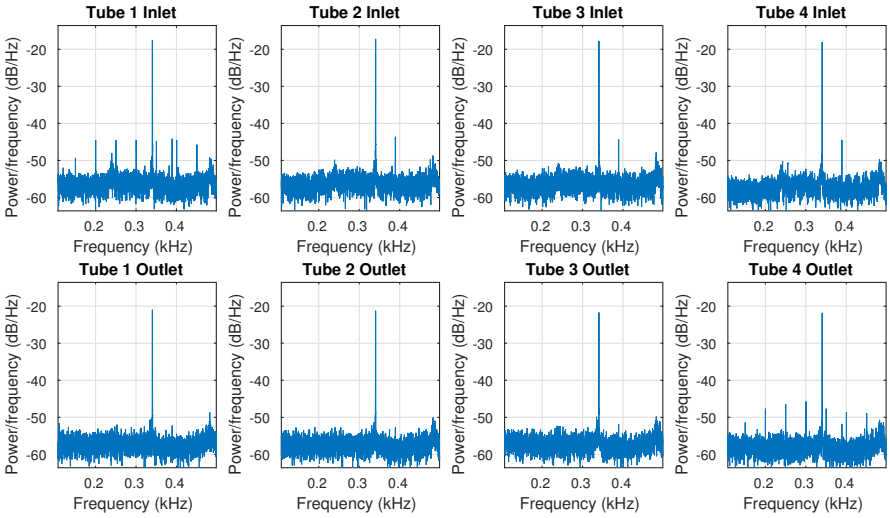

Figure 4.6. Case 10a power spectral density plot (T_{inlet}=333.2F, p=418.3 psi, Tubes 1 and 4 heated)

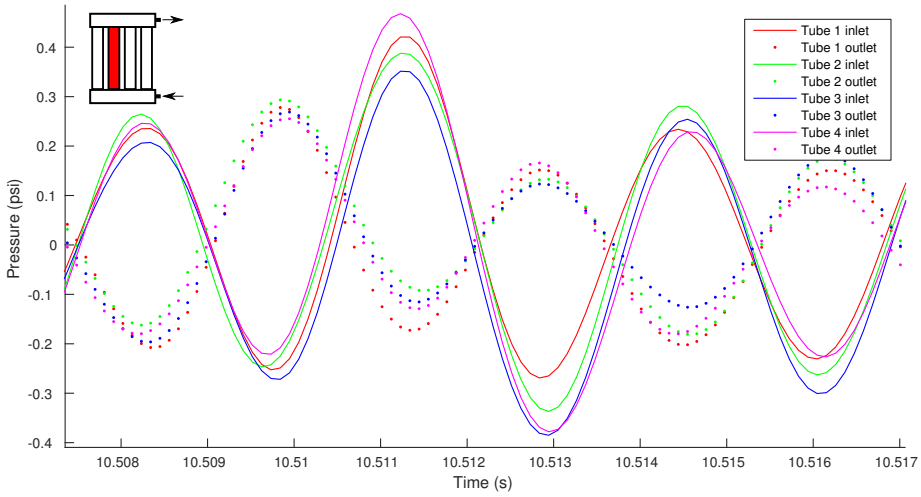

Figure 4.7. Case 11a pressure trace (T_{inlet}=268.1F, p=398.1 psi, Tube 2 heated)

Figures 4.7 and 4.8 provide a pressure trace and power spectral density plot for Case 11a. Only Tube 1 was heated in Case 8a, whereas only Tube 2 was heated in Case 11a. This case yielded much larger and more strongly-coupled oscillations with a dominant frequency of 344 Hz. Activity was also detected at 144 Hz; however, this lower-frequency mode is small enough in amplitude to be invisible on the pressure trace. These aforementioned frequencies were typically detected in cases in which only Tube 2 was heated during the second test campaign.

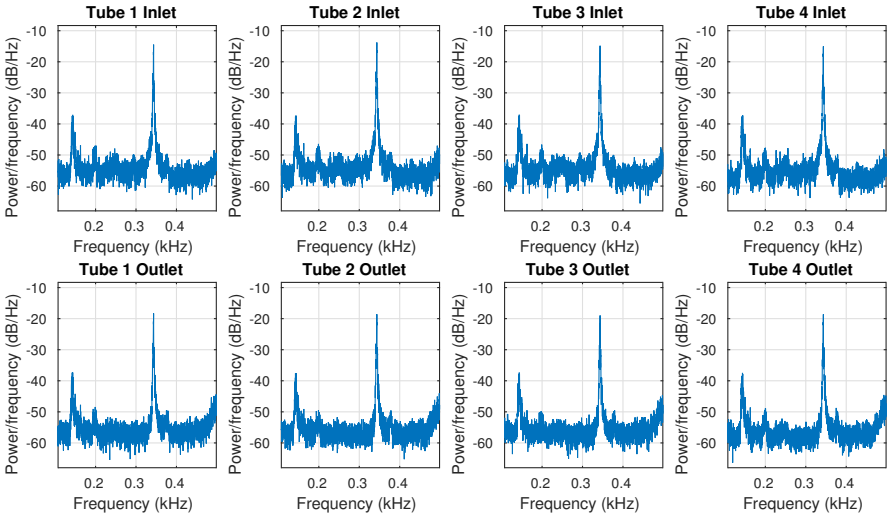

Figure 4.8. Case 11a power spectral density plot (T_{inlet}=268.1F, p=398.1 psi, Tube 2 heated)

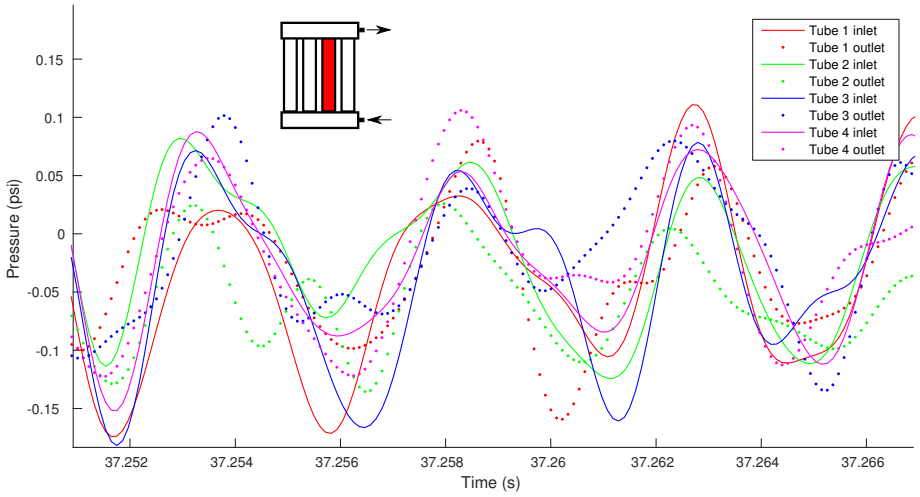

Figure 4.9. Case 12a pressure trace (T_{inlet}=318.9F, p= 420.3 psi, Tube 3 heated)

Figures 4.9 and 4.10 provide a pressure trace and power spectral density plot for Case 12a, in which only Tube 3 was heated. Case 12a showed oscillations at 244, 336, and 389 Hz - the typical frequencies for cases with Tube 3 heated. The 244 Hz mode was the strongest of the group, and tended to occur with minimal phase lag between all inlet and outlet probes. Small phase lags between inlet and outlet were commonly observed in cases in which the $\tilde{3}40$ Hz mode did not dominate.

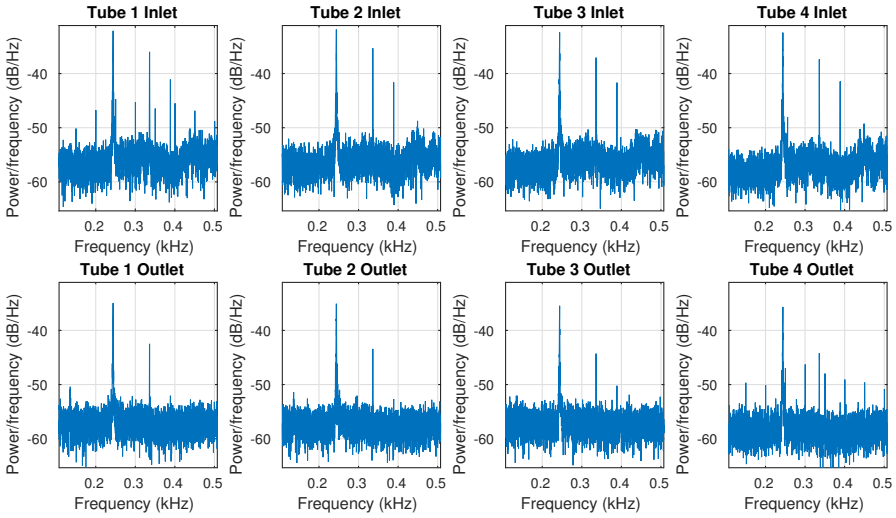

Figure 4.10. Case 12a power spectral density plot (T_{inlet}=318.9F, p= 420.3 psi, Tube 3 heated)

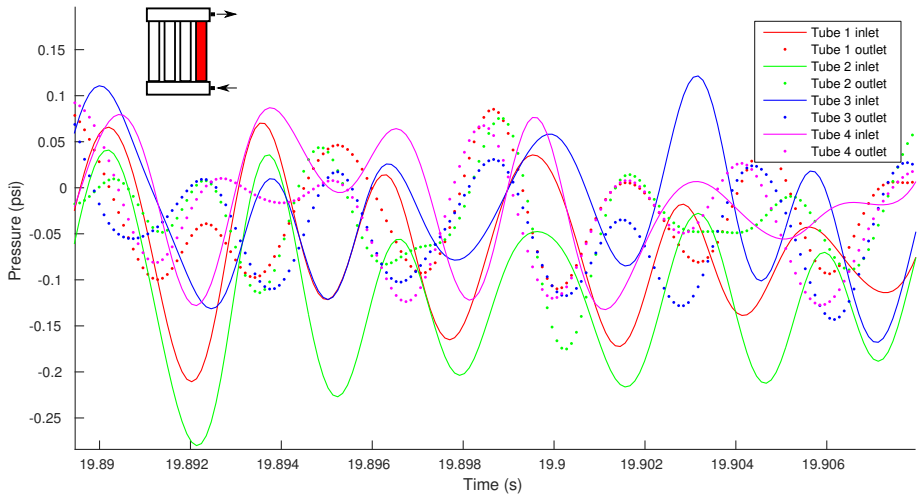

Figure 4.11. Case 13a pressure trace (T_{inlet}=317.2F, p=407.9 psi, Tube 4 heated)

Figures 4.11 and 4.12 provide a pressure trace and power spectral density plot for Case 13a, in which only Tube 4 was heated. Case 13a showed strong frequency content at 342 Hz for all tubes. Weaker frequency content was detected at 236 Hz. These frequencies were often observed in cases in which Tube 4 was heated.

Power spectral density plots shown previously were representative of the entire data set of conditions where a single tube was heated. Table 4.3 lists frequencies detected for every test condition. Every cell represents a single test condition. Similar to the first test campaign, frequencies between 330 and 355 Hz were frequently detected. There is also strong trend between which tube is heated and which other frequencies were detected: Heating Tubes 1 or 2 tended to generate 140 and 280 Hz oscillations, whereas heating Tube 3 or 4 generated 244 Hz oscillations. This trend was not seen in the first test campaign. However, more cases were intentionally performed in the second campaign with conditions known to induce acoustic-mode oscillations - that is, cases with low preheating and maximum tube heating to maximize

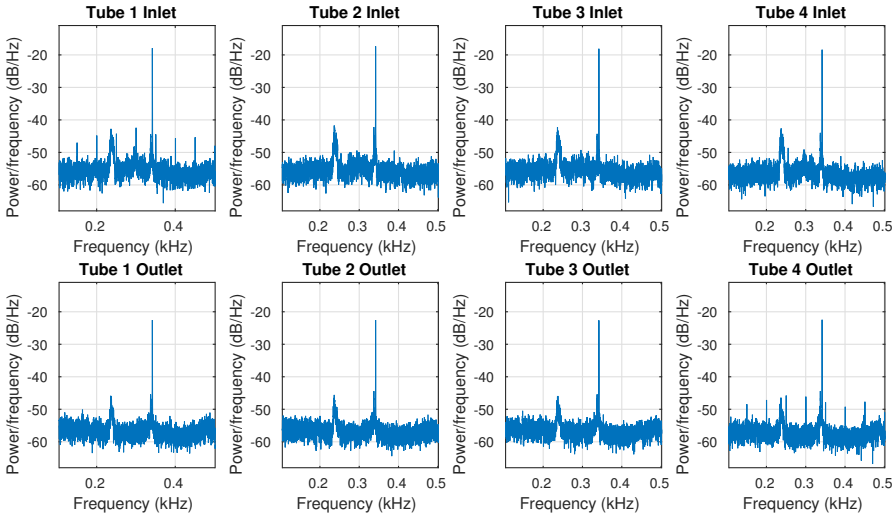

Figure 4.12. Case 13a power spectral density plot (T_{inlet}=317.2F, p=407.9 psi, Tube 4 heated)

the temperature gradient inside the fuel tubes. The first campaign was conducted with coarser property increments, producing a smaller number of cases with strong acoustic oscillations, which made trends more difficult to establish.

The frequency at which oscillations resonance is presumed to be largely a function of the speed of sound of the fluid, which is a derived function of the fluid's temperature. Inlet temperatures were varied throughout the test campaign; however, the vast majority of oscillating cases displayed frequencies between 330 and 355 Hz. The invariance of frequency for changing inlet temperature, mass flow rate, and pressure may come as a surprise. However, this invariance can be explained by an unintended similarity between test cases in which oscillations were observed: tube outlet temperatures tended to remain nearly constant.

Tube outlet temperatures are suspected to remain within a narrow range for oscillating cases due to a natural heating barrier illustrated in Figure 4.13, which is a plot of specific heat versus temperature for Jet-A fuel. Specific heat spikes near the critical temperature; as outlet temperature approaches this neighborhood, the effect of a unit of heat input on temperature rise diminishes by an order of magnitude. Consider a case in which fuel is heated from room temperature to near-critical conditions. For a fixed heat input within the test section, a 100F inlet temperature increase would result in a mere 25F outlet temperature increase. Furthermore, highly-preheated fuel would receive less heat input inside the test section than non-preheated fuel due to the smaller difference between fluid and wall temperature; this further diminishes the effect of preheating on outlet temperature.

Thermocouples were installed upstream and downstream of each tube, but the long residence times for fuel inside the manifolds prohibit accurate measurement of individual tubes' outlet temperatures due to conduction and mixing effects. However, due to the natural heating barrier around the critical temperature, cases in which one tube was heated with maximum nitrogen temperature and flow rate can be reasonably assumed to have outlet temperatures within the neighborhood of Jet-A's critical temperature (750F). This assumption was used for the definition of temperature profiles

Table 4.3. Frequencies detected for every test condition in which a single tube was heated

Heated tube	Tube 1	Tube 2	Tube 3	Tube 4
Frequencies detected (Hz)	141	340, 140, 280	244, 335, 389	343
	141, 283, 352	140, 279	243, 335	343, 239
	142, 250, 284, 353	139, 279	243, 336	344, 238
	141, 282, 353, 423	140, 279	244, 336, 389	342, 236
	141, 282, 352, 423	139, 280	244, 334, 434	343, 238
	142,284, 353, 426	139, 279	245, 338, 448	345, 240
	141, 283, 353, 424	344, 144		
		340, 144		
		342, 141		

generated for acoustic simulations. These simulations were performed to corroborate frequencies observed in experiments, and are described in the following chapter.

Only coarse changes in heating nitrogen temperature and flow rate were made for the two test campaigns. When nitrogen flow rate and temperature were set to their maximum attainable settings, and this flow was directed at a single tube, oscillations were detected under most circumstances. Oscillations were never detected when 1/4th of the maximum nitrogen flow rate was applied. However, intermediate heating settings were not considered for the present study. It is hypothesized that intermediate heating settings may increase the frequency of acoustic oscillations due to higher associated sound speeds, while still providing sufficient energy to drive these oscillations.

Although the majority of oscillating cases exhibited frequencies around 340 Hz, some displayed other excited modes. If the 340 Hz mode is assumed to occur due to open tube resonance of a single heated tube, an effective speed of sound for this tube may be calculated with Equation 4.1.

$$a_{eff} = 2L_{tube}f = 2(7.75\text{in})(340\text{Hz}) = 5270\text{in/s} = 440\text{ft/s} \tag{4.1}$$

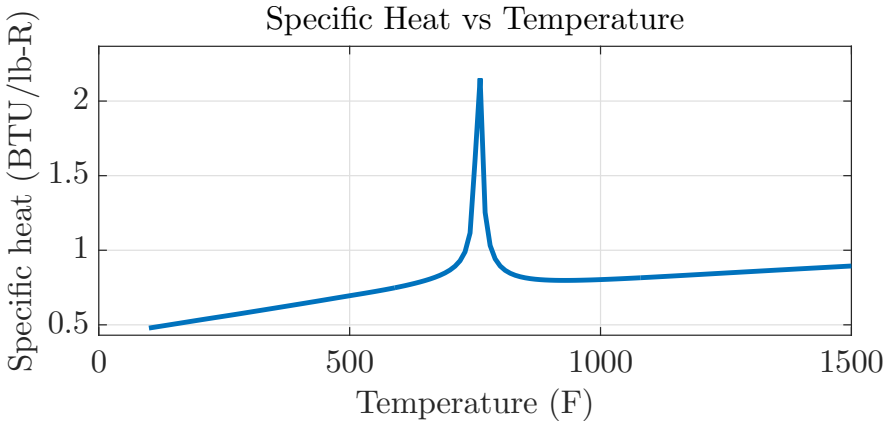

Figure 4.13. Specific heat versus temperature for Jet-A fuel

The length of 7.75 in corresponds to the length of the physical tube plus the small holes inside the manifold leading to the cross passages. A local speed of sound of 440 ft/s matches that of 740F fuel, which is slightly subcritical in temperature. Using this effective sound speed, the frequency for open-tube resonance based on the length of the heated tube (7.75 in) plus that of the outlet passage (1.5 in) is calculated in Equation 4.2.

$$f_2 = \frac{a_{eff}}{2L} = \frac{5270 \text{ in/s}}{2(7.75 + 1.5)\text{in}} = 285\text{Hz} \tag{4.2}$$

This result closely matches a frequency commononly observed in experiments: most cases in which either Tube 1 or 2 was heated yielded frequencies between 279 and 284 Hz. The 140 Hz subharmonic was also detected under similar conditions. The 280 Hz modes tended to exhibit nearly 180 degree phase lag between inlet and outlet, which is consistent with the theory that the inlet and outlet transducers lie near opposite antinodes of a 2L mode acting at around 280 Hz. The 140 Hz modes tended to occur with minimal phase lag between each signal. The length of this mode may span one heated tube and the outlet manifold passage, as predicted by the simple calculation. However, it most likely spans both cross passages. The added length of the inlet manifold does not substantially affect the frequency calculated in Equation 4.2 because it is filled with cold fuel having a sound speed an order of magnitude faster than that inside the outlet manifold. Addition of a unit length of passage containing cold fuel affects frequency less than a unit length of passage with fuel near the critical temperature. Cases in which Tubes 3 or 4 were heated did not exhibit the 140 or 280 Hz modes, possibly due to the lack of hot fuel in the outlet manifold. Tubes 3 and 4 were closer to the outlet port, so fuel residing in the outlet manifold tended to be cooler in these cases.

5. RESULTS OF ACOUSTIC SIMULATION

An acoustic model was developed using the linear acoustics solver in COMSOL Multiphysics 5.2. The fundamental frequency for the flow geometry is predicted by solving the Helmholtz equation, Equation 5.1, for eigenfrequencies ω. The lowest eigenfrequency was selected for each case.

$$\nabla\cdot\left(\frac{-1}{\rho}(\nabla p)\right) = \frac{\omega^2 p}{\rho c^2} \tag{5.1}$$

Here, p is total acoustic pressure, c is the speed of sound, and ρ is density. Thermal conduction, mean flow, and buoyancy effects are neglected for this analysis. The linear acoustics solver only calculates eigenfrequencies for the system; no information regarding amplitudes can be obtained from this analysis. A detailed description of the COMSOL linear acoustics solver is provided in the COMSOL Acoustics Module User's Guide [20].

Temperature distributions were specified along the tubes and manifold passages' axial directions. Temperatures were approximated as radially and tangentially constant inside each cylinder. Mean inlet and outlet manifold temperatures were specified, and it was presumed that when a single tube was heated, the temperature difference between its inlet and outlet would equal four times the temperature difference of the inlet and outlet mean temperatures.

A tetrahedral grid consisting of 40,342 elements, shown in Figure 5.1, was generated to simulate the fuel flow path used for the second test campaign. Quarter-inch diameter manifold cross passages connected the four parallel fuel tubes to the fuel inlet and outlet ports, the latter of which was larger in diameter. Both ports were treated as open-wall acoustic boundaries. A grid independence study was performed

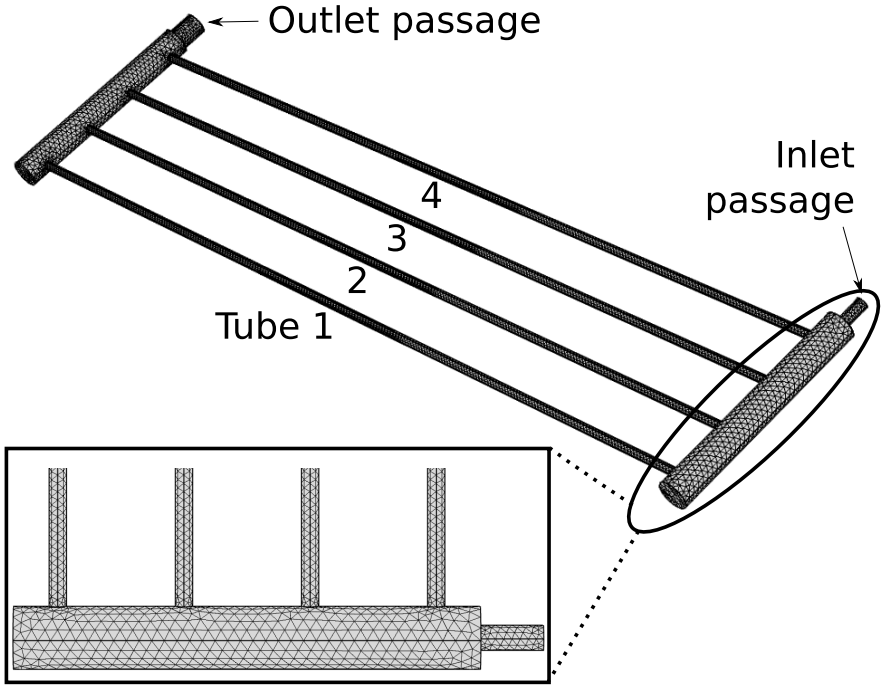

Figure 5.1. Tetrahedral mesh of fuel flow path used for acoustic simulation consisting of 40,342 elements

based on predicted frequencies to ensure accurate results, as illustrated in Figure 5.2 below.

The predicted frequency for a typical test case; in which T_{inlet}=300F, T_{outlet}=450F, p_{mean}=400psi, and only Tube 1 is heated; is plotted versus the number of grid elements in Figure 5.2. A simulation using a grid with 40,342 elements predicted a frequency within 1 Hz from that using a grid containing over ten times as many elements. This level of accuracy was deemed acceptable, thus the grid was used for all simulations.

A summary of simulated cases is shown in Table 5.1. These cases were chosen to determine the effect of several parameters on frequency: which tube is heated, inlet temperature, and pressure.

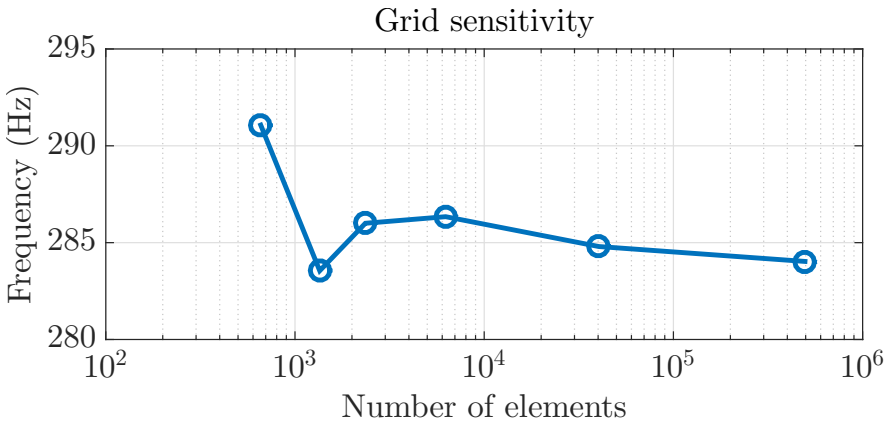

Figure 5.2. Fundamental frequencies obtained from grid sensitivity study for acoustic simulation; T_{inlet}=300F, T_{outlet}=450F, p_{mean}=400psi, only Tube 1 heated

Table 5.1: List of cases simulated with COMSOL acoustic model

T_{inlet} (F)	T_{outlet} (F)	Heated tubes	Pressure (psi)	Primary freq (Hz)
100	288	Tube 1	400	337.2
200	359	Tube 1	400	339.7
300	431	Tube 1	400	339.1
400	502	Tube 1	400	337.4
500	574	Tube 1	400	331.1
600	645	Tube 1	400	313.4
700	717	Tube 1	400	256.0
300	450	Tube 1	400	284.8
300	450	Tube 2	400	333.0
300	450	Tube 3	400	363.3
300	450	Tube 4	400	389.2
300	450	All tubes	400	1550.3
300	350	Tube 1	400	1585.2
300	400	Tube 1	400	1084
300	410	Tube 1	400	948.8
300	420	Tube 1	400	771.5
300	430	Tube 1	400	381.6
300	440	Tube 1	400	299.6
300	475	Tube 1	400	264.4
300	500	Tube 1	400	254.9
300	525	Tube 1	400	258.0
300	550	Tube 1	400	263.1
300	600	Tube 1	400	275.6
300	650	Tube 1	400	296.1
300	700	Tube 1	400	316.4

300	350	Tube 3	400	1638.5
300	400	Tube 3	400	1137.4
300	420	Tube 3	400	841.5
300	440	Tube 3	400	399.4
300	460	Tube 3	400	341.4
300	480	Tube 3	400	319.8
300	500	Tube 3	400	311.8
300	525	Tube 3	400	310.2
300	550	Tube 3	400	313.0
300	600	Tube 3	400	324.0
300	650	Tube 3	400	337.4
300	700	Tube 3	400	354.0
300	350	All tubes	400	1758.8
300	400	All tubes	400	1658.5
300	500	All tubes	400	1433
300	550	All tubes	400	1304.6
300	600	All tubes	400	1162.4
300	650	All tubes	400	1000.4
300	700	All tubes	400	793.9
300	725	All tubes	400	640.5
300	750	All tubes	400	361.3
300	800	All tubes	400	359.6
300	300	None	400	1851.9
300	450	Tube 1	450	311.4
300	450	Tube 1	500	344.1
300	450	Tube 1	550	400.5
300	450	Tube 1	600	470.0
300	450	Tube 1	700	602.5
300	450	Tube 1	800	699.5

300	450	Tube 1	900	772.9
300	450	Tube 1	1000	832.5

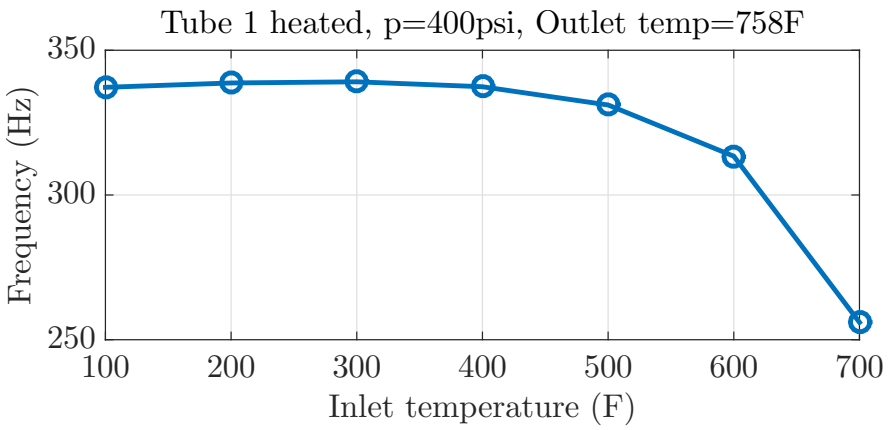

Figure 5.3. Predicted primary frequency versus inlet temperature for cases in which Tube 1 is heated, p=400 psi, T_{outlet}=758F

As explained in the previous chapter, experimental cases associated with accoustic oscillations had the following conditions: fuel inlet temperature was at or below 300F and tube heating was maximized to hardware constraints. The large amount of heat input most likely caused the fuel to be heated to a temperature in the neighborhood of the critical temperature. Several cases were simulated with varying inlet temperatures, and the heated tube's outlet temperature constant. Predicted oscillation frequencies for different inlet temperatures are plotted in Figure 5.3. Tube 1 was heated for all of these cases; the temperature distribution was approximated with a logarithmic profile, and mean pressure was fixed at 400psi. Cases with inlet temperatures under 400F yielded oscillations with consistent frequencies around 340Hz - the most commonly observed frequency in experiments. Inlet temperature had little effect on frequency within the range known to produce acoustic oscillations in experiments. Above this range, frequencies decreased with rising inlet temperature.

The acoustic mode associated with a 200F inlet temperature is depicted by Figure 5.4, a color plot in which regions of high acoustic pressure are shaded with warm colors. Hot fluid in the manifold allows the acoustic mode to enter that region. The

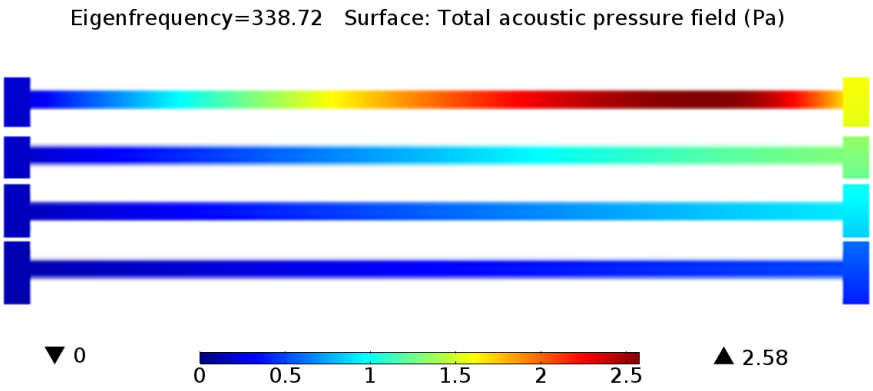

Figure 5.4. Acoustic pressure field for case in which Tube 1 is heated, p=400 psi, T_{inlet}=200F, and T_{outlet}=758F

aspect ratio of the geometry has been altered, and the manifold cross passages have been truncated in this figure to improve clarity.

Figure 5.5 depicts the primary accoustic oscillation frequency versus which tube was heated for test cases in which mean pressure was held at 400 psi, inlet temperature was maintained at 300F, and outlet temperature was maintained at 450F. Recall that the fuel inlet and outlet ports were located near Tube 4, as shown in Figure 3.1. Heating a tube far from the inlet and outlet ports caused low-frequency oscillations. Heating a tube near the ports caused high-frequency oscillations. This trend owes itself to the presence of hot fuel inside the manifold when far-away tubes are heated; this hot, compressible fuel allows for waves to stretch into the outlet manifold, resulting in oscillations having longer-wavelengths and lower frequencies. Conversely, when tubes near the ports are heated, the passages remain relatively cool; this cool, incompressible fuel does not participate as much in acoustic oscillations, so oscillations are constrained to the heated fuel tube.

Effective sound speeds were calculated based on the frequencies shown in Figure 5.5 and the corresponding distance between the heated tube inlet and manifold outlet. These effective sound speed calculations assume open tube resonance, and are plotted

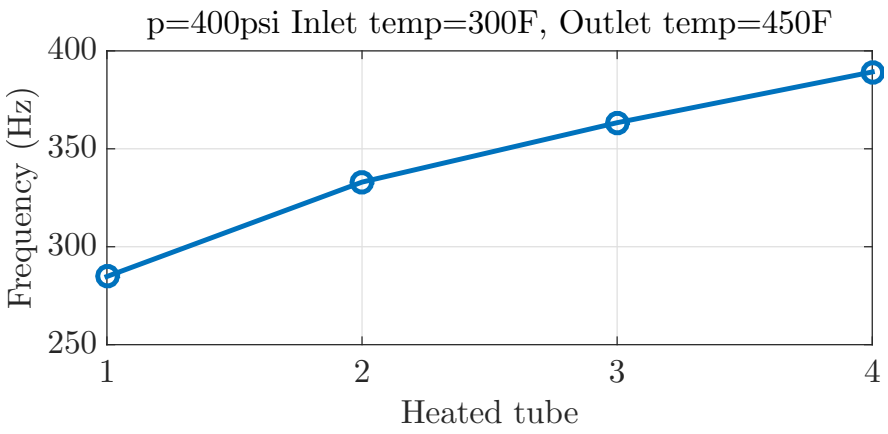

Figure 5.5. Predicted primary frequency versus which tube is heated for cases in which p=400 psi, T_{inlet}=300F, and T_{outlet}=450F

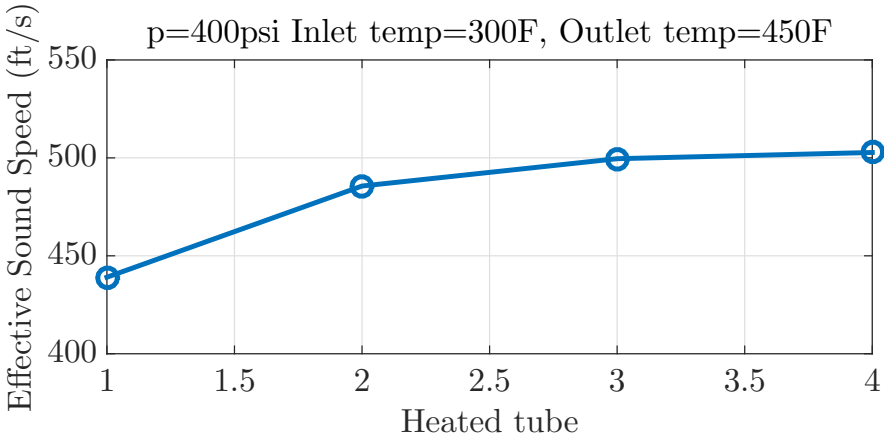

Figure 5.6. Predicted effective sound speed versus which tube is heated for cases in which p=400 psi, T_{inlet}=300F, and T_{outlet}=450F

in Figure 5.6. The resulting plot indicates that the effective sound speed follows the trend mentioned in the previous paragraph. This trend is not linear, however, because the temperature profiles and relationships between sound speed and temperature are highly nonlinear.

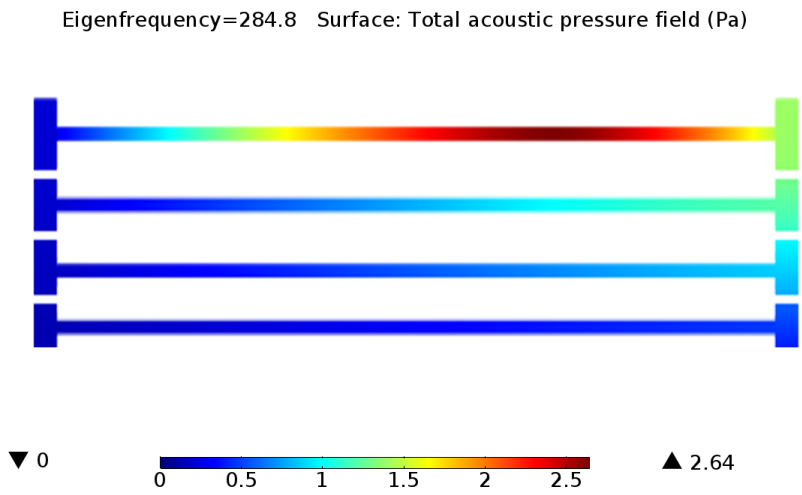

Figure 5.7. Acoustic pressure field for case in which Tube 1 is heated, p=400 psi, T_{inlet}=300F, and T_{outlet}=450F

The acoustic mode caused by heating Tube 1 is depicted by Figure 5.7, a color plot in which regions of high acoustic pressure are shaded with warm colors. Hot fluid in the manifold allows the acoustic mode to enter that region. Figure 5.8 depicts a case in which Tube 3 is heated; here, the acoustic mode remains more constrained inside the heated tube.

A limitation of this acoustic simulation used is that property profiles within each domain (i.e. tubes and manifolds) only vary in a single direction. To prevent erroneous results, temperature profiles at domain interfaces must be continuous. Temperatures inside the outlet manifold must, therefore, match tube outlet temperatures. For cases in which Tube 1 is heated, a gradual temperature decrease is imposed along the outlet manifold, which likely approximates the acutal temperature distribution reasonably well. In contrast, when Tube 4 is heated, a steep temperature rise and drop surrounding Tube 4 are imposed in order to match tube outlet temperatures while maintaining a manifold outlet temperature representing the average of the four tubes. Such a temperature profile is unrealistic, as the actual temperature distribu-

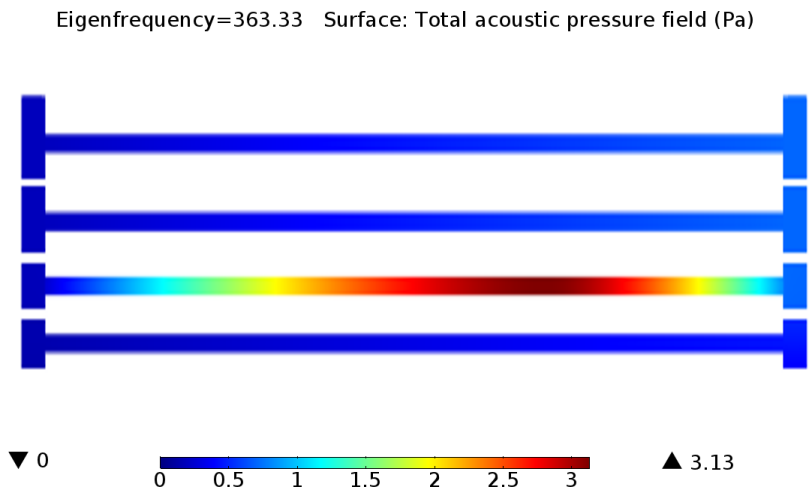

Figure 5.8. Acoustic pressure field for case in which Tube 3 is heated, p=400 psi, T_{inlet}=300F, and T_{outlet}=450F

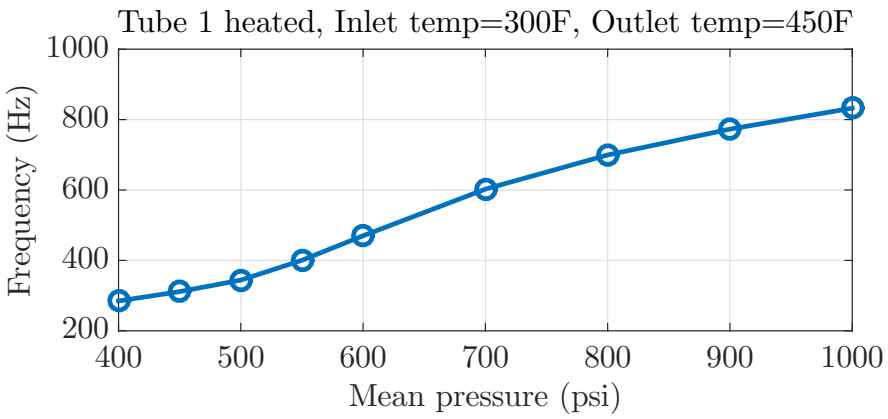

Figure 5.9. Predicted primary frequency versus mean pressure for cases in which Tube 1 is heated, T_{inlet}=300F, and T_{outlet}=450F

tion for this case is highly two-dimensional. In conclusion, more confidence can be placed in simulations in which a tube far from the outlet ports was heated than those in which a tube near the inlet was heated.

Figure 5.9 depicts the primary accoustic oscillation frequency versus mean pressure for test cases in which Tube 1 was heated, mean pressure was held at 400 psi, and inlet temperature was maintained at 300F. Sound speed correlates directly with pressure, and accordingly, the simulation predicts higher frequencies for higher mean pressures.

Figure 5.10 depicts the primary accoustic oscillation frequency versus system-wide temperature for test cases in which the mean pressure was held at 400 psi. No heat is input to the tubes for these cases. The frequencies vary with the speed of sound of the fluid. However, oscillations under these conditions would not be thermoacoustic in nature because no temperature gradient exists within the flowpath.

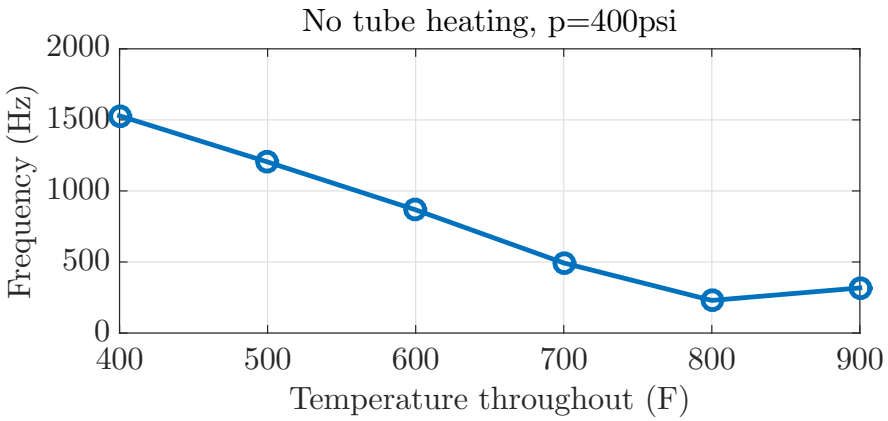

Figure 5.10. Predicted primary frequency versus system-wide temperature for cases in which p=400 psi

6. CONCLUSIONS

Measurable pressure oscillations have been generated under flow conditions and geometry relevant to fuel-air heat exchangers for gas turbine engines. Bulk mode oscillations, such as those shown in Figure 6.1, were observed with frequencies on the order of 1Hz and amplitudes of 1-10 psi. Acoustic mode oscillations, such as those shown in 6.2, were observed with frequencies on the order of 100-1000Hz, and with amplitudes from 0.1-1.0 psi.

Bulk mode oscillations were originated from an external fuel preheater rather than the test section itself; bulk-mode amplitudes were correlated with preheater exit temperature. Acoustic-mode oscillations originated inside the heated test section tubes; although they occurred at low pressure amplitudes with respect to the structural

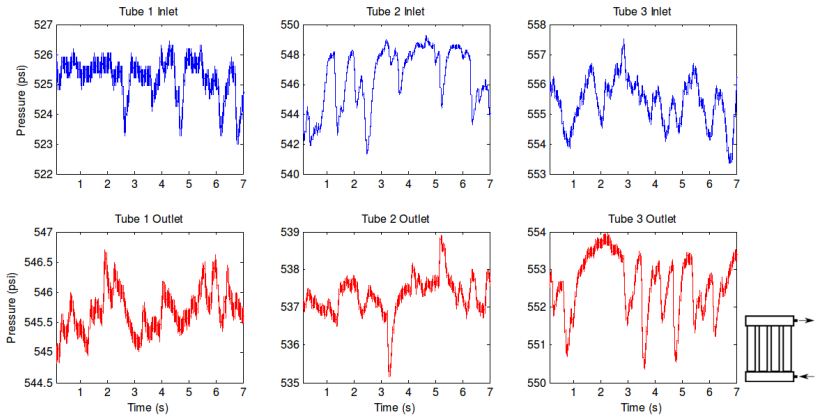

Figure 6.1. Case 5b pressure traces (T_{inlet}=500degF, p=500 psi, no nitrogen flow)

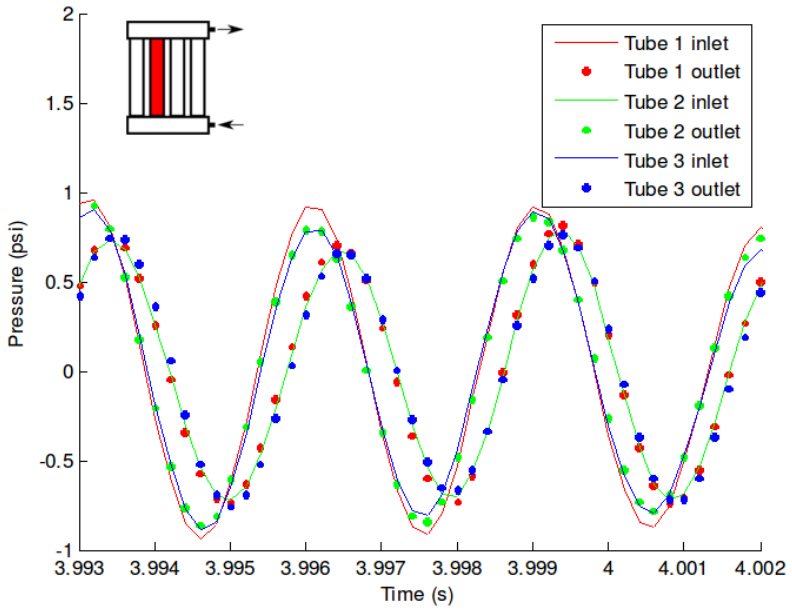

Figure 6.2. Case 7a pressure trace

strength of metal tubes, these high frequency oscillations do pose a high-cycle fatigue risk for heat exchanger components.

Conditions conducive to acoustic-mode oscillations consist of low fuel preheating and large amounts of heating inside the test section. Oscillations tend to occur in such settings because of the large temperature gradients, and associated density gradients, these conditions provide. The experimental hardware was capable of flowing nitrogen across fuel tubes at roughly 900F, which is 150F higher than the critical temperature of Jet-A fuel. The spike in the fuel's specific heat near the critical temperature, depicted by Figure 4.13, created a natural heating barrier near the critical temperature. Therefore, most cases with acoustic-mode oscillations were heated to near-critical temperatures.

The most common oscillation frequency was around 340 Hz. These oscillations are hypothesized to originate from a single heated fuel tube and travel into the fuel manifolds. This oscillation mode was predicted by a COMSOL acoustic model, in which realistic one-dimensional temperature profiles were input. Inlet temperature had little effect on the frequency of this mode in both experimental and simulated test cases. Inlet pressure signals remained in phase with one another, and outlet pressure signals remained in phase with one another. The inlet and outlet pressure signals were offset by a phase lag that was a function of the diameter of the fuel manifolds' cross passages; large cross passage diameters yielded larger phase lags.

The second most common oscillation frequency was 280 Hz. Alongside it was often its subharmonic oscillation at 140Hz. These modes were often observed when tubes far from the fuel outlet passage (i.e. Tubes 1 and 2) were heated. A simple calculation, shown in Equations 4.1 and 4.2, indicates that if an effective speed of sound is calculated based on the length of a heated tube and a frequency of 340Hz, the characteristic frequency of the heated tube plus the outlet manifold passage is around 280 Hz. Inlet and outlet signals are all in phase for the 140Hz mode, but are offset by a phase lag for the 280 Hz mode. This would indicate that the 280 Hz mode

corresponds to a 2L open-tube resonance mode, whereas the 140 Hz signal shows half-wave resonance.

6.1 Recommendations for Future Work

In the present study, heat input was varied coarsely, and was not accurately measured. The measurement of tube wall temperature at multiple axial locations would allow for the calculation of heat input into the fuel; such a measurement could be made with an infrared camera placed with each of the tubes in view, or thermocouples welded to the fuel tubes. Fine sweeps of heat input could be performed to determine the power required for the onset of acoustic-mode instabilities. Effort was made for the present study to describe the shape and character of several commonly-occurring acoustic modes based on observations from experiments and a preliminary acoustic simuation. However, more sophisticated acoustic simulations with three-dimensional property variations could aid in the accurate prediction of mode shapes. Fluid simulations considering the effect of mean flow could further improve accuracy.

The equipment used for experiments was incapable of generating bulk-mode oscillations in Jet-A fuel within the heated test section. Bulk-mode instabilities could be studied within the current flow geometry by either heating nitrogen with a more powerful heater or choosing a simulent to Jet-A with a lower critical temperature, such as methanol or a variety of refrigerants.

By measuring the amount of heat input required to induce oscillations at a variety of flow conditions, one may attempt the formulation of a stability criterion using dimensionless analysis. Such a dimensionless analysis has been performed on a data set from an experiment in which a single tube was heated, and is included in Appendix A.

REFERENCES

REFERENCES

[1] C Sondhaus. Ueber die Schallschwingungen der Luft in erhitzten Glasroehren und in gedeckten Pfeifen von ungleicher Weite. *Annalen der Physik*, 1850.

[2] H. A. Kramers. Vibrations of a gas column. *Physica*, 15(11-12):971, 1949.

[3] Vijay Chatoorgoon. Supercritical Flow Stability in Two Parallel Channels. volume 2006, pages 723–730. ASME, 2006.

[4] Daniel Fritsche. *Origin and Control of Thermoacoustic Instabilities in Lean Premixed Gas Turbine Combustion*. PhD thesis, Swiss Federal Institute of Technology Zurich, 2005.

[5] Jerry D. Griffith. An investigation of the mechanism of heat transfer near the critical state of a fluid, 1960.

[6] W. S. Hines and H Wolf. Pressure Oscillations Associated With Heat Transfer to Hydrocarbon Fluids at Supercritical Pressures and Temperatures. *ARS Journal*, 32(3):361–366, January 1962.

[7] Diane Linne, Michael Meyer, Donald Braun, and Dennis Keller. Investigation of Instabilities and Heat Transfer Phenomena in Supercritical Fuels at High Heat Flux and Temperatures, July 2000.

[8] Nikolaus Rott. Damped and thermally driven acoustic oscillations in wide and narrow tubes. *Zeitschrift fr Angewandte Mathematik und Physik (ZAMP)*, 20(2):230–243, 1969.

[9] Nikolaus Rott. Thermally Driven Acoustic Oscillations. Part II: Stability Limit for Helium. *Journal of Applied Mathematics and Physics*, 24, 1973.

[10] L.E. Faith, G.H. Ackerman, and H.T. Henderson. Heat Sink Capability of Jet A Fuel: Heat Transfer and Coking Studies. Technical report, Shell Development Company, July 1971.

[11] Brad Hitch and Michael Karpuk. Enhancement of Heat Transfer and Elimination of Flow Oscillations in Supercritical Fuels. Technical Report AIAA-98-3759, 1997.

[12] Neal Herring. *On the Development of Compact, High Performance Heat Exchangers for Gas Turbine Applications*. PhD thesis, Purdue University, August 2007.

[13] Michael Palumbo. *Predicting the Onset of Thermoacoustic Oscillations in Supercritical Fluids*. PhD thesis, Purdue University, October 2009.

[14] R. S. Thurston. Pressure Oscillations Induced by Forced Convection Heat Transfer to Two Phase and Supercritical Hydrogen. Technical Report LAMS-3070, Los Alamos Scientific Laboratory, February 1964.

[15] R. D. Blevins and M. M. Bressler. Acoustic Resonance in Heat Exchanger Tube BundlesPart I: Physical Nature of the Phenomenon. *Journal of Pressure Vessel Technology*, 109(3):275–281, August 1987.

[16] R. D. Blevins and M. M. Bressler. Acoustic Resonance in Heat Exchanger Tube BundlesPart II: Prediction and Suppression of Resonance. *Journal of Pressure Vessel Technology*, 109(3):282–288, August 1987.

[17] R. E. Sullivan F. L. Eisinger. Unusual acoustic vibration in heat exchanger and steam generator tube banks possibly caused by fluid-acoustic instability. *Journal of Engineering for Gas Turbines and Power; (United States)*, 115:2, 1993.

[18] Anthony F Mills. Error Analysis of Experiments - a Manual for Engineering Students, 2004.

[19] Cross-correlation - MATLAB xcorr.

[20] COMSOL. Acoustics Module Users Guide, May 2013.

[21] Hui Wang, Jin Zhou, Yu Pan, and Ning Wang. Experimental investigation on the onset of thermo-acoustic instability of supercritical hydrocarbon fuel flowing in a small-scale channel. *Acta Astronautica*, 117:296–304, December 2015.

APPENDICES

A. ANALYSIS OF PALUMBO'S SINGLE-TUBE EXPERIMENT

A.1 Introduction

The objective of the present study is to more accurately predict the onset of thermoacoustic instabilities under conditions relevant to hydrocarbon-based aviation fuel systems. In order to safely and cheaply perform experiments, a simulant fluid was selected to replicate a typical hydrocarbon fuel. Using the simulant fluid, a range of variables believed to influence thermoacoustic oscillations will be examined. Dimensionless groups of these variables have been created, from which a stability criterion has been established. Additionally, a one-dimensional CFD code will be written to aid characterization of oscillations observed in experiments.

A.2 Facility Description

Fig. A.1 is a summary of the main facility hardware. Methanol test fluid is loaded into the run tank and pressurized with nitrogen. A pneumatic valve is used to connect or disconnect the methanol tank with the test section. A Coriolis flow meter between the tank and pneumatic valve measures the mass flow rate of the test fluid. The fluid continues to a filter, and then an electric preheater, which consists of an array of tubes sandwiched by copper blocks heated with cartridge heaters. The preheated fuel then enters the test section, which consists of a tube undergoing electric resistance heating. The test section is electrically insulated on each end with isolation flanges. Downstream of the test section, the fluid passes through a cooling bath, filter, flow control valve, sampling station, and finally a waste drum. A manual valve provides

nitrogen for purging the test section.

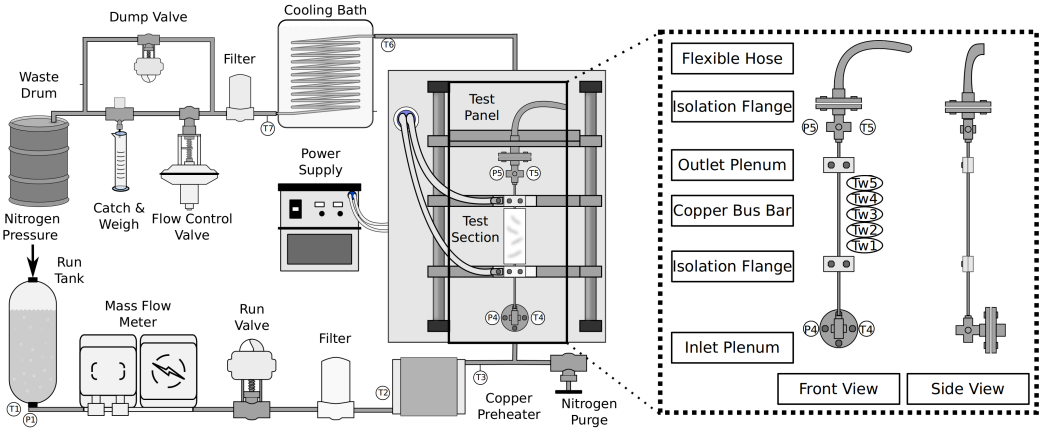

Figure A.1. Overall facility schematic.

The fluid enters the apparatus via the bottom isolation flange where it makes a 90-degree turn and flows vertically through the inlet plenum. The fluid then enters the test section where it enetually enters the heated length of the test section, which is the length between the electrical bus bars. The fluid then enters the outlet plenum and exits via the isolation flange and a flexible hose.

Type K thermocouples were mounted in both the inlet and outlet plenums. The tubes tested were too small to accomodate thermocouples, so only outer wall temperatures were measured along the test section. Ungrounded thermocouples were selected despite their relatively slow response times in order to minimize instrumentation noise from the resistively-heated tube. Thermocouple locations are shown in Fig. A.1 as annotations with the letter T. Wall temperatures are designated with a 'w' subscript; fluid temperatures are designated with no subscript.

Kulite ETL-GTS-190 (M) pressure transducers were placed in the inlet and outlet plenum. These transducers are rated to temperatures up to 1025F and pressures of 3000 PSI. The special high frequency amplifier allows the transducer to be used up to 150 KHz. Data recorded during experiments were sampled at 4 KHz. Transducer locations are shown in Fig. A.1 as annotations with the letter P. Tab. A.1 lists values for parameters varied throughout the experiments. The chosen reduced pressures of 1.0, 1.2, and 1.4 correspond to pressures of 1175, 1410, and 1645 psi.

Test Parameters			
Heated Length	ℓ	[in]	4,6
Tube O.D.	D_{out}	[in]	0.125
Tube I.D.	D_{in}	[in]	0.027,0.069,0.093
Reduced Pressure	p_r		1.0,1.2,1.4
Mass Flow	$\dot{m}$	[$\frac{lbm}{hr}$]	4,5,6,7
Heat Input	$\dot{Q}$	[Watts]	0-800

Table A.1. Thermoacoustic testing matrix for methanol

Tab. A.2 lists distances between major components of the experiment.

A.3 Measurements

Unfiltered pressure traces obtained near the tube inlet and tank, as well as a mass flow rate trace, are shown in Fig. A.2. Test section wall temperatures are shown in Fig. A.3. Seven probes were evenly spaced along the tube; however, the fifth and sixth thermocouples from the inlet failed, so results from the seventh have been assigned to the T_{w5}. Fluid temperatures measured at the heated tube inlet and exit are also included.

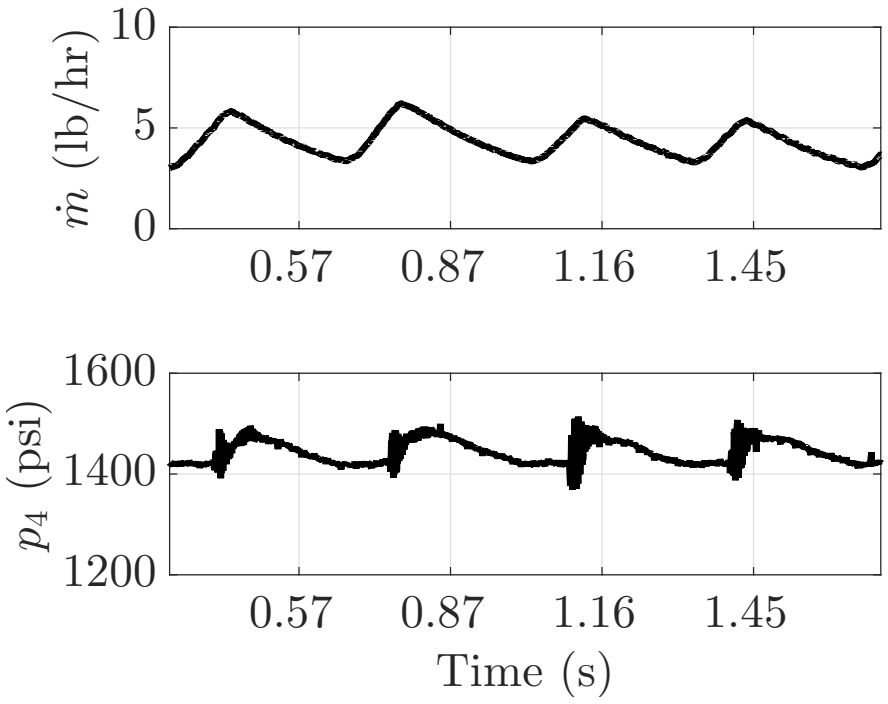

Figure A.2. Unfiltered mass flow rate, tank pressure, and tube inlet pressure of a sample selected case: $\dot{Q}$ =550W, D_{in} =0.069in, ℓ =6in, $\dot{m}$ =5lb/hr, P_r =1.2

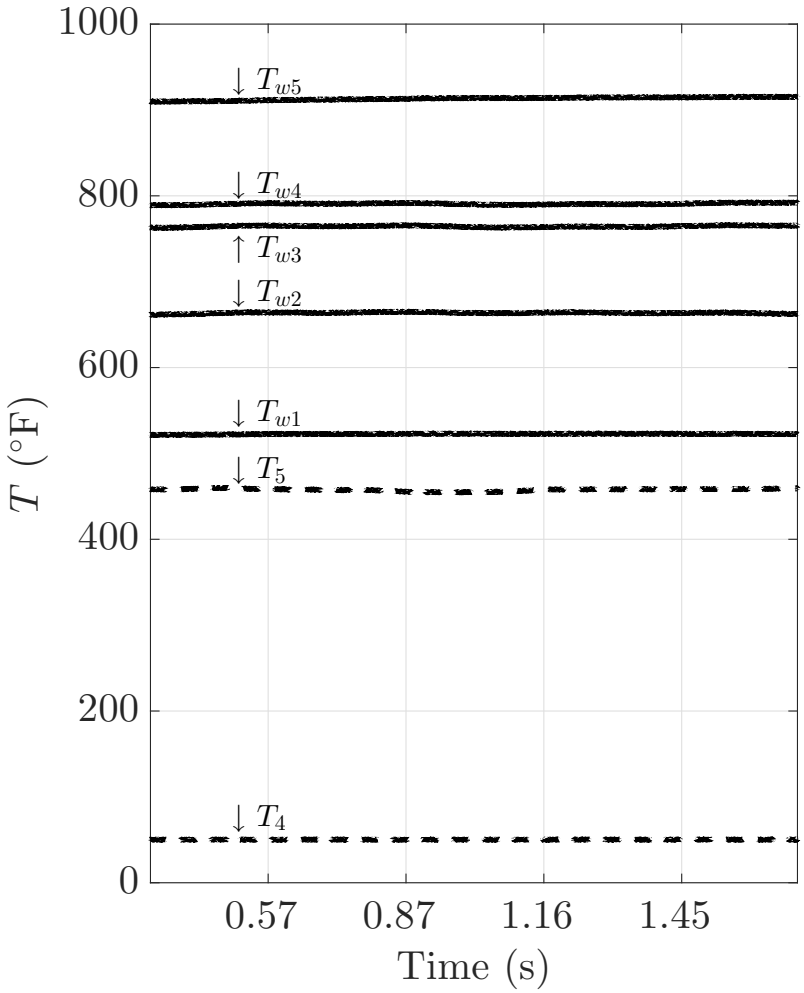

Figure A.3. Unfiltered temperature traces of a sample selected case: $\dot{Q}$ =550W, D_{in} =0.069in, ℓ =6in, $\dot{m}$ =5lb/hr, P_r =1.2

Table A.2. Distances along fuel flow path.

Flow Lengths		
Tank to preheater	L_{12}	6 ft
Preheater inlet to exit	L_{23}	16 in
Preheater exit to test section inlet	L_{34}	22 in
Test section inlet to outlet	L_{45}	9.5 or 11 in
Test section outlet to cooling bath inlet	L_{56}	21 in
Cooling bath inlet to exit	L_{56}	80 ft
Cooling bath exit to control valve	L_{67}	2 ft

Oscillations are most prominently displayed in pressure traces near the test section tube and the mass flow rate measurements. Throughout the test campaign, similar to previous studies, two modes of oscillations were detected: the acoustic mode, characterized by frequencies of 100-500 Hz; and the bulk mode, characterized by frequencies from 1-5 Hz. Bulk mode oscillations tend to have amplitudes of over one order of magnitude larger than the acoustic mode. The case illustrated in Figs. A.2-A.3 is representative of the test campaign; both oscillation modes are present, but the bulk mode dominates.

Bulk-mode oscillations are visible in some wall temperature traces, but the amplitudes here are much smaller than those in the tube pressure and mass flow rate. These wall temperature signals undergo damping and lag due to the thermal resistance of the stainless steel tube. The bulk-mode is not well-displayed by thermocouples located anywhere in the flow-path; this may be because the thermocouples are located in wide plenums in which significant mixing occurs, interfering with the temperature oscillations due to bulk-mode oscillations. Because tube pressure and mass flow rate measurements displayed the strongest oscillations, these measurements were cho-

sen for the characterization of the phenomena and in the formulation of a stability criterion.

A.4 Data Analysis

Data from the thermoacoustic instability test article have been analyzed to determine thresholds of several flow parameters for the occurrence of oscillations. Independent variables include mean pressure (p_{mean}), fuel mass flow rate ($\dot{m}$), heated tube diameter (D_{in}), heat input ($\dot{Q}$), fuel density (ρ), and fuel viscosity (μ). Density and viscosity were considered at the heated tube inlet. The dependent variable was the pressure amplitude of the major acoustic mode.

A non dimensional analysis was performed in the interest of finding a window of all independent variables that is non-conducive to oscillations. The Buckingham Pi method yielded four dimensionless groups defined by Eq. A.1.

$$\Pi_1 = \frac{D_{in}^4 \rho p_{mean}}{\dot{m}^2}, \Pi_2 = \frac{D_{in}^4 \rho p_{amp}}{\dot{m}^2}, \Pi_3 = \frac{D_{in}^4 \rho^2 \dot{Q}}{\dot{m}^3}, \Pi_4 = \frac{D_{in}\mu}{\dot{m}} = \frac{const}{Re_D} \tag{A.1}$$

The significance of these dimensionless groups are as follows: Π_1 relates mean pressure and dynamic pressure. Π_2, the only output group, relates pressure oscillation amplitude and dynamic pressure. Π_3 relates thermal and kinetic energy transport. Π_4 acts like the Reynolds number for internal flow, relating viscous forces and momentum forces.

Eighty eight test cases were selected for examination from the 175 cases of Palumbo's entire data set. Cases with strong and consistent acoustic oscillations having distinct major frequencies were chosen for analysis. Fig. A.4 shows example pressure and mass flow rate waveforms of a selected case. Thick solid lines indicate signals filtered to only pass the major frequency; dashed lines indicate raw signals.

Figure A.5 plots Π_2 (dimensionless pressure amplitude) versus Π_3 (dimensionless heat input). Each line in the plot represents a range of Π_1 (dimensionless mean pressure) values; the median of each Π_1 range is denoted on the legend. All values of Π_4

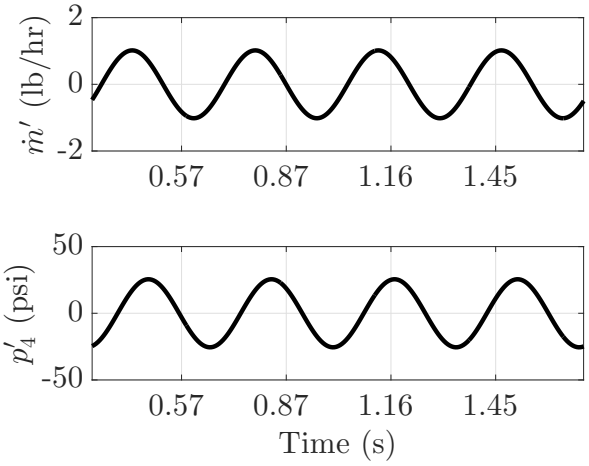

Figure A.4. Mean-subtracted mass flow rate, tank pressure, and tube inlet pressure of a sample selected case: $\dot{Q}$ =550W, D_{in} =0.069in, ℓ =6in, $\dot{m}$ =5lb/hr, P_r =1.2

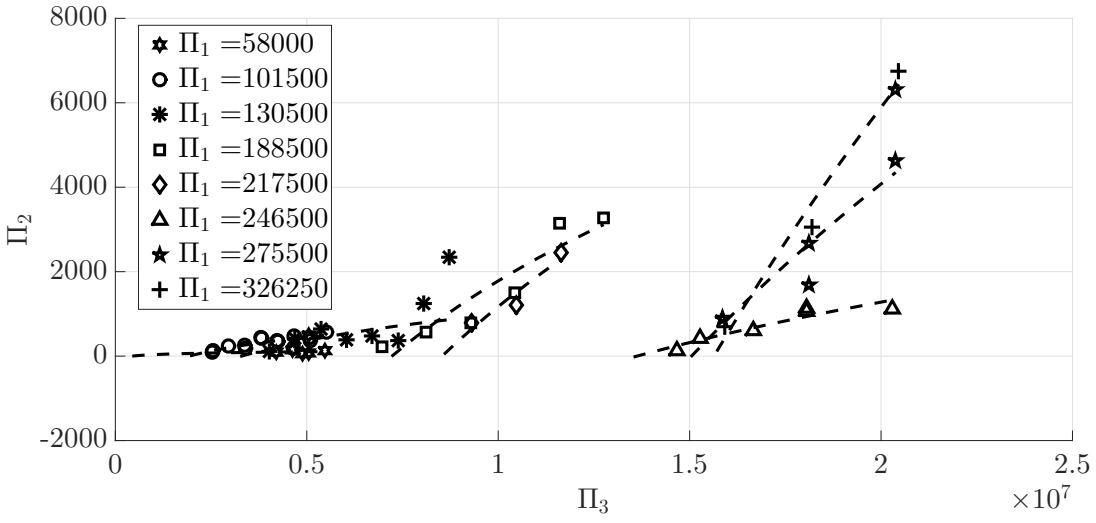

Figure A.5. Dimensionless pressure amplitude versus dimensionless heat input

(inverse Reynolds number) were included in the plot indiscriminately, as the entire range of its values was relatively small.

Unsurprisingly, the oscillation amplitude group tends to increase as the power input group increases. A test case is considered stable if Π_2, the dimensionless group representing pressure amplitude, is near zero. Therefore, for each Π_1 line, the location of the x intercept represents the threshold dimensionless power input required for oscillations to occur. This threshold power increases monotonically with increasing Π_1 (dimensionless mean pressure).

A predictive stability criterion, shown in Eq. A.2, quantifies the critical dimensionless power causing oscillations as a function of dimensionless mean pressure.

$$\Pi_{3,crit} = f(\Pi_1) \tag{A.2}$$

Figure A.6 plots $\Pi_{3,crit}$ (critical dimensionless power) for several values of Π_1 (dimensionless mean pressure). Operating points beneath this curve would be predicted as stable, and those above would be predicted to exhibit oscillations. A power-law regression for $\Pi_{3,crit}$ versus Π_1, is shown in Eq. A.3.

$$\Pi_{3,crit} = 8.643{\Pi_1}^{1.155} - 2.945 \times 10^6 \tag{A.3}$$

A linear regression for $\Pi_{3,crit}$ versus Π_1, in which the y-intercept is forced to equal zero, is shown in Eq. A.4.

$$\Pi_{3,crit} = 46.2\Pi_1 \tag{A.4}$$

Substituting variables for the dimensionless groups and canceling like terms yields the approximate maximum heat input for non-oscillating flow as a function of mean pressure, mass flow rate, and fluid density. This relation is given in Eq. A.5.

$$\dot{Q}_{crit} = 46.2\frac{p_{mean}\dot{m}}{\rho} \tag{A.5}$$

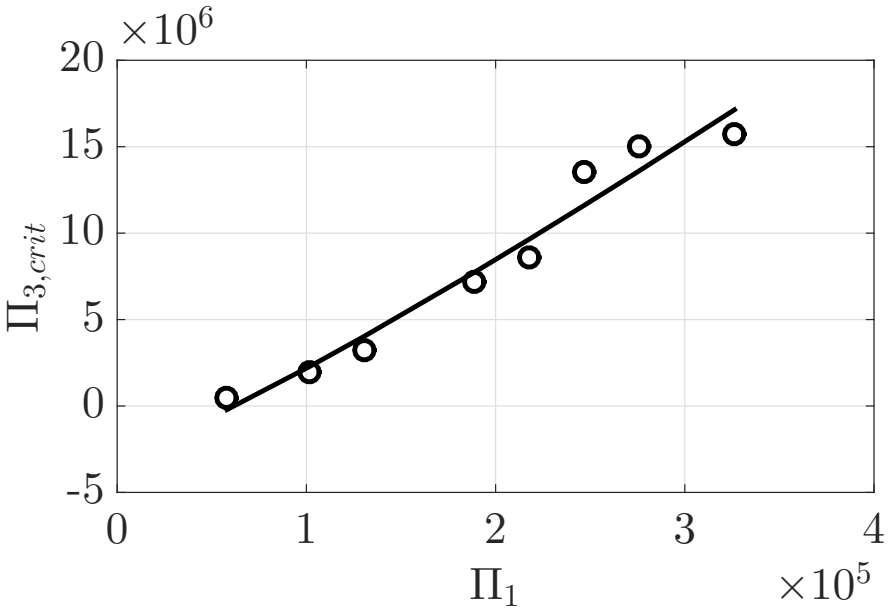

Figure A.6. Critical dimensionless heat input versus dimensionless mean pressure

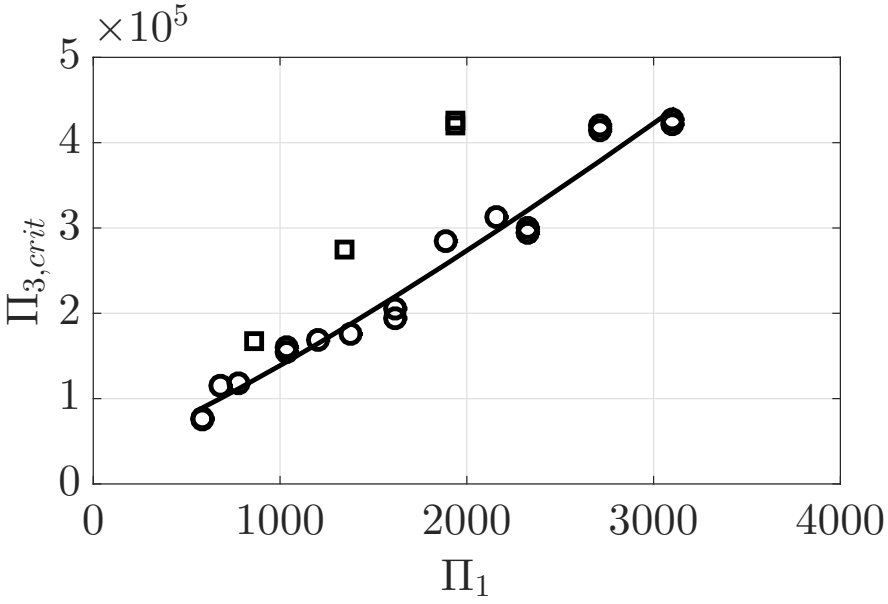

Figure A.7. Critical dimensionless heat input versus dimensionless mean pressure for all 24 non-preheated cases from Wang et al. Cases performed at p=2.5MPa designated by squares.

A.5 Comparison with Wang et al. Data

Wang et al. [21] heated RP-3 to supercritical temperatures, and investigated thermoacoustic oscillations therein. The method of generating a stability criterion discussed in the previous section shall be used with the data set reported by Wang et al. Cases with preheating were excluded from this analysis. Figure A.7 depicts $\Pi_{3,crit}$ (critical dimensionless power) for several values of Π_1 (dimensionless mean pressure). Operating points beneath this curve would be predicted as stable, and those above would be predicted to exhibit oscillations.

Although a trend is evident, notable outliers exist on this plot. The worst outliers corresponded to cases run with p=2.5MPa, which was the lowest pressure setting run by Wang et al. This pressure corresponds to a reduced pressure of 1.09. These five points, designated by squares in Fig. A.7, were excluded from the curve fit. The

remaining 19 points, designated by circles, produced a much stronger trend. Several factors may prevent the stability analysis from correctly predicting the threshold power for low-pressure cases. The fuel may have unintentionally been pressurized to a subcritical pressure in the lowest-pressure setting cases, due to either abnormal fuel composition or pressure transducer error. Although this cannot be proven, the behavior does match that which may be expected with subcritical-p fluids: the fluid remains stable throughout the liquid phase, but will eventually exhibit instabilities once sufficient power is input to boil a significant amount of the fuel. The energy required to undergo actual boiling is larger than that required for pseudo-boiling.

A power-law regression for $\Pi_{3,crit}$ versus Π_1 for Wang et al. data is shown in Eq. A.6.

$$\Pi_{3,crit} = 27.29{\Pi_1}^{0.7186} - 3.412 \times 10^4 \tag{A.6}$$

A linear regression for $\Pi_{3,crit}$ versus Π_1, in which the y-intercept is forced to equal zero, is shown in Eq. A.7.

$$\Pi_{3,crit} = 139.1\Pi_1 \tag{A.7}$$

Substituting variables for the dimensionless groups and canceling like terms yields the approximate maximum heat input for non-oscillating flow as a function of mean pressure, mass flow rate, and fluid density. This relation is given in Eq. A.8.

$$\dot{Q}_{crit} = 139.1\frac{p_{mean}\dot{m}}{\rho} \tag{A.8}$$

Although the correlation for Wang's results does not match that for Palumbo's, the general behavior is the same: critical dimensionless power scales nearly linearly with dimensionless mean pressure. The two correlations merely differ by their coefficients. This coefficient may be a function of variables not captured within the dimensionless groups selected, such as flow path geometry (viz. tube length or heated length) or fluid properties. More experiments would need to be performed in order to determine how to predict this coefficient.

B. Supplementary Material

B.1 Test Procedures

The following test procedures were performed for all experiments.

Section 1: Pre-test setup

			Test Numbers			
Step #		**Operation**				
1.000		VERIFY no lightning storms occuring within 10 miles				
1.001		VERIFY the test article and instrumentation are installed per the test plan and the appropriate drawings				
1.002		VERIFY Instrumentation Power & Valve Power switches are OFF				
		TURN ON Magma chassis				
1.003		START both computers				
1.004		START DataFlex system				
1.005		Turn on SCXI Chassis Power				
1.006		Turn on Instrumentation Power				
1.007		Set Active DAQ configuration in MAX (under Tools/Traditional NI-DAQ Configuration/)---filepath: C:\\Documents and Settings\Test Operator\Desktop\Master (select file with most recent date in name)				
1.008		Repeat step above to ensure DAQ configuration is loaded				
1.009		Close MAX				
1.010		Open SIR LabView program				
1.011		Run VI				
1.012		Verify the data on display				
1.013		Open the "File and Data Details" tab				
1.014		Verify all file directories are correct				
1.015		Switch "Manual Acquire" to true				
1.016		Switch "Obtain Zero Data" to true				
1.017		Wait for "Obtain Zero Data" switch to reset to false				
1.018		Switch "Display Zero Data" to true				
1.019		Switch "Set File Details" to true				
1.020		Switch the "Acquire Data" switch to true for about five seconds to obtain zero data				
1.021		On hi-freq computer, launch DSPCon software				
1.022		VERIFY pressure transducer settings are correct				
1.023		CLICK Record; take 5 seconds of zero data.				
1.024		Log zero data files for both hi-freq and lo-freq systems				
1.025		Turn on cell video cameras power				
1.026		Verify that video cameras, microphones, and monitors are in position and functioning				
1.027		Proceed to Gas Turbine Cell				
1.028		Verify CO2 fire extinguisher is in place				
1.029		TURN ON power to dissolved O2 sensor and flow meter transmitter (power strip behind flow meter transmistters)				
1.030		VERIFY operation of dissolved O2 sensor				
1.031		Clear the test area of all extraneous personnel				
1.032		Close and lock courtyard gates				
1.033		Place courtyard key in GT control room, in a visible area				
1.034		Fill cooling bath with water				
1.035		Connect cooling bath and backpressure valve CV-SIR-001 to manifolds.				
1.036		Ensure waste drum is not too full for test.				
1.037		Connect backpressure valve to waste drum.				
1.038		Ensure fuel tube from preheater is connected to SIR				
1.039		Verify Fuel System Purge Pressure Reg **MR-GT-00** is unloaded				
1.040		Verify N2 100 psi Pilot Pressure Reg **MR-GT-01** is unloaded				
1.041		Verify Fuel Purge Reg **MR-GT-02** is unloaded				
1.042		Verify Fuel Sparging System Pressure Reg **MR-GT-03** is unloaded				
1.043		CLOSE N2 100 psi Pilot Pressure Isolation Valve **MV-GT-01**				
1.044		CLOSE N2 Sparge Valve **MV-GT-03**				
1.045		CLOSE N2 Purge Valve to ACE Rig (green, on control room wall)				
1.046		OPEN N2 Purge Valve to SIR (black, on control room wall)				
1.047		Place the Main Liquid Fuel Panel 3-Way Selector Valve in SIR Position				
1.048		Place the N2 Purge 3-Way Selector Valve near rig in SIR position				
1.049		Disconnect ACE Rig 1/4" Fuel Line *(if applicable)*				
1.050		Ensure High Frequency Pressure transducers are plugged into system.				
1.051		Verify correct sonic venturi is installed upstream of secondary air heater				
1.052		Verify SIR is the only rig connected to secondary air (ask rig owners to disconnect their rigs)				

			Test Numbers			
Step #		**Operation**				
Prepare Nitrogen Supply						
1.053		If lab nitrogen is already up, proceed to step 1.079				
1.054		Proceed to Ox Room				
1.055		UNLOAD 1500 psi Pilot Source Pressure Regulator **MR-N2-04**				
1.056		CLOSE 1500 Pilot Pressure Source Isolation Valve **MV-N2-11**				
1.057		UNLOAD 100 psi Pilot Source Pressure Regulator **MR-N2-03**				
1.058		CLOSE 100 psi Pilot Source Pressure Isolation Valve **MV-N2-10**				
1.059		UNLOAD Fuel Trickle Purge Pressure Regulator **MR-N2-02**				
1.060		CLOSE Fuel Trickle Purge Isolation Valve **MV-N2-07**				
1.061		UNLOAD Ox Trickle Purge Pressure Regulator **MR-N2-01**				
1.062		CLOSE Ox Trickle Purge Isolation Valve **MV-N2-08**				
1.063		UNLOAD Cell C Trickle Purge Regulator **MR-204**				
1.064		CLOSE Cell C Trickle Purge Isolation Valve				
1.065		Proceed to Nitrogen Tube Trailer				
1.066		VERIFY Nitrogen Supply Vent Valve **MV-N2-05** (black valve connected to tee) is CLOSED				
1.067		OPEN Nitrogen Trailer Main Supply Isolation Valve **MV-N2-04**				
1.068		OPEN Nitrogen Source Start-Up Valve **MV-N2-06**				
1.069		OPEN Trickle Purge & Pilot Pressure Isolation Valve **MV-N2-09**				
1.070		OPEN all Nitrogen Tube Trailer valves SLOWLY				
1.071		Return to Ox Room				
1.072		VERIFY that 1/2" Nitrogen Line Pressure **PG-8** has equalized with Nitrogen Tube Trailer Pressure **PG-1.** Make sure there's enough pressure; notify Scott if it's running low (<3000 psi)				
1.073		OPEN Cell C Trickle Purge Regulator Isolation Valve **MV-N2-204**				
1.074		LOAD Cell C Trickle Purge Regulator **MR-204** to 20 psig				
1.075		OPEN Ox Trickle Purge Regulator Isolation Valve **MV-N2-08**				
1.076		LOAD Ox Trickle Purge Pressure Regulator **MR-N2-01** to 20 psig				
1.077		OPEN Fuel Trickle Purge Regulator Isolation Valve **MV-N2-07**				
1.078		LOAD Fuel Trickle Purge Pressure Regulator **MR-N2-02** to 10 psig (Never higher than Ox Trickle Purge)				
1.079		Proceed to Deluge Room				
1.080		Switch Secondary Air Heater Control Toggle Switch to Gas Turbine Cell Control (switch down, verify blue light on)				
1.081		Proceed to Gas Turbine Test Cell				
1.082		OPEN **MV-GT-01** 100 psi pilot pressure valve *for valve actuation*				
1.083		LOAD N2 100 psi Pilot Pressure Regulator **MR-GT-01** to 100 psig				
Verify the Remotely Controlled Valves Operate Properly						
1.084		Verify All Valves on VI are in De-Energized State				
1.085		Turn on Gas Turbine Valve Power Toggle Switch in the Control Room				
1.086		Turn on Valve Power switch in Gas Turbine Instrument Room				
1.087		CYCLE and verify **PV-FU-001** (Main Fuel Isolation Valve)				
1.088		CLOSE **PV-FU-001**				
1.089		CYCLE and verify **PV-FU-004** (SIR fuel panel fuel valve)				
1.090		CLOSE **PV-FU-004**				
1.091		CYCLE and verify **PV-N2-004** (SIR fuel panel nitrogen purge valve)				
1.092		OPEN **PV-N2-004**				
1.093		CYCLE and verify **CV-SIR-001** (SIR backpressure valve)				
1.094		SET **CV-SIR-001** to 100%				
1.095		CYCLE and verify **PV-GT-03** (Nitrogen isolation valve)				
1.096		CLOSE **PV-GT-03**				
1.097		CYCLE and verify **RR-GT-03** (Nitrogen control valve)				
1.098		SET **RR-GT-03** to 0%				
1.099		CYCLE and verify **CV-FU-001** (fuel control valve)				
1.100		SET **CV-FU-001** to 0%				
1.101		CYCLE and verify louver control servo motors				
1.102		SET louvers to FULLY-OPEN position				
1.103		VERIFY secondary air heat toggle switches are OFF				
1.104		VERIFY **CTG-FU-001** (fuel preheater toggle switch) is OFF				

			Test Numbers			
Step #		**Operation**				
Prepare Secondary Air Heater and Tape Heaters						
1.105		Proceed to secondary air heater control (green box)				
1.106		SET metal toggle switch in down position				
1.107		TURN ON red breaker switch				
1.108		VERIFY blue light turned on				
1.109		PRESS both reset buttons				
1.110		VERIFY both temperatures on display near ambient				
1.111		TURN ON heat switch				
1.112		PRESS both reset buttons again				
1.113		Proceed to tape heater control (wall bordering control room)				
1.114		TURN ON three "Square D" breakers				
Begin N2 Purge and Prepare Fuel Preheater						
1.115		LOAD Fuel System Purge **MR-GT-02** to 150 psi				
1.116		Ensure fuel preheater control switch set to off (located beneath loudspeaker)				
1.117		Turn on power to fuel preheater				
1.118		Verify scrolling display shows ambient temperature in all zones				
1.119		SET fuel preheater control switch to auto				
1.120		Turn on fuel preheater on VI for a few seconds				
1.121		Verify scrolling display shows rising temperatures				
1.122		Turn off fuel preheater on VI				

			Test Numbers			
Step #		**Operation**				
Section 2: Jet Fuel System Setup and Sparging						
2.000		Proceed to Fuel Tank Pump Station				
2.001		Visually inspect fuel level in Jet-A fuel tank				
2.002		VERIFY CLOSE ALL ALTERNATIVE FUEL TANK VALVES				
2.003		VERIFY CLOSE **MV-GTF-02**				
2.004		VERIFY CLOSE **MV-GTF-06**				
2.005		VERIFY CLOSE **MV-GTF-08**				
2.006		VERIFY CLOSE **MV-GTF-10**				
2.007		CLOSE Nitrogen Blanket Purge Valve **MV-GTF-07**				
2.008		OPEN Sparge Valve **MV-GTF-09**				
2.009		VERIFY CLOSE **MV-GTF-01**				
2.010		VERIFY CLOSE **MV-GTF-03**				
2.011		VERIFY CLOSE **MV-GTF-04**				
2.012		VERIFY CLOSE **MV-GTF-05**				
2.013		VERIFY CLOSE **MV-GTF-11**				
2.014		(2 people) Open Sparge Valve **MV-GT-03** in cell				
2.015		(2 people) LOAD the Sparge Regulator **MR-GT-03** to 6-8 psi while teammate monitors the fuel tank **Wait 25 minutes.**				
2.016		Proceed to Fuel Tank Pump Station				
2.017		OPEN the Nitrogen Blanket Purge Valve **MV-GTF-07**				
2.018		CLOSE the Sparge Valve **MV-GTF-09**				
2.019		OPEN **MV-GTF-01**				
2.020		OPEN **MV-GTF-04** (fuel to cell)				
2.021		OPEN **MV-GTF-05** (fuel return)				
2.022		SET 480V Service Switch (for fuel pump, located across Jet-A tank from pump) to Start				
2.023		Proceed to GT cell				
2.024		VERIFY manual valve (black valve on fuel panel) on sampling circuit is open				
2.025		Return to control room				
2.026		VERIFY fuel pump control switch (opposite monitors) is set to AUTO				
2.027		TURN ON 480 V power to pump				
2.028		VERIFY on VI that **PV-FU-001** is CLOSED				
2.029		TURN ON jet fuel pump on VI				
2.030		CHECK **PT-FU-001** on VI to ensure fuel is being pumped				
2.031		Proceed to Fuel Tank Pump Station				
2.032		ADJUST pressure relief valve (outside by pump) to desired fuel supply pressure (ask for help)				
2.033		Proceed to GT cell				
2.034		VERIFY feed pressure to O2 sensor under 20 psi				
2.035		Monitor dissolved O2 percentage until <1%				
2.036		VERIFY manual valve for secondary air is closed				
2.037		OPEN manual valve for nitrogen				

			Test Numbers			
Step #		**Operation**				

Section 3: Clear Test Cell

3.000		Clear GT cell of all personnel, and notify all in rocket control room and cell of testing activity				
3.001		Turn on Warning Lights, Traffic: yellow, 134A: Red, 133A: yellow and blue, 127A: yellow and blue, 128: yellow and blue				
3.002		Install test cell barrier chain				

Section 4: Rig Warmup

4.000		Open **PV-GT-03**				
4.001		Adjust **RR-GT-03** for desired heating nitrogen pressure				
4.002		TURN ON **EHEX-SA-001** on VI				
4.003		TURN ON **DO-EH-01** on VI				
4.004		SET **EHEX-SA-SET** on VI to desired temperature; increase in 100F increments to prevent overshoot				
4.005		Once desired rig temperature is attained, continue to next section				

Section 5: Heated Fuel Tests

5.000		OPEN **PV-FU-001** to actuate main fuel isolation valve				
5.001		SET **CV-FU-001** for desired fuel flow rate				
5.002		CLOSE **PV-N2-004** to stop purge through hot fuel heater system.				
5.003		OPEN **PV-FU-004** to run main fuel through heaters.				
5.004		SET **CV-SIR-001** for desired fuel pressure				
5.005		READJUST **CV-FU-001** for desired fuel flow rate				
5.006		TURN ON **CTG-FU-001** to provide power to fuel preheater				
5.007		ADJUST High Temperature Fuel Heaters until desired fuel inlet temperature is reached.				
5.008		ADJUST servo-controlled louvers until desired fuel outlet temperature is reached.				
5.009		**If oscillations occur:**				
5.010		TOGGLE **Acquire Data** on LabVIEW VI to begin recording				
5.011		CLICK **Record** on high frequency data system				
5.012		Wait 5-10 seconds				
5.013		TOGGLE **Acquire Data** on LabVIEW VI to stop recording				
5.014		CLICK **Stop** on high frequency data system				
5.015		ADJUST CV-SIR-001 to obtain next pressure condition				
5.016		ADJUST High Temperature Fuel Heaters until desired fuel inlet temperature is reached.				
5.017		Repeat this subsection for all data points				
5.018		**When testing is complete:**				
5.020		SET fuel preheater set points to 0				
5.021		TURN OFF **CTG-FU-001** (fuel preheater power)				
5.022		SET **EHEX-SA-SET** (secondary air heater) to 0				
5.023		TURN OFF **EHEX-SA-001** (secondary air heater power)				
5.024		TURN OFF **DO-EH-01** (tape heaters)				
5.025		Close **PV-FU-004** (Main Fuel Flow to Heater System)				
5.026		Open **PV-N2-004** (Heater System Purge)				
5.027		TURN OFF fuel pump **PMP-FU-001**				
5.028		WAIT for **PT-FU-001** to show ambient pressure				
5.029		SET **CV-FU-001** to 0%				
5.030		TURN OFF **EF-FU-01**				
5.031		CLOSE **PV-FU-001**				
5.032		SET **CV-SIR-001** to 100%				
5.033		WAIT for **TC-SIR-BOX-L** and **TC-SIR-BOX-R** to decrease below 300F				
5.034		SET **RR-GT-03** to 0%				
5.035		CLOSE **PV-GT-03**				

			Test Numbers			
Step #		**Operation**				
Section 6: Test Completion						
6.000		REMOVE test cell chain barrier				
6.001		SET warning light for room 134A to YELLOW				
6.002		Proceed to Gas Turbine Cell				
6.003		TURN OFF fuel preheater master switch				
6.004		TURN OFF tape heater master switch				
6.005		TURN OFF secondary air heater master switch				
6.006		CLOSE manual nitrogen valve upstream of secondary air heater				
6.007		UNLOAD **MR-GT-01** (pilot regulator)				
6.008		UNLOAD **MR-GT-03** (sparge regulator)				
6.009		CLOSE **MV-GT-03** (sparge valve)				
6.010		WAIT until pilot pressure is below 60%				
6.011		Proceed to GT Control Room				
6.012		TURN OFF Valve Power switch in Gas Turbine Instrument Room. VI may now be left unattended.				
6.013		TURN OFFJet Fuel Pump from Auto				
6.014		TURN OFF 480V power to pump				
6.015		Proceed to Fuel Tank Pump System				
6.016		CLOSE **MV-GT-04**				
6.017		CLOSE **MV-GT-05**				
6.018		CLOSE **MV-GT-01**				
6.019		CLOSE Blanket Purge Valve **MV-GTF-07**				
6.020		VERIFY Sparge Valve **MV-GTF-09** is CLOSED				
6.021		CLOSE 480V service switch				
6.022		WAIT for fuel preheater temperatures to drop below 200F.				
6.023		Proceed to GT Cell				
6.024		UNLOAD **MR-GT-02** (fuel purge regulator)				
6.022		Vent Secondary Air Lines.				

B.2 Facility Drawings and Specifications

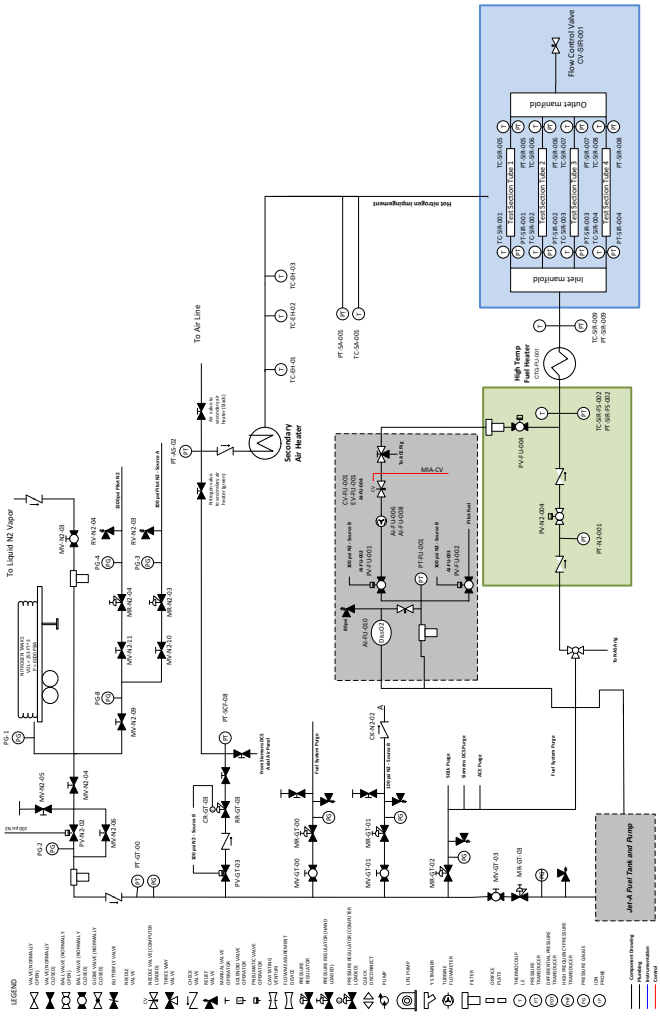

Figure B.1. Plumbing and instrumentation diagram

kulite®

HIGH TEMPERATURE HIGH BANDWIDTH AMPLIFIED GAS TURBINE IS® PRESSURE TRANSDUCER

ETL-GTS-X-190 (M) SERIES

- Miniature, Robust Construction
- High Temperature
- Acceleration & Vibration Insensitive
- High Bandwidth Amplifier
- Patented Leadless Technology **VIS®**
- Separate DC and AC Outputs
- Dynamic and Static Capability
- Excellent Long Term Stability Coupled with High Accuracy

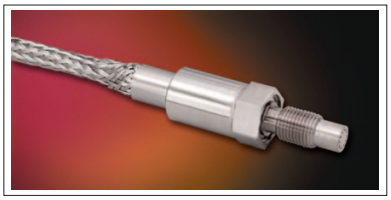

The ETL-GTS Series are high temperature, extremely rugged pressure transducers which are ideal for the measurement of instabilities and steady pressures in gas turbine combustors and compressors. They use a patented acceleration insensitive leadless sensing element that is more than 1000 times less sensitive to vibration than other Kulite transducers. The front of the transducers can withstand temperatures of 1000°F (538°C)* while the in-line amplifier can be placed in a cooler area. The amplifier is compatible with both existing and new data acquisition systems with a measurement bandwidth of up to 150KHz, specified by Option X.

CONSULT FACTORY FOR SPECS. ON SEALED GAGE
*NO SCREEN FOR 50 KHz (AND ABOVE) BANDWIDTH

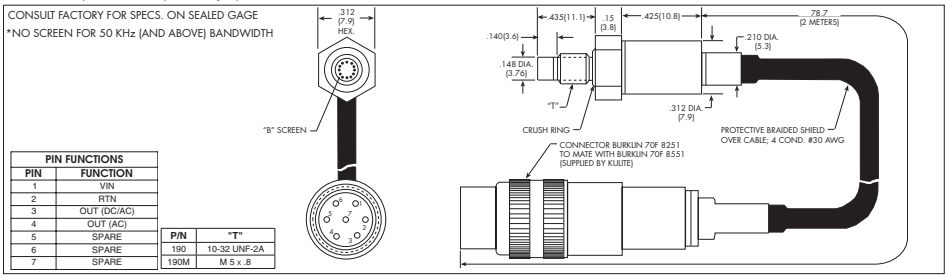

PIN FUNCTIONS	
PIN	FUNCTION
1	VIN
2	RTN
3	OUT (DC/AC)
4	OUT (AC)
5	SPARE
6	SPARE
7	SPARE

P/N	"T"
190	10-32 UNF-2A
190M	M 5 x .8

INPUT Pressure Range	3.5 50 / 7 100 / 14 200 / 21 300 / 35 500 / 70 BAR 1000 PSI
Operational Mode	Absolute, Sealed Gage
Over Pressure	2 Times Rated Pressure
Burst Pressure	3 Times Rated Pressure
Pressure Media	All Nonconductive, Noncorrosive Liquids or Gases (Most Conductive Liquids and Gases - Please Consult Factory)
ELECTRICAL PERFORMANCE Rated Electrical Excitation	12 ± 4VDC or 28 ± 4VDC
Maximum Electrical Current	25 mA
Output Impedance	200 Ohms (Typ.)
Output Range	0.5V to 5V ± 3% (2 Outputs)
Bandwidth (-3dB)	Output 1: DC to 5kHz (Option A), 50kHz* (Option B) or 150kHz* (Option C) Output 2: AC 10Hz to 5kHz (Option A), 50kHz* (Option B) or 150kHz* (Option C) (X10 Additional gain)
Output Filter	Low Pass Filter Available per Customer Specification
Residual Unbalance	500mV ±1%
OUTPUT Resolution	Infinitesimal
Natural Frequency (KHz) (Typ.)	Greater Than 1000 KHz
Insulation Resistance	100 Megohm Min. @ 50 VDC
ENVIRONMENTAL Operating Temperature Range	-65°F to +1000°F* (-55°C to +538°C) (Front End) -65°F to +257°F (-55°C to +125°C) (Connector + Amplifier)
Compensated Temperature Range	+80°F to +850°F (+25°C to +454°C)
Thermal Zero Shift	± 1.5% FS/100°F (Typ.)
Thermal Sensitivity Shift	± 1.5% /100°F (Typ.)
Linear Vibration	50g Peak, Sine 10 to 2000 Hz
Humidity	100% Relative Humidity
Mechanical Shock	100g half Sine Wave 11 msec. Duation
PHYSICAL Electrical Connection	Burklin 70F 8251 Connector (Mating Connnector Supplied)
Weight	10 Grams (Nom.) Excluding Cable and Connector
Pressure Sensing Principle	Fully Active Four Arm Wheatstone Bridge Dielectrically Isolated Silicon on Silicon Patented Leadless Technology
Mounting Torque	15 Inch-Pounds (Max.) 1.7 N-m

** Limited life above 850°F (454°C) dependent on operating conditions.*
Note: Custom pressure ranges, accuracies, amplifiers and mechanical configurations available. Dimensions are in inches. Dimensions in parenthesis are in millimeters.
Continuous development and refinement of our products may result in specification changes without notice - all dimensions nominal. (L)

KULITE SEMICONDUCTOR PRODUCTS, INC. • One Willow Tree Road • Leonia, New Jersey 07605 • Tel: 201 461-0900 • Fax: 201 461-0990 • http://www.kulite.com

Figure B.2. Pressure transducer specification sheet, courtesy of Kulite

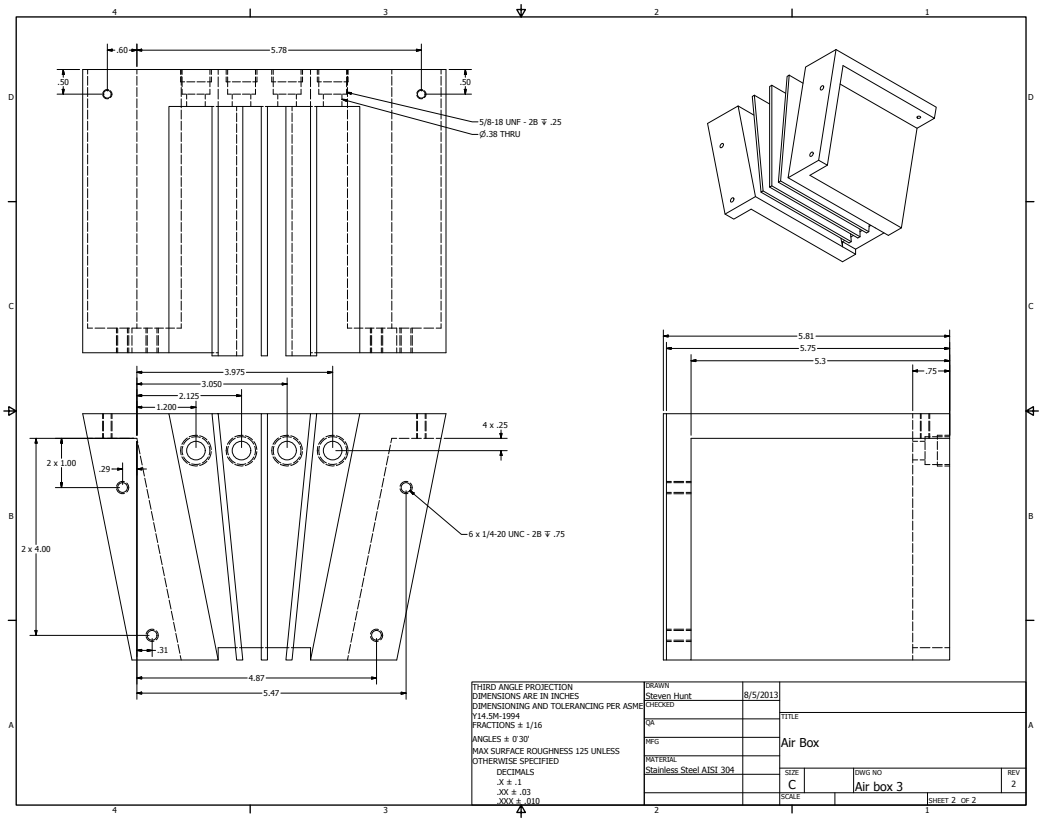

Figure B.3. Drawing of nitrogen flow path enclosure (aka air box)

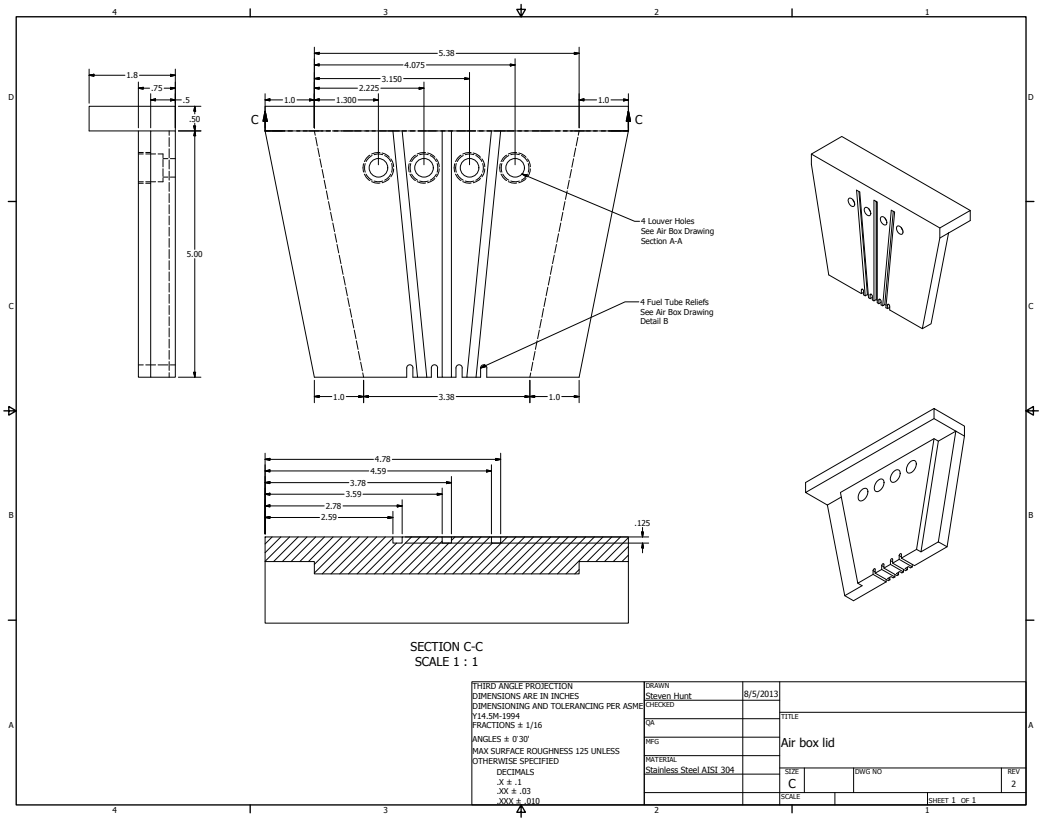

Figure B.4. Drawing of top cover plate for nitrogen flow path enclosure

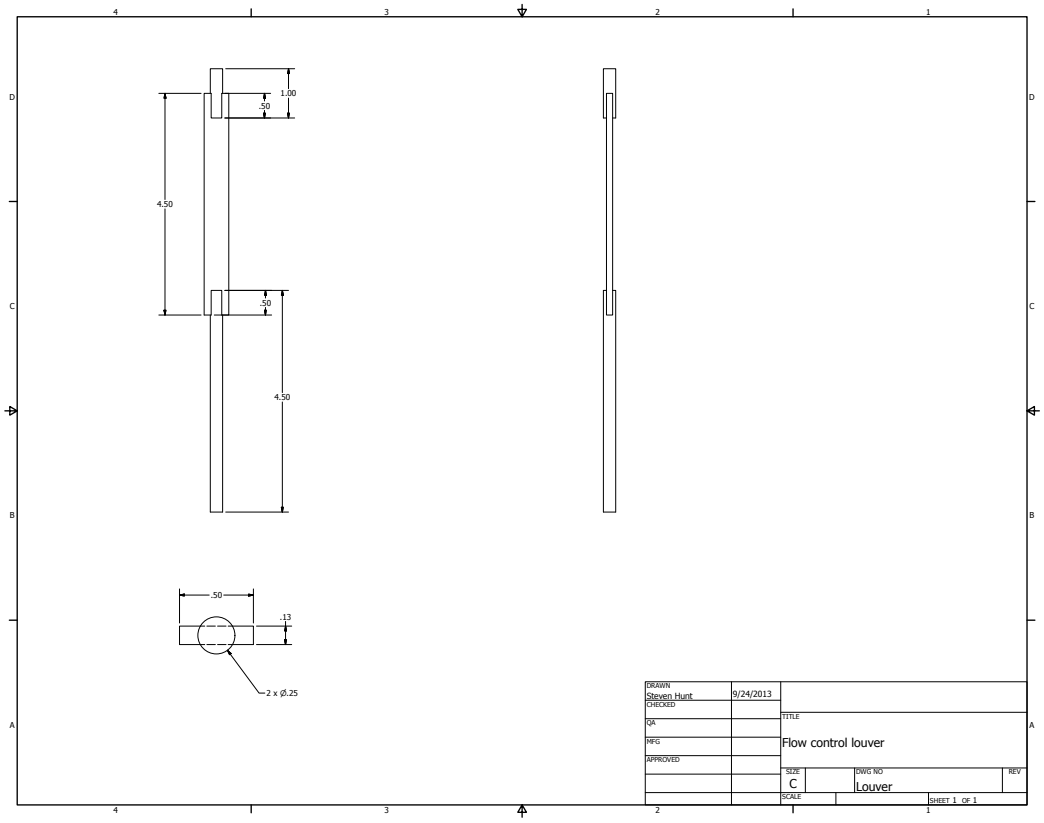

Figure B.5. Drawing of nitrogen flow control louver vane

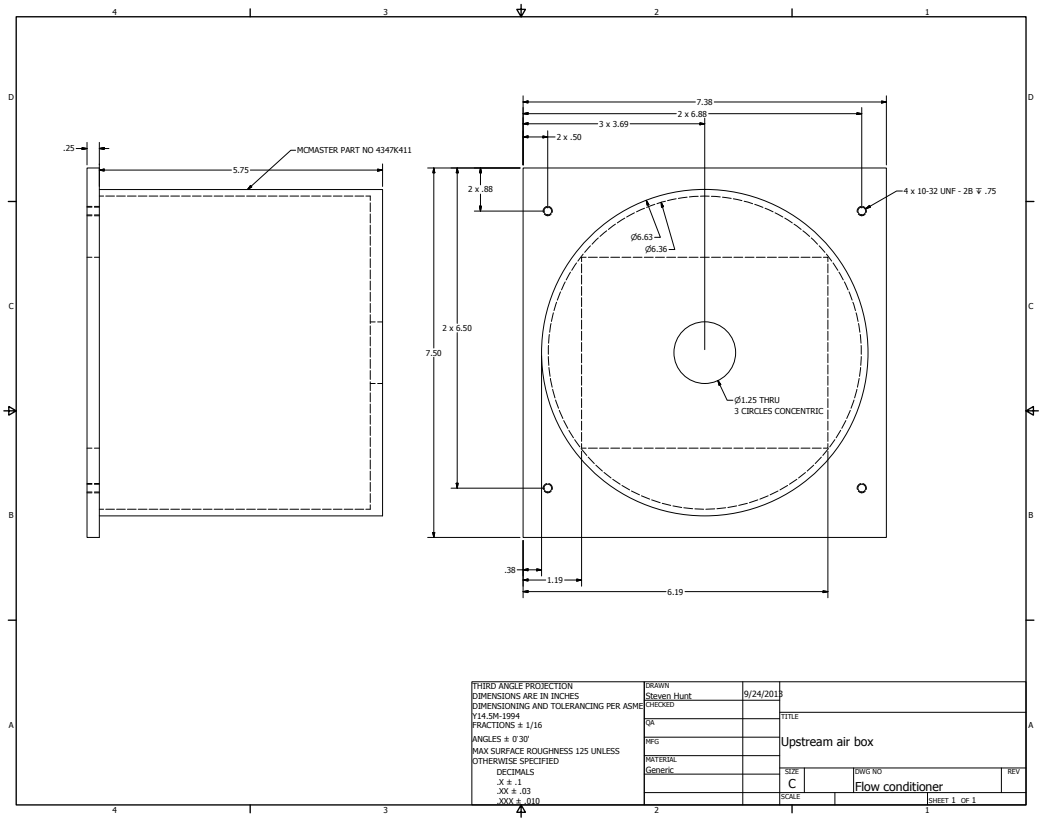

Figure B.6. Drawing of nitrogen flow conditioning housing

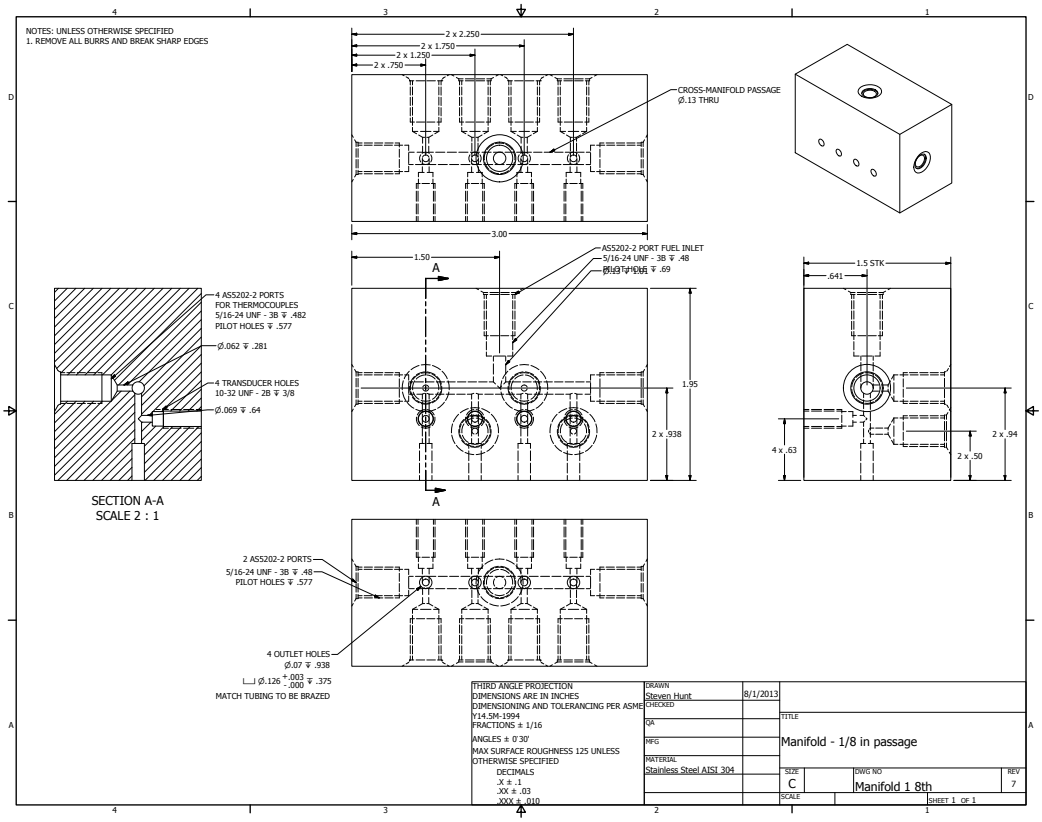

Figure B.7. Drawing of fuel manifold

B.3 Additional Data Samples from Second Test Campaign

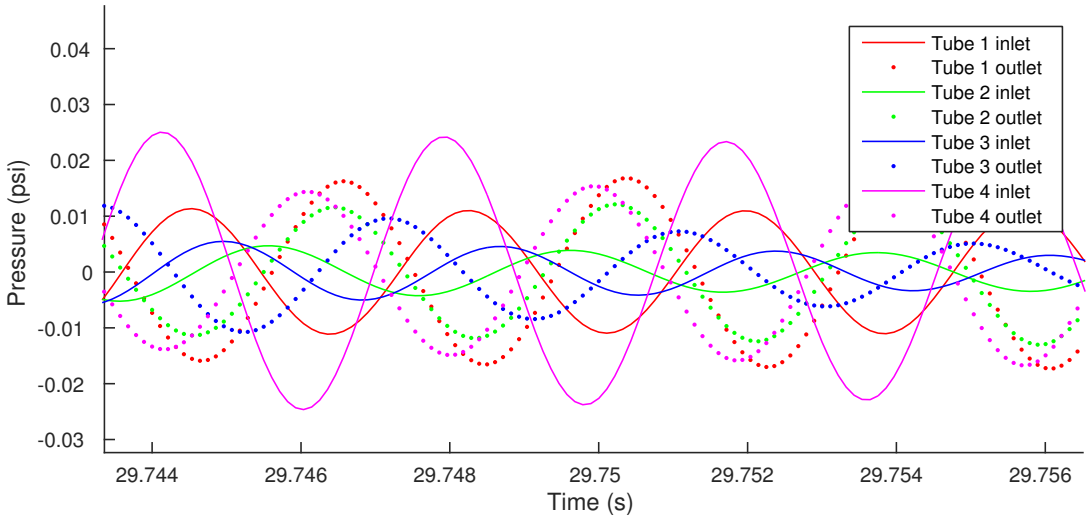

Figure B.8. Pressure traces for file ID 20150624_1428592

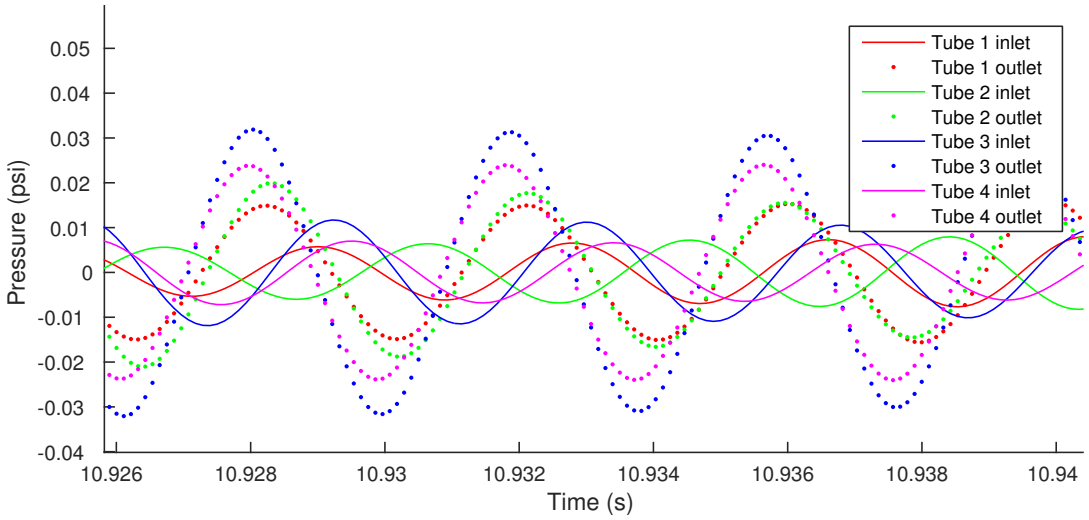

Figure B.9. Pressure traces for file ID 20150625_0828352

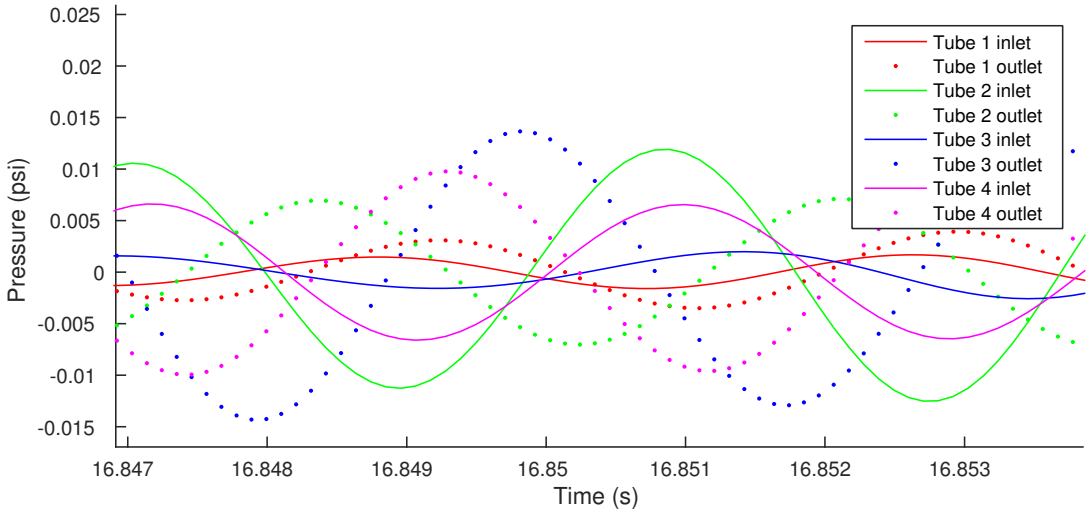

Figure B.10. Pressure traces for file ID 20150624_1431177

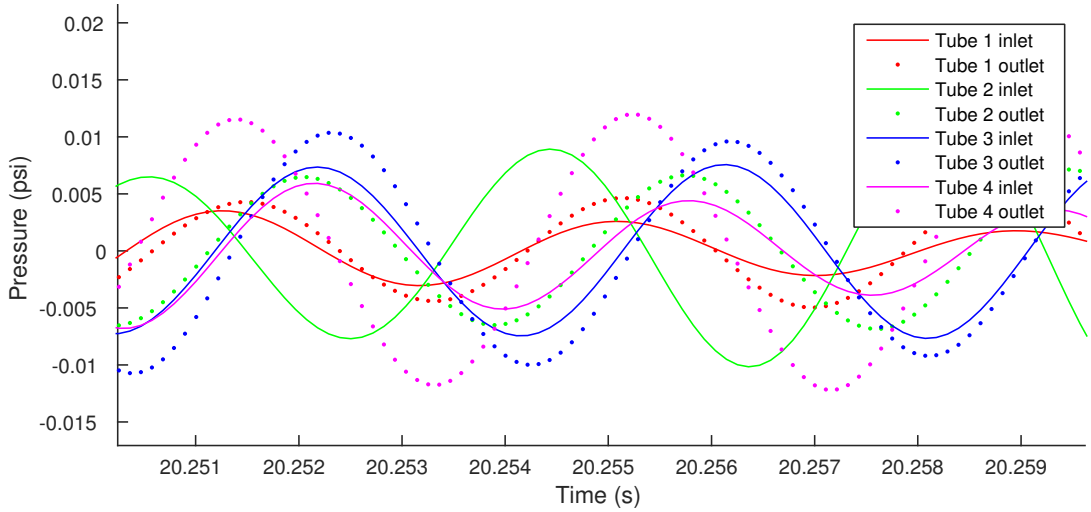

Figure B.11. Pressure traces for file ID 20150624_1447052

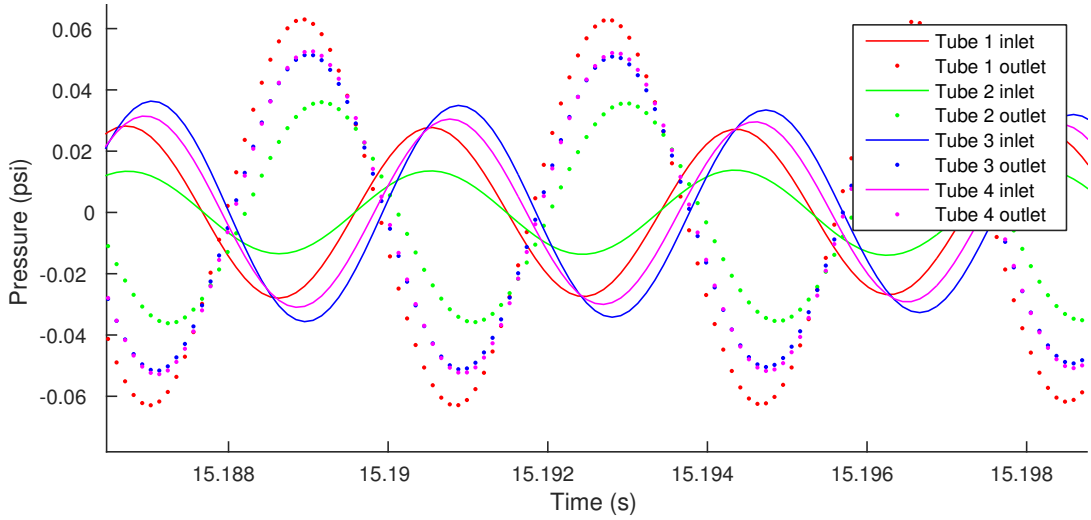

Figure B.12. Pressure traces for file ID 20150625_0832125

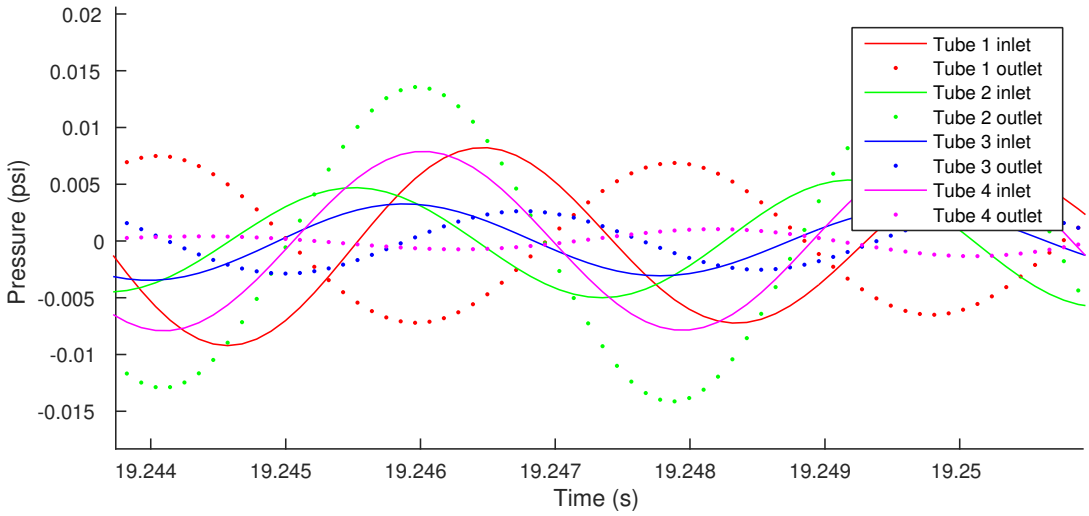

Figure B.13. Pressure traces for file ID 20150624_1448503

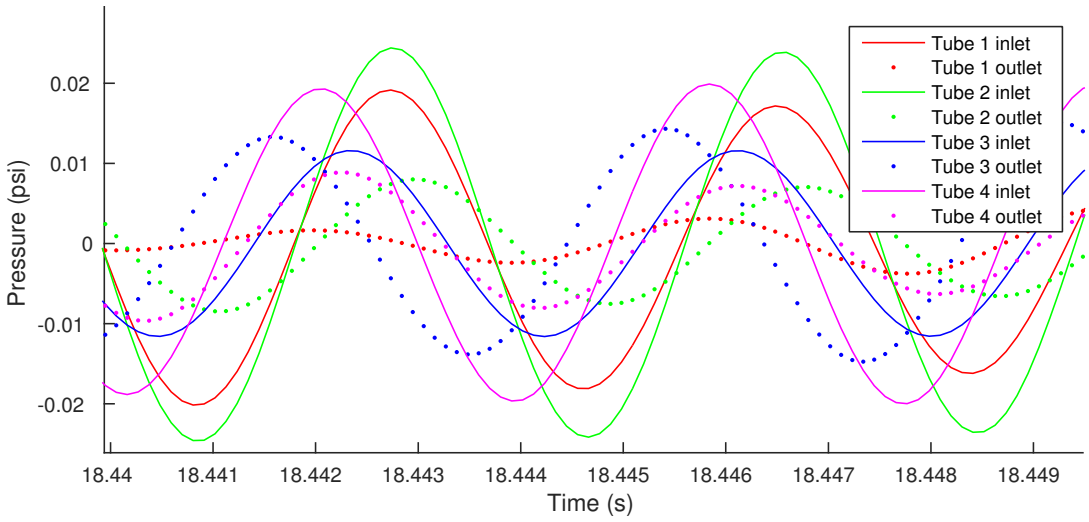

Figure B.14. Pressure traces for file ID 20150624_1501508

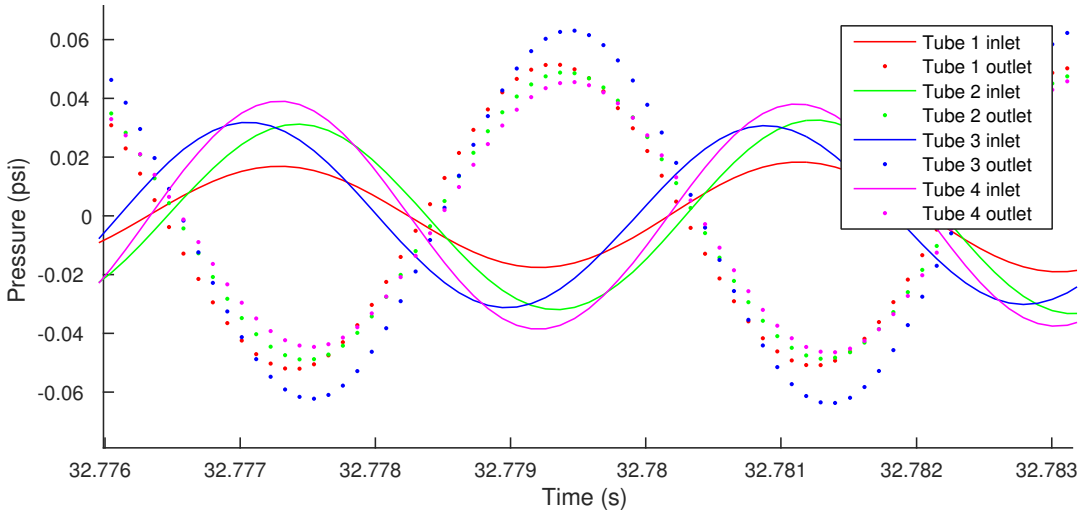

Figure B.15. Pressure traces for file ID 20150625_0835172

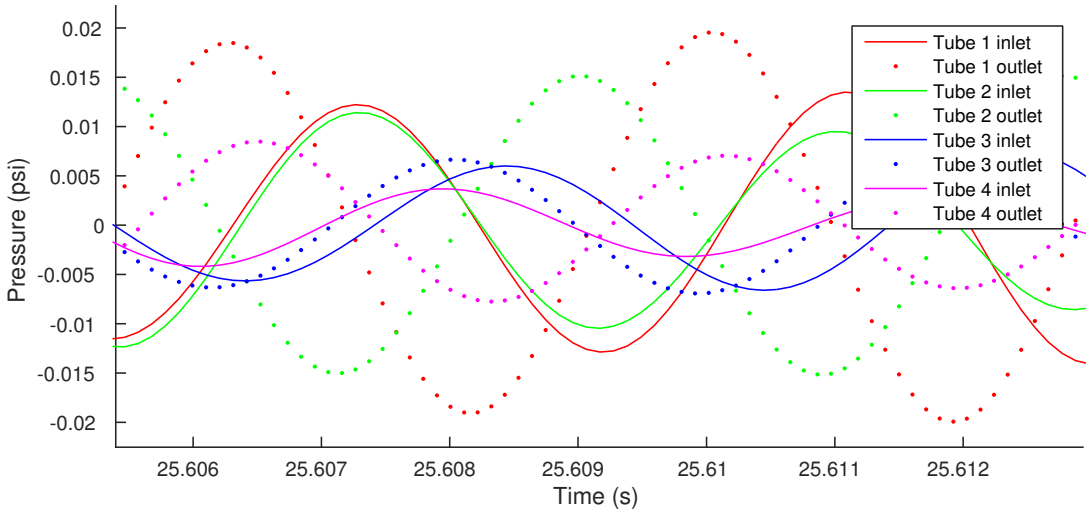

Figure B.16. Pressure traces for file ID 20150624_1503366

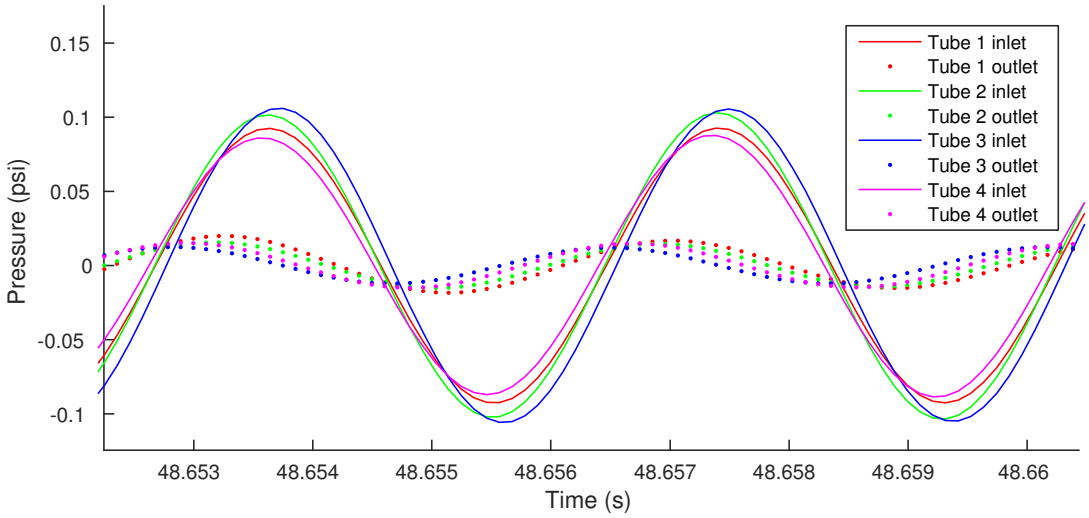

Figure B.17. Pressure traces for file ID 20150624_1529029

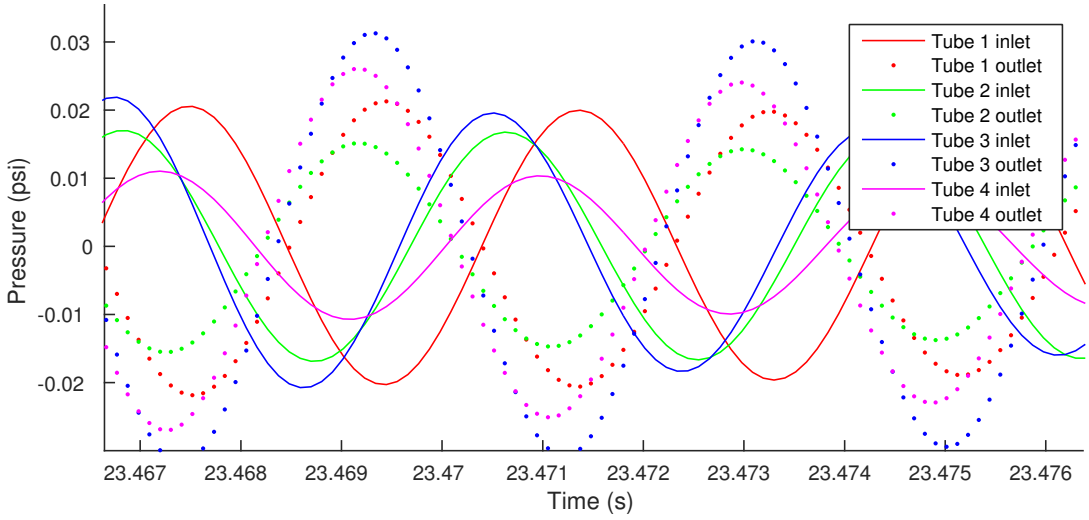

Figure B.18. Pressure traces for file ID 20150625_0850427

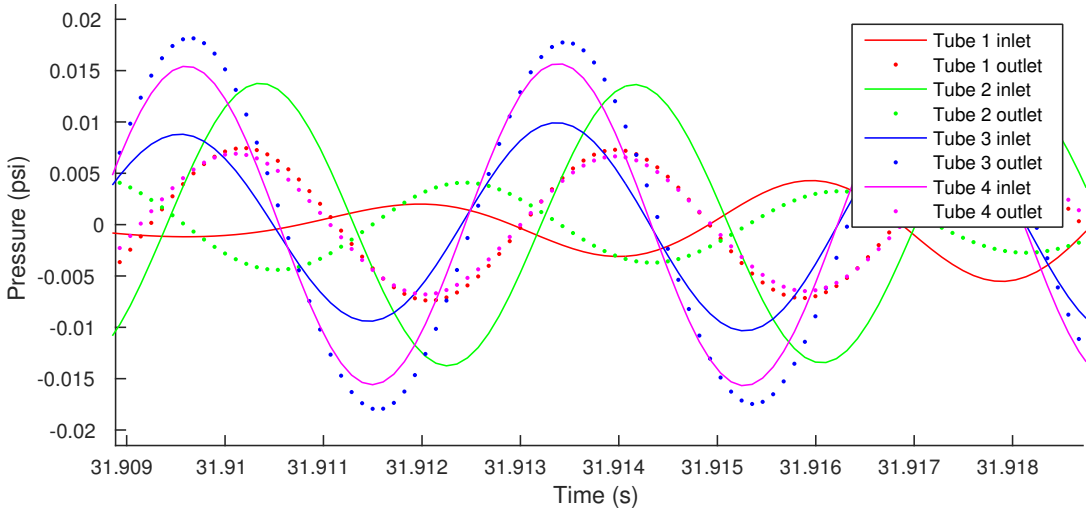

Figure B.19. Pressure traces for file ID 20150624_1653492

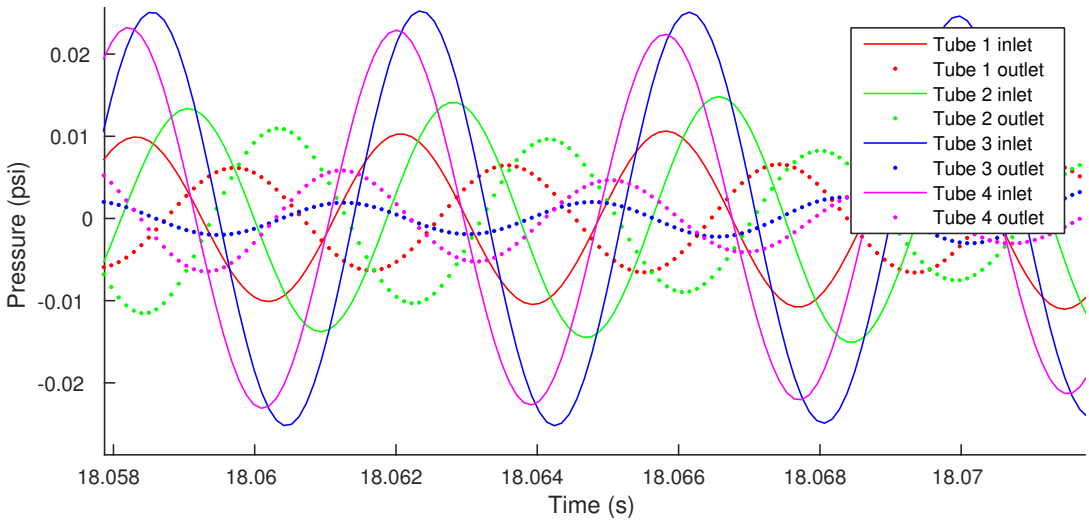

Figure B.20. Pressure traces for file ID 20150625_0855519

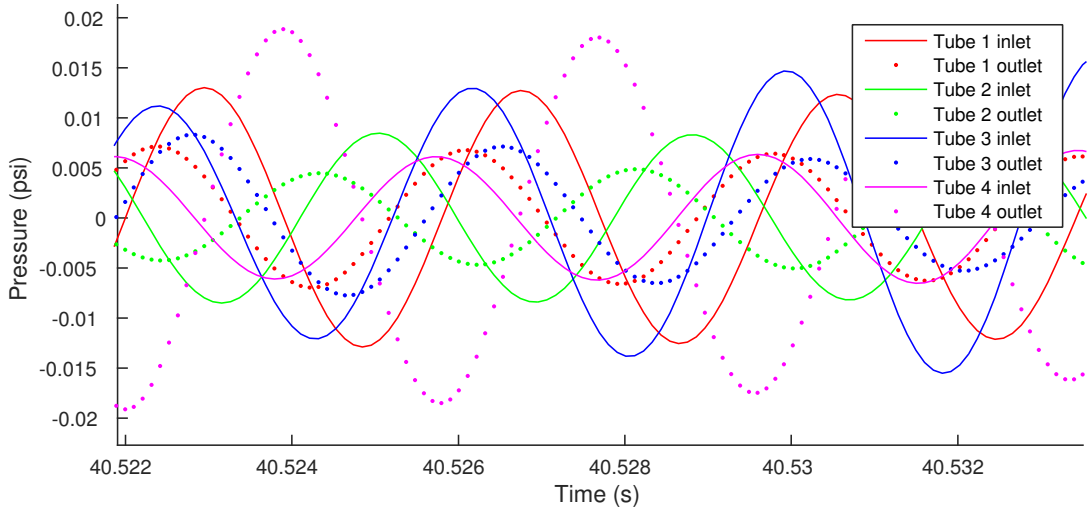

Figure B.21. Pressure traces for file ID 20150624_1702459

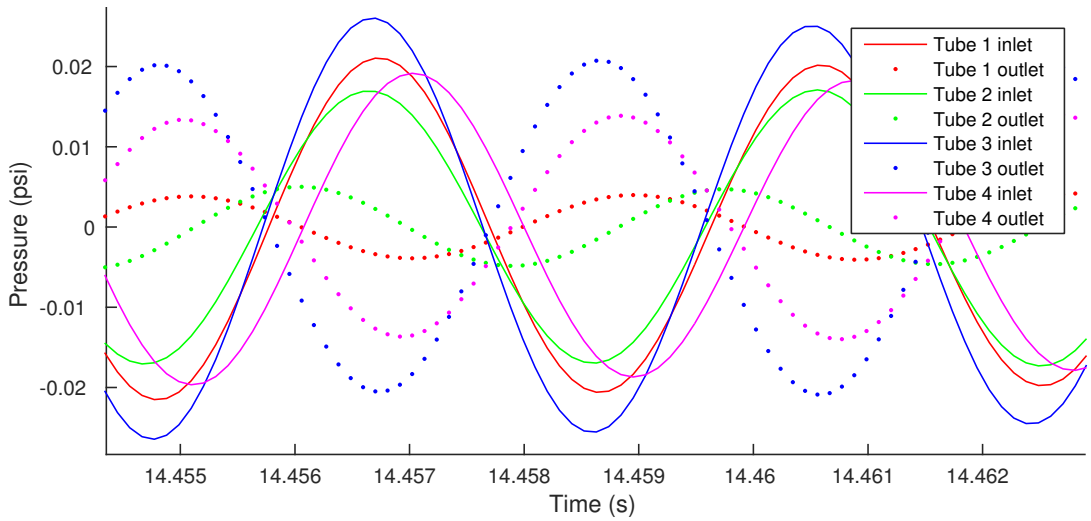

Figure B.22. Pressure traces for file ID 20150625_0858515

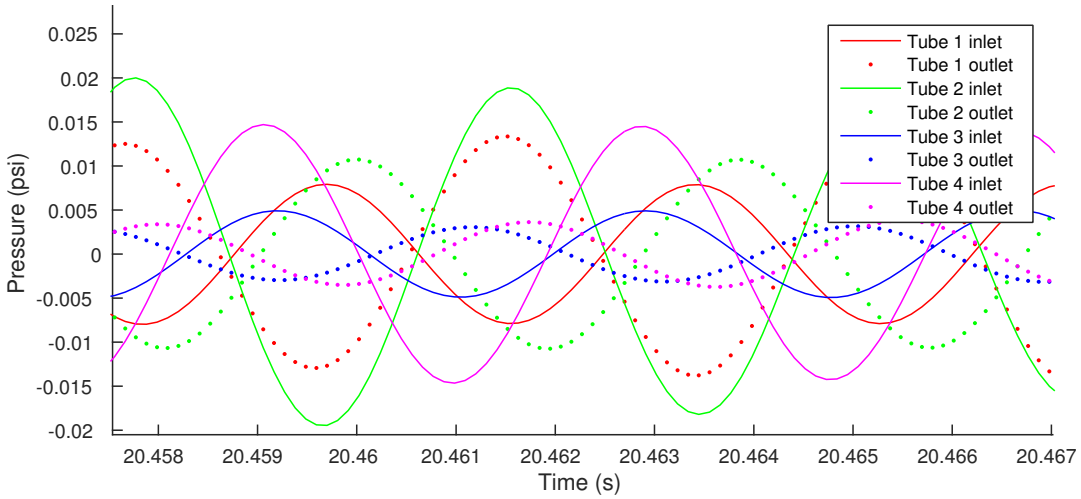

Figure B.23. Pressure traces for file ID 20150624_1707559

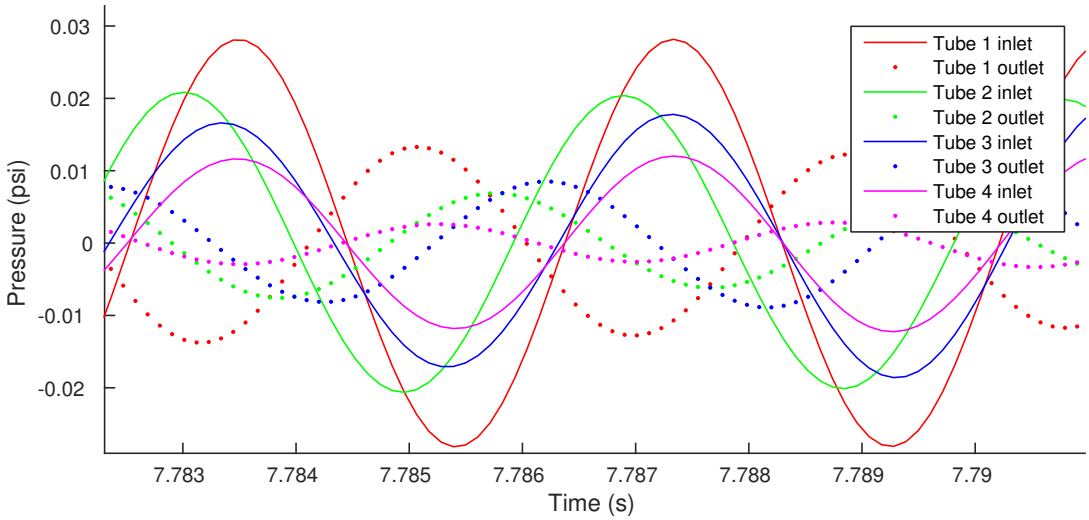

Figure B.24. Pressure traces for file ID 20150624_1557129

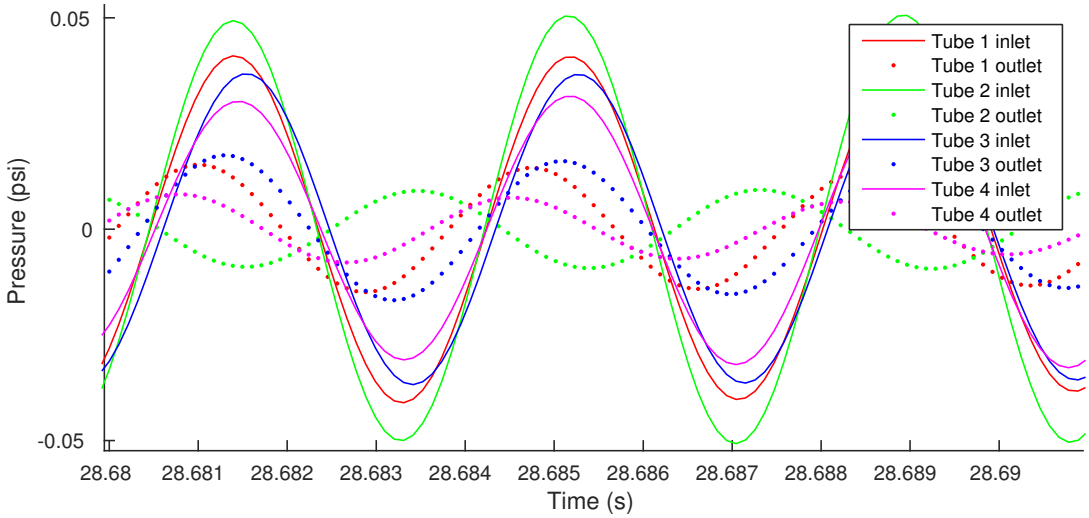

Figure B.25. Pressure traces for file ID 20150625_0919045

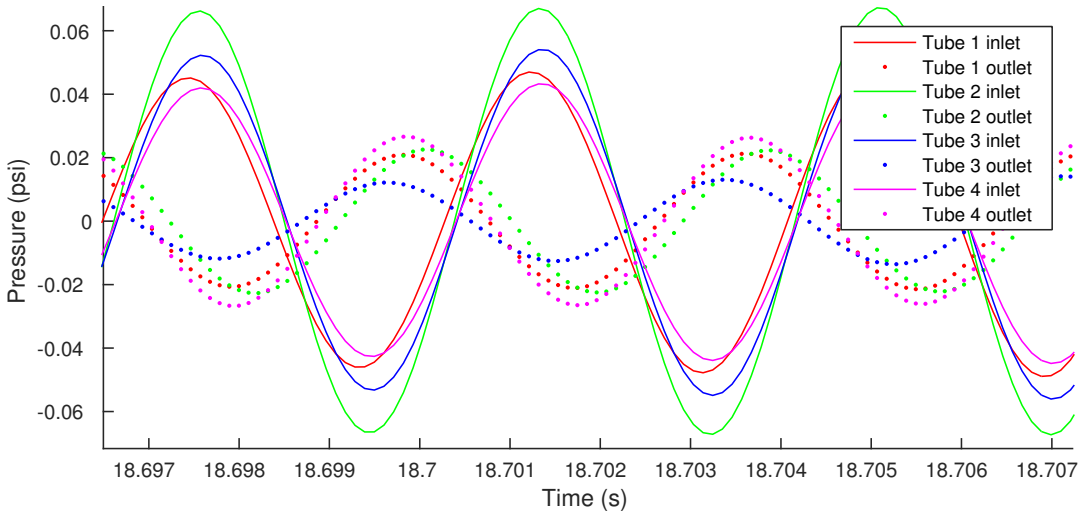

Figure B.26. Pressure traces for file ID 20150624_1605591

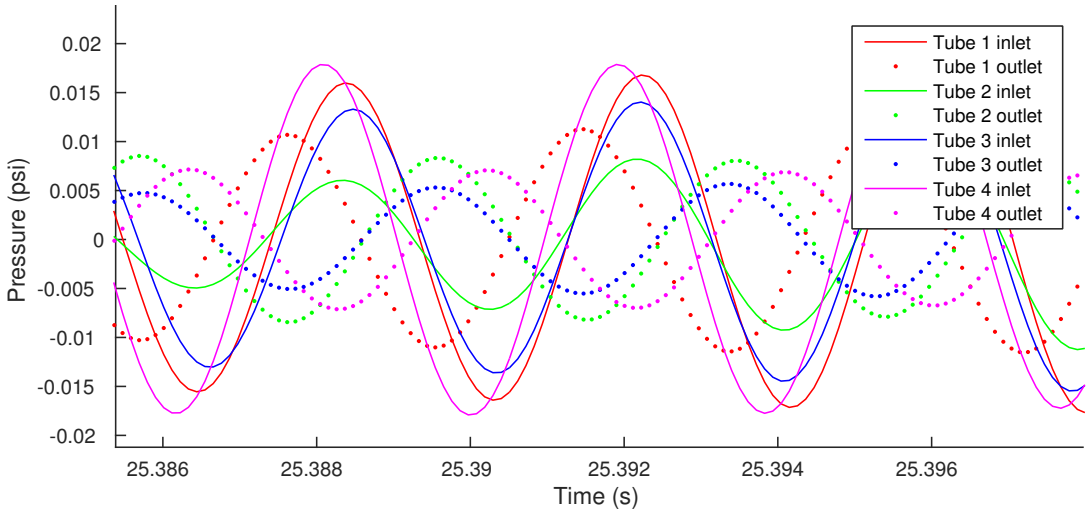

Figure B.27. Pressure traces for file ID 20150624_1638415

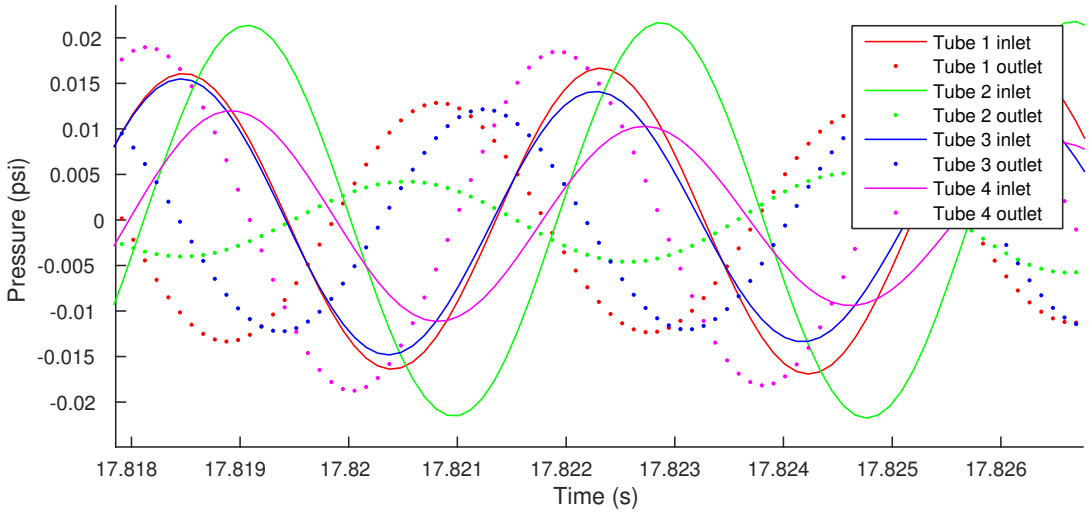

Figure B.28. Pressure traces for file ID 20150624_1607338

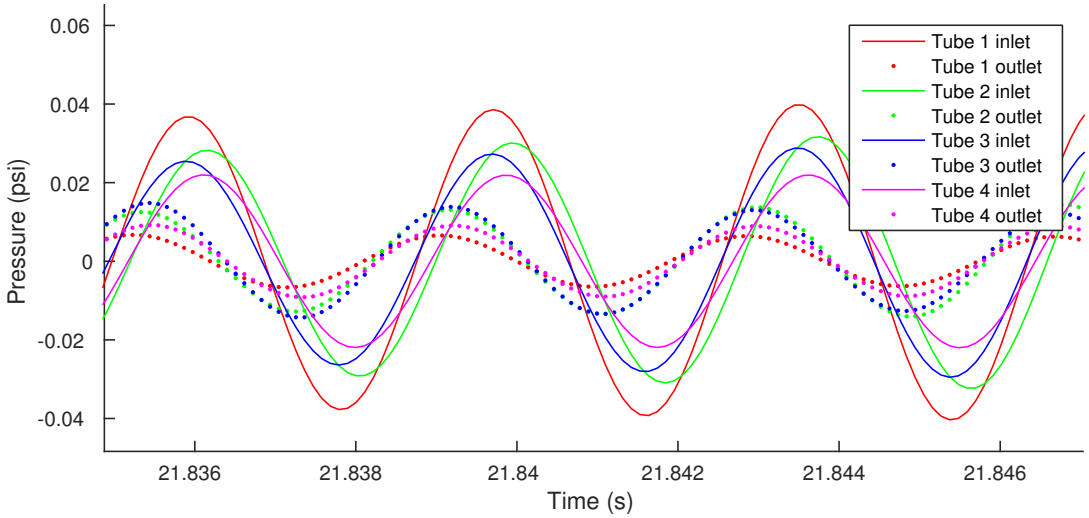

Figure B.29. Pressure traces for file ID 20150624_1625560

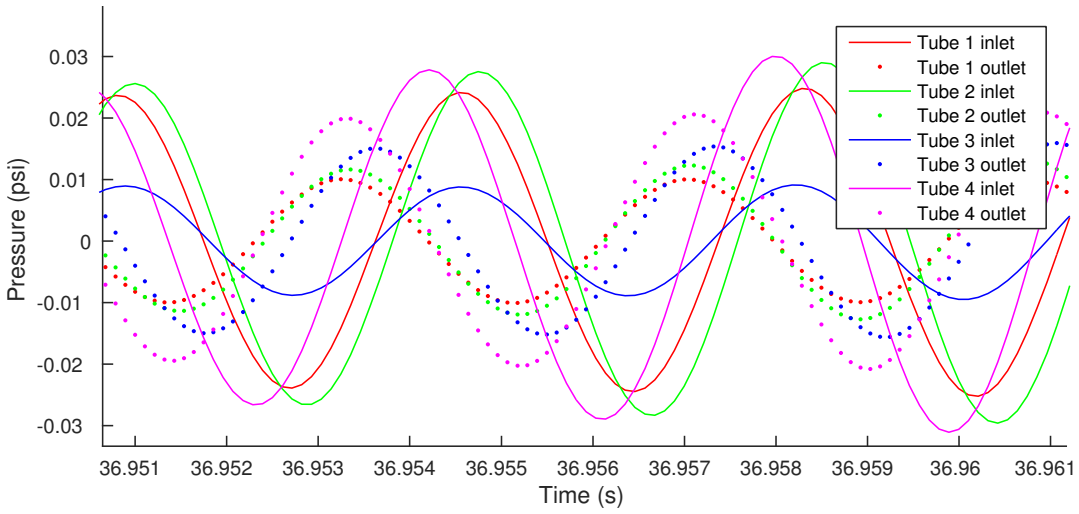

Figure B.30. Pressure traces for file ID 20150625_0921508

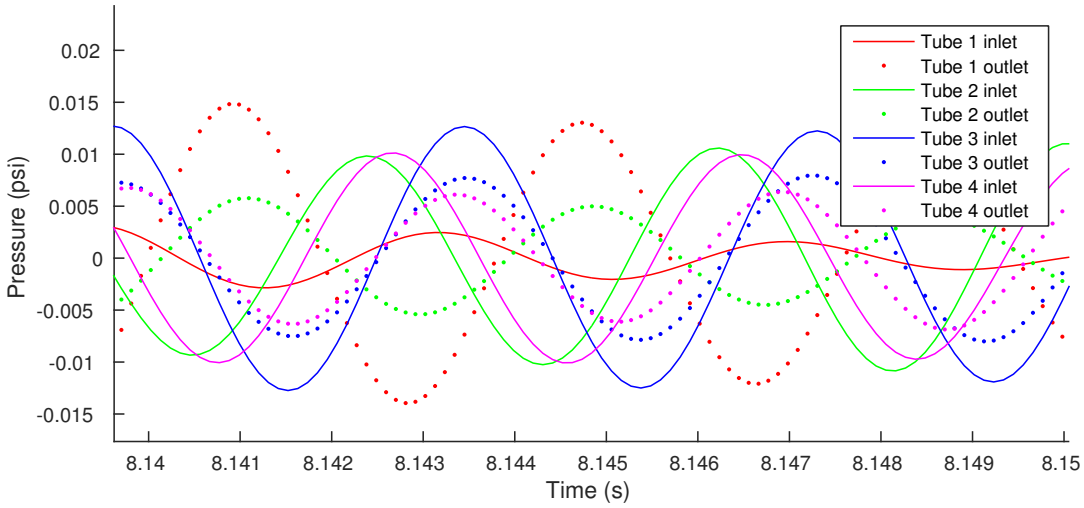

Figure B.31. Pressure traces for file ID 20150624_1634384

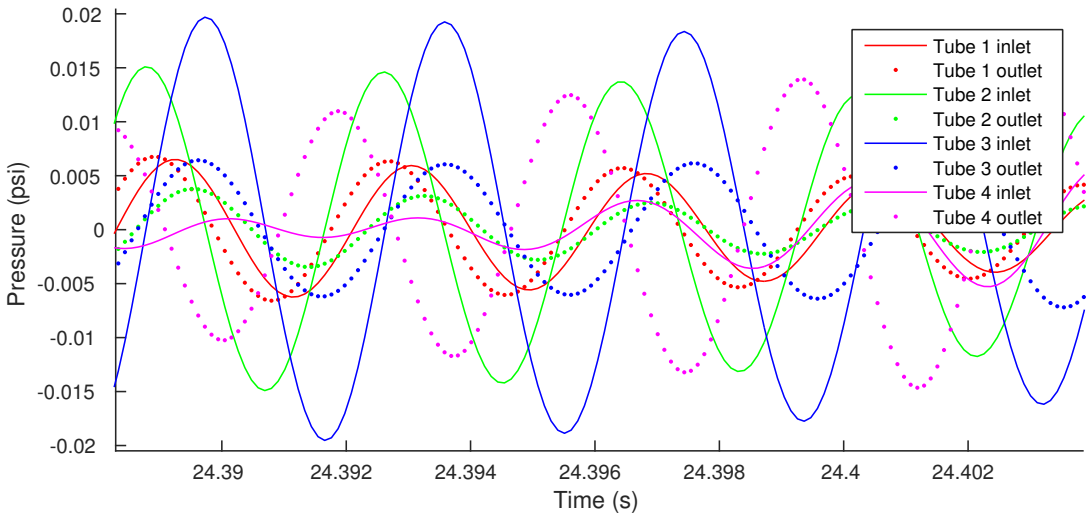

Figure B.32. Pressure traces for file ID 20150624_1622049

B.4 Test Matrices

B.4.1 First Test Campaign, Small Manifold Passage Cases

Target Inlet Fuel Temp	Target Fuel Pressure	Target Fuel Mass Flow Rate	Louver Setting	Lo freq file	Hi freq ID	Hi freq file	N2 Flow rate	Inlet N2 Temp
200	400	20	All open	184320	861	20140524_0359509	0.306	850
			Chan 1 open	185359	862	20140524_0401360	0.306	850
			Chan 2 open	185512	863	20140524_0403138	0.306	850
300			All open	160706	883	20140531_0118203	0.307	864
			Chan 1 open	161143	884	20140531_0119564	0.307	864
			Chan 2 open	161322	885	20140531_0121427	0.307	864
400			All open	185935	864	20140524_0425131	0.256	870
			Chan 1 open	191839	865	20140524_0426288	0.256	870
500			All open	192914	867	20140524_0436466	0.204	870
			Chan 1 open	192946	868	20140524_0437475	0.204	870
			Chan 2 open	193050	869	20140524_0438332	0.204	870
600			All open	163933	887	20140531_0149370	0.305	861
			Chan 1 open	164318	888	20140531_0151236	0.305	861
			Chan 2 open	164426	889	20140531_0152512	0.305	861
600	400	20	All open	150931	918	20140621_0023009	0.307	856
			Chan 1 open	151718	919	20140621_0025205	0.307	853
			Chan 2 open	151921	920	20140621_0028236	0.307	848
	600		All open	152520	921	20140621_0034058	0.307	845
			Chan 1 open	152827	922	20140621_0036317	0.307	845
			Chan 2 open	153039	923	20140621_0038590	0.307	845
	700		All open	153601	924	20140621_0043395	0.306	845
			Chan 1 open	153719	925	20140621_0044593	0.306	845
			Chan 2 open	153851	926	20140621_0046369	0.306	845
			Chan 3 open	154034	927	20140621_0048248	0.306	845
700	400	20	All open	135125	907	20140620_2334172	0.309	835
			Chan 1 open	142823	908	20140620_2336537	0.309	835
			Chan 2 open	143106	909	20140620_2338516	0.309	835
	500		All open	144147	910	20140620_2349277	0.309	833
			Chan 1 open	144349	911	20140620_2352015	0.309	833
			Chan 2 open	144543	912	20140620_2353376	0.308	834
			Chan 3 open	144735	913	20140620_2355185	0.308	834
			Chan 4 open	144901	914	20140620_2357283	0.308	834
	600		All open	145218	915	20140621_0000121	0.308	834
			Chan 1 open	145410	916	20140621_0002107	0.308	834
			Chan 2 open	145606	917	20140621_0004275	0.308	834

Target Inlet Fuel Temp	Target Fuel Pressure	Fuel mass flow rate	Louver Setting	Lo freq file	Hi freq ID	Hi freq file	N2 Flow Rate	Inlet N2 Temp
500	500	7	All open	140137	952	20140703_2310047	0.312	834
		7	Chan 1 open	140536	953	20140703_2313032	0.312	834
		7	Chan 2 open	140728	954	20140703_2315087	0.312	834
	500	13	All open	142311	955	20140703_2330351	0.311	821
		13	Chan 1 open	142529	956	20140703_2333167	0.311	820
		13	Chan 2 open	142750	957	20140703_2335199	0.311	820
		13	Chan 3 open	143044	958	20140703_2338075	0.311	820
		13	Chan 4 open	143317	959	20140703_2340487	0.311	820
	500	25	All open	150131	964	20140704_0009201	0.309	826
		25	Chan 1 open	150428	965	20140703_0011387	0.309	826
		25	Chan 2 open	150640	966	20140703_0014020	0.309	827
	600	13	All open	144108	960	20140703_2348378	0.311	822
		13	Chan 1 open	144318	961	20140703_2350581	0.31	822
		13	Chan 2 open	144625	962	20140703_2354048	0.311	823

B.4.2 First Test Campaign, Large Manifold Passage Cases

Target Inlet Fuel Temp	Target Fuel Pressure	Fuel mass flow rate	Louver Setting	Lo freq file	Hi freq ID	Hi freq file	N2 Flow Rate	Inlet N2 Temp
600	400	28	All open	125930	1089	20140905_1700226	0.296	832
			Chan 1 open	130125	1090	20140905_1702202	0.295	820
			Chan 2 open	130248	1091	20140905_1703463	0.295	825
		20	All open	130554	1092	20140905_1708430	0.301	850
			Chan 1 open	130908	1093	20140905_1710377	0.3	852
			Chan 2 open	131054	1094	20140905_1712159	0.3	855
			Chan 3 open	131240	1095	20140905_1714001	0.3	856
			Chan 4 open	131414	1096	20140905_1715419	0.299	859
	500	20	All open	131936	1097	20140905_1720559	0.299	866
			Chan 1 open	132711	1099	20140905_1731261	0.295	862
			Chan 2 open	133133	1100	20140905_1733158	0.298	864
	400	12	All open	133959	1101	20140905_1741334	0.297	857
			Chan 1 open	134159	1102	20140905_1743322	0.297	858
			Chan 2 open	134337	1103	20140905_1745038	0.297	859
500	500	6	All open	134802	1104	20140905_1749167	0.296	862
			Chan 1 open	134931	1105	20140905_1750441	0.296	864
			Chan 2 open	135059	1106	20140905_1752125	0.296	864
600	500	12	All open	142848	1153	20141028_1328028	0.291	882
			Chan 1 open	143035	1154	20141028_1330018	0.291	883
			Chan 2 open	143212	1155	20141028_1331445	0.291	883
	600		All open	141834	1149	20141028_1317450	0.291	875
			Chan 1 open	141946	1150	20141028_1320493	0.291	878
			Chan 2 open	142259	1151	20141028_1322292	0.291	878
			Chan 3 open	142432	1152	20141028_1323576	0.291	878
	500	37	All open	135530	1140	20141028_1257338	0.291	867
			Chan 1 open	140323	1142	20141028_1302376	0.291	872
			Chan 2 open	140540	1143	20141028_1304535	0.291	873
			Chan 3 open	140711	1144	20141028_1306444	0.291	874
			Chan 4 open	140851	1145	20141028_1308453	0.291	875
	600		All open	141136	1146	20141028_1310549	0.291	875
			Chan 1 open	141350	1147	20141028_1313025	0.291	875
			Chan 2 open	141516	1148	20141028_1314343	0.291	875

B.4.3 Second Test Campaign, Large Manifold Passage Cases

Target Inlet Fuel Temp	Target Fuel Pressure	Fuel mass flow rate	Louver Setting	Lo freq file	Hi freq ID	Hi freq file	N2 Flow Rate	Inlet N2 Temp
650	400	8	All open	2355_24	1518	20150617_1803381	0.27	930
			Chan 1 open	2357_19	1519	20150617_1805337	0.3	934
			Chan 2 open	2359_02	1520	20150617_1807168	0.29	936
			Chan 3 open	0000_45	1521	20150617_1808595	0.29	933
			Chan 4 open	0002_36	1522	20150617_1810501	0.29	929
			Chan 2 open, slowly sweeping 3 open	0004_30	1523	20150617_1812443	0.29	925
			Chan 2 open, slowly sweeping 1 open	0005_51	1524	20150617_1814054	0.29	923
750		1	All open					
			Chan 1 open	0010_26	1525	20150617_1818408	0.29	919
			Lost flow rate of fuel	0012_20	1526	20150617_1820349	0.29	919
750	450	40	All open	2331_46	1511	20150617_1740009	0.29	928
			Chan 1 open	2334_50	1512	20150617_1743043	0.29	928
			Chan 2 open	2336_57	1513	20150617_1745117	0.29	928
			Chan 3 open	2339_03	1514	20150617_1747174	0.29	929
			Chan 4 open	2340_59	1515	20150617_1749135	0.29	929
			Chan 2 open, slowly sweeping 3 open	2342_54	1516	20150617_1751077	0.29	930
			Chan 2 open, slowly sweeping 1 open	2344_49	1517	20150617_1753027		
700	700	55	All open	0021_26	1527	20150617_1829402	0.29	918
			Chan 1 open					
			Chan 2 open	0036_02	1528	20150617_1844165	0.3	900
			Chan 3 open	0037_56	1529	20150617_1846111	0.3	905
675	450	23	All open					
			Chan 3 open	0046_25	1530	20150617_1854396	0.3	915

Target Inlet Fuel Temp	Target Fuel Pressure	Fuel mass flow rate	Louver Setting	Other Settings	Lo freq file	Hi freq ID	Hi freq file	Set Point	N2 Flow Rate	Inlet N2 Temp	Strong oscillation freqs
Ambient	400	30	1 and 4 open		2018_14	1549	20150624_1426405	70	0.29	881	
			Chan 1 open		2020_33	1550	20150624_1428592	70	0.29	882	141
			Chan 2 open		1420_10	1595	20150625_0828352	70	0.3	851	140, 280, 340
			Chan 4 open		2022_52	1551	20150624_1431177	70	0.29	883	343
			Chan 1 open, slowly sweeping 4 open		2025_31	1552	20150624_1433568	70	0.29	887	
			Chan 1 open	1/4 N2 flowrate	2028_20	1553	20150624_1436458	70	0.09	852	
			Chan 4 open	1/4 N2 flowrate	2030_00	1554	20150624_1438262	70	0.09	840	
		10	1 and 4 open		2036_39	1555	20150624_1445048	70	0.29	861	
			Chan 1 open		2038_39	1556	20150624_1447052	70	0.29	866	141,283,352
			Chan 2 open		1423_46	1596	20150625_0832125		0.3	864	140, 279
			Chan 4 open		2040_24	1557	20150624_1448503	70	0.29	877	343,239
			Chan 1 open	1/4 N2 flowrate	2044_09	1559	20150624_1452350	70	0.09	840	
			Chan 4 open	1/4 N2 flowrate	2042_28	1558	20150624_1450538	70	0.09	845	
		5	1 and 4 open		2051_54	1560	20150624_1500205	70	0.28	811	
			Chan 1 open		2053_25	1561	20150624_1501508	70	0.28	843	142,250,284, 353
			Chan 2 open		1426_50	1597	20150625_0835172		0.3	873	139,279
			Chan 4 open		2055_10	1562	20150624_1503366	70	0.28	852	344,238
			Chan 4 open, slowly sweeping 1 open		2056_53	1563	20150624_1505189	70	0.28	873	
			Chan 1 open	1/4 N2 flowrate	2059_18	1564	20150624_1507444	70	0.09	834	
			Chan 4 open	1/4 N2 flowrate	2100_59	1565	20150624_1509251	70	0.09	826	
200	400	30	1 and 4 open		2118_29	1566	20150624_1526547	200	0.19	873	
			Chan 1 open		2120_37	1567	20150624_1529029	240	0.29	872	141, 282, 353,423
			Chan 2 open		1442_16	1598	20150625_0850427	180	0.3	836	140, 279
			Chan 3 open		2245_23	1589	20150624_1653492	250	0.29	925	244,335,389
			Chan 3 open	1/4 N2 flowrate	2247_05	1590	20150624_1655306	240	0.09	882	
		10	1 and 4 open								
			Chan 1 open								
			Chan 2 open		1447_25	1599	20150625_0855519	195	0.3	849	139,280
			Chan 3 open		2254_20	1591	20150624_1702459	250	0.29	894	243,335
			Chan 4 open								

Target Inlet Fuel Temp	Target Fuel Pressure	Fuel mass flow rate	Louver Setting	Other Settings	Lo freq file	Hi freq ID	Hi freq file	Set Point	N2 Flow Rate	Inlet N2 Temp	Strong oscillation freqs
			1 and 4 open								
			Chan 1 open								
		Min	Chan 2 open		1450_25	1600	20150625_0858515	200	0.3	860	139,279
			Chan 3 open		2259_30	1592	20150624_1707559	250	0.29	914	243,336
			Chan 3 open	1/4 N2 flowrate	2302_46	1593	20150624_1711121	255	0.08	856	
			1 and 4 open		2127_43	1569	20150624_1536095	335	0.29	889	
			Chan 1 open		2129_22	1570	20150624_1537483	340	0.29	896	141, 282, 352,423
			Chan 2 open		1507_02	1601	20150625_0915291	270	0.3	845	344,144
			Chan 3 open		2234_57	1588	20150624_1643232	320	0.29	919	244,336,389
		30	Chan 4 open		2125_47	1568	20150624_1534134	310	0.29	882	342,236
			Chan 1 open, slowly sweeping 4 open		2133_56	1571	20150624_1542219	340	0.29	940	
			1 and 4 open	1/4 N2 flowrate	2136_33	1572	20150624_1544595	340	0.09	886	
			Chan 1 open	1/4 N2 flowrate	2139_12	1573	20150624_1547385	340	0.09	867	
			Chan 4 open	1/4 N2 flowrate	2140_51	1574	20150624_1549175	340	0.09	859	
			1 and 4 open		2147_05	1575	20150624_1555311	360	0.29	957	
			Chan 2 open		1510_38	1602	20150625_0919045	280	0.3	844	340,144
300	400		Chan 1 open		2157_33	1577	20150624_1605591	370	0.29	821	142,284, 353,426
		10	Chan 3 open		2230_15	1587	20150624_1638415	360	0.29	908	244,334,434
			Chan 4 open		2159_08	1578	20150624_1607338	370	0.29	844	343,238
			Chan 1 open	1/4 N2 flowrate	2202_37	1580	20150624_1611036	380	0.09	811	
			Chan 4 open	1/4 N2 flowrate	2200_59	1579	20150624_1609252	370	0.09	823	
			1 and 4 open		2215_55	1584	20150624_1624217	370	0.29	879	
			Chan 1 open		2217_30	1585	20150624_1625560	370	0.29	886	141, 283, 353,424
			Chan 2 open		1513_24	1603	20150625_0921508	295	0.3	856	342,141
		Min	Chan 3 open		2226_12	1586	20150624_1634384	370	0.29	885	448,338,245
			Chan 4 open		2213_39	1583	20150624_1622049	380	0.29	873	345,240
			Chan 1 open	1/4 N2 flowrate	2208_35	1581	20150624_1617014	390	0.09	815	
			Chan 4 open	1/4 N2 flowrate	2210_00	1582	20150624_1618262	390	0.09	814	

VITA

VITA

Steven Hunt grew up in Greenwood, MI and attended Yale High School in Yale, MI. He received his bachelors of science in mechanical engineering from UCLA in 2009 and his masters of science from the NYU Polytechnic Institute in 2011. He worked as a product engineer in Chrysler's SRT Engine Group from 2011 to 2012. From 2012 to 2016, he attended the Purdue University School of Aeronautics and Astronautics, from which he earned a doctorate of philosophy. His research, under the guidance of Prof. Stephen Heister, focused on thermoacoustic instabilities in heat exchangers and thermoacoustic engines for waste heat reclamation.